INFORMATION TO USERS

This reproduction was made from a copy of a document sent to us for microfilming. While the most advanced technology has been used to photograph and reproduce this document, the quality of the reproduction is heavily dependent upon the quality of the material submitted.

The following explanation of techniques is provided to help clarify markings or notations which may appear on this reproduction.

1. The sign or "target" for pages apparently lacking from the document photographed is "Missing Page(s)". If it was possible to obtain the missing page(s) or section, they are spliced into the film along with adjacent pages. This may have necessitated cutting through an image and duplicating adjacent pages to assure complete continuity.

2. When an image on the film is obliterated with a round black mark, it is an indication of either blurred copy because of movement during exposure, duplicate copy, or copyrighted materials that should not have been filmed. For blurred pages, a good image of the page can be found in the adjacent frame. If copyrighted materials were deleted, a target note will appear listing the pages in the adjacent frame.

3. When a map, drawing or chart, etc., is part of the material being photographed, a definite method of "sectioning" the material has been followed. It is customary to begin filming at the upper left hand corner of a large sheet and to continue from left to right in equal sections with small overlaps. If necessary, sectioning is continued again—beginning below the first row and continuing on until complete.

4. For illustrations that cannot be satisfactorily reproduced by xerographic means, photographic prints can be purchased at additional cost and inserted into your xerographic copy. These prints are available upon request from the Dissertations Customer Services Department.

5. Some pages in any document may have indistinct print. In all cases the best available copy has been filmed.

University Microfilms International
300 N. Zeeb Road
Ann Arbor, MI 48106

Order Number 1330515

Geochemical and isotopic study of calcite stockworks at La Encantada mining district, Coahuila, Mexico: relationships with orebodies and implications for exploration

Diaz-Unzueta, Raul, M.S.

THE UNIVERSITY OF ARIZONA, 1987

U·M·I
300 N. Zeeb Rd.
Ann Arbor, MI 48106

PLEASE NOTE:

In all cases this material has been filmed in the best possible way from the available copy. Problems encountered with this document have been identified here with a check mark ✓.

1. Glossy photographs or pages ✓
2. Colored illustrations, paper or print ✓
3. Photographs with dark background ✓
4. Illustrations are poor copy _____
5. Pages with black marks, not original copy ✓
6. Print shows through as there is text on both sides of page _____
7. Indistinct, broken or small print on several pages ✓
8. Print exceeds margin requirements _____
9. Tightly bound copy with print lost in spine _____
10. Computer printout pages with indistinct print _____
11. Page(s) _____ lacking when material received, and not available from school or author.
12. Page(s) _____ seem to be missing in numbering only as text follows.
13. Two pages numbered _____. Text follows.
14. Curling and wrinkled pages _____
15. Dissertation contains pages with print at a slant, filmed as received _____
16. Other _____

_____

_____

University
Microfilms
International

GEOCHEMICAL AND ISOTOPIC STUDY OF CALCITE STOCKWORKS AT LA ENCANTADA MINING DISTRICT, COAHUILA, MEXICO: RELATIONSHIPS WITH OREBODIES AND IMPLICATIONS FOR EXPLORATION

by

Raul Diaz-Unzueta

A Thesis Submitted to the Faculty of the

DEPARTMENT OF MINING AND GEOLOGICAL ENGINEERING

In Partial Fulfillment of the Requirements
For the Degree of

MASTER OF SCIENCE
WITH A MAJOR IN GEOLOGICAL ENGINEERING

In the Graduate College

THE UNIVERSITY OF ARIZONA

1 9 8 7

STATEMENT BY AUTHOR

This thesis has been submitted in partial fulfillment of requirements for an advanced degree at The University of Arizona and is deposited in the University Library to be made available to borrowers under rules of the Library.

Brief quotations from this thesis are allowable without special permission, provided that accurate acknowledgment of source is made. Requests for permission for extended quotations from or reproduction of this manuscript in whole or in part may be granted by the head of the major department or the Dean of the Graduate School when in his or her judgment the proposed use of the material is in the interests of scholarship. In all other instances, however, permission must be obtained from the author.

SIGNED: 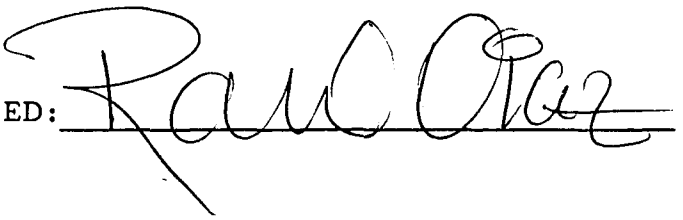

APPROVAL BY THESIS DIRECTOR

This thesis has been approved on the date shown below:

William C. Peters

April 28, 1987

William C. Peters
Professor Emeritus of Mining
and Geological Engineering

Date

ACKNOWLEDGMENTS

Funding for this thesis was provided by Servicios Industriales Peñoles S.A. de C.V. to which I gratefully acknowledge. In particular, thanks to José E. Gaytán. Octavio Alvidrez, and Joaquín Echavez. I am grateful also to Baltazar Solano and Gustavo Lozano, who provided valuable information and helped in arranging the visit to the mine. The cooperation of Oscar Comadurán, Roberto Banda, and the La Encantada mine staff, who helped in the field and assisted my work at La Encantada, is gratefully acknowledged.

I also wish to thank Dr. Joaquín Ruiz for his guidance and advice throughout the project and to Dr. William C. Peters for his enthusiasm and interest in the thesis and reading of the manuscript. My sincere appreciation to Dr. Chris J. Eastoe for his comments and suggestions, which greatly benefited the isotope section, and to Professors Spencer R. Titley and Peter J. Coney for their communications on different topics. Special thanks go to Carla Higgins for her encouragement and whose typing and patient reviews greatly improved the manuscript, and to H. R. Hauck who edited the final version of the thesis.

TABLE OF CONTENTS

TABLE OF CONTENTS--Continued

LIST OF ILLUSTRATIONS

LIST OF ILLUSTRATIONS--Continued

LIST OF TABLES

ABSTRACT

The La Encantada lead-silver district, Coahuila, Mexico, is an example of a high-temperature, carbonate-hosted intrusive-centered deposit. Calcite stockworks and veinlets with iron and manganese are a surface expressions of these deposits. Ore-bearing calcites contain Ag, Pb, Zn, As, Sb, Mo, Mn, Bi, and Hg equivalent to tens to hundreds times the concentration of these elements in either barren calcites or local or average limestone. This enrichment indicates that the metal anomalies are best detected as leakage anomalies in calcite veinlets. Ag, Pb, and As are the best geochemical indicator elements; Sb and Hg appear to be good indicators of deep orebodies, and Mo closely reflects the productive intrusive center. Stable isotope analyses indicate that a $\delta^{18}O$ and $\delta^{13}C$ halo extends at least 70 m away from ore. Geochemical and isotopic data suggest that distance from orebodies and depth of ore can be estimated with averaged Pb/As, Pb/Sb, or C-O compositions.

CHAPTER 1

INTRODUCTION

Base- and precious-metal carbonate-hosted deposits in Mexico occupy a prime position in world lead and silver production and represent a large portion of the country's potential resources of these metals. However, these deposits are also among the most difficult to explore for due to their limited surface expression and the ambiguity of their outcrops. Typical famous examples in Mexico of high-temperature carbonate-hosted deposits are Santa Eulalia and Naica in Chihuahua, Mapimí and Velardena in Durango, San Martín and Providencia in Zacatecas, and La Encantada in Coahuila, which all together produce a substantial part of Mexico's silver and lead.

Problems encountered in prospecting and exploring for these deposits are related to their poor surface expression, the irregularity of orebodies, the irregularity of their distribution, and an insufficient understanding of the controls of the mineralization. In view of the location of mineralization with specific stratigraphic horizons, early studies held that the orebody distribution was due to a stratigraphic horizon favorability for replacement (Prescott, 1926; Hewitt, 1928; Fletcher, 1929; Hayward and Tripplet, 1931). Extensive and more recent studies of chemical composition and primary permeability (Hayward and Tripplet, 1931; Wehrenberg and Silberman, 1965) show, however, that these factors are not consistent controls of mineralization. Among

the factors that have been proposed in several studies to explain the controls of mineralization (morphology and orebody distribution) are carbonate and solution chemistry, primary carbonate textures and composition, grain size, solubility and permeability. Recently, Ruiz, Megaw, and Lofquist (n.d.) in their work on Naica and Santa Eulalia concluded that the mineralization is jointly controlled by secondarily enhanced permeability and impermeable barriers; primary carbonate chemistry, porosity, and permeability do not appear to be as important to ore localization. Thus, it becomes evident that no single factor can be used alone in exploration and that a combination of factors must be used to provide a reasonable explanation of the control of the mineralization. Prospecting based on lithologic and stratigraphic guides alone does not provide an efficient method of exploration; other techniques should be included. There are several secondary characteristics of carbonate-hosted deposits that can be used in exploration.

Carbonate-hosted deposits have a particular surface expression that may be an excellent exploration guide, if its significance is recognized. Calcite breccias, veinlets, stockworks, and oxidizing halos have been recognized as being associated with mineralization. Similar occurrences are, however, widespread in barren carbonate terranes or may occur at the base of eroded orebodies, making these expressions ambiguous. Carbonate-hosted deposits also commonly have manganiferous- and ferrous-calcite stockworks and veinlets with variable diffusion halos of trace elements and oxides. The size of the veinlets and alteration halos can be so small that many deposits of this type have

probably been overlooked during exploration. Typical examples of outcrops of carbonate-hosted deposits are found in Naica, Chihuahua, where large chimneys crop out as either, or both, small brecciated zones or scarce calcite stockworks with oxides content, and in Mapimí, Durango, where large non-outcropping orebodies are seen at surface as long calcite runs or veinlets with traces of iron and copper; these runs occasionally widen out into pockets of silicified limestone and (or) blebs of limestone with iron oxides and into small spots of calcite stockworks or brecciated rock.

Recent studies have emphasized the significance of Fe-Mn-rich veinlets and stockworks found in these deposits. Current research is focusing on the use of these expressions in exploration (Beaty, 1985, 1986; Megaw, 1986). Megaw have recognized the presence of extensive Fe-Mn-rich stockworks above ore at Santa Eulalia. Beaty (1985, 1986) has studied ^{18}O isotope distribution in limestones and calcites of the Leadville formation in Colorado and has shown that calcites, as well as the limestones associated with mineralization have a lower ^{18}O halo than do the host carbonates. In summary, Fe-Mn calcite stockworks, veinlet swarming, and brecciated oxidized outcrops appear to be common features of carbonate-hosted deposits that can be used as an exploration tool.

Accordingly, the purpose of this thesis was to determine the relationships between these stockworks and orebodies at La Encantada mining district to apply these surface manifestations as an exploration tool for carbonate-hosted deposits. The main purpose was to distinguish ore-bearing calcites from barren ones and to find a measure to

estimate the depth of mineralization. Accordingly, the chemical composition, isotopic data, fluorescence, fracture density relations, and geological setting of the calcite stockworks were used to evaluate these surface expressions. Surface-sampling data was used for geochemical interpretation, with both surface and underground for isotopic and surface measurements for fracture-density interpretation. Due to the excellent exposures and, unlike other deposits of its kind, the representation of a complete system including the intrusive center, La Encantada offers a unique setting for its study.

This thesis is intended to provide a general concept and treatment of the use of isotope and veinlet geochemistry in grass-roots as well as detailed exploration.

Location, Geography, History, and Production

The La Encantada mining district is located in the northwest part of the State of Coahuila, 120 km N. 65° W. of the City of Musquiz, Coahuila (Fig. 1). The district is divided into three main areas connected by a trend of faults and joints scarcely mineralized (Fig. 2). The west area, referred to as La Prieta, comprises the La Prieta and La Escondida chimneys and is the area in production; the middle area, San Javier, comprises a chimney and mantos currently under exploration and development; and in the northeast, the La Escalera area, is a prospective zone currently undergoing surface exploration. Collectively, the district occupies approximately 1.5 km^2. Geographically, the district lies at the southern end of the Sierra de la Encantada, a northwest-trending mountain range 30 km long and 10 km wide, which rises

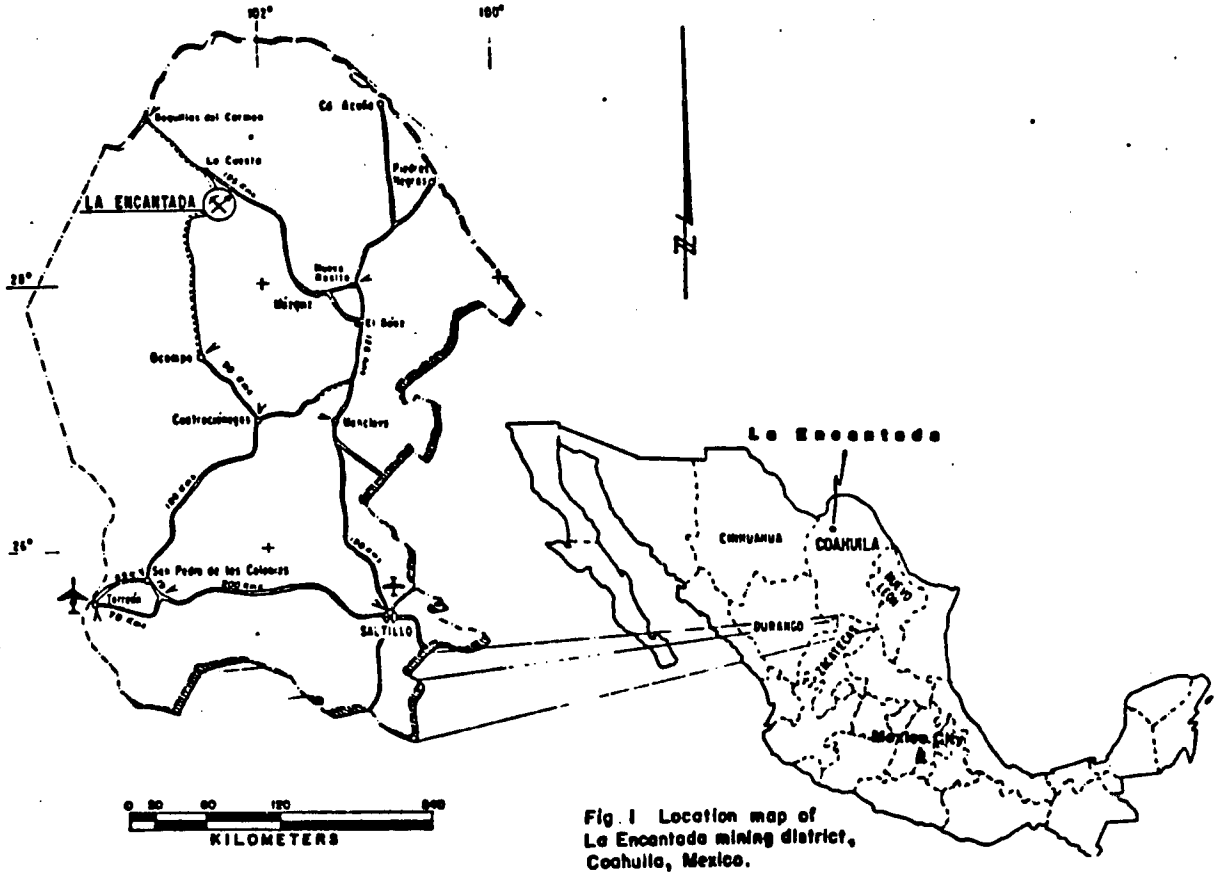

Fig. 1 Location map of La Encantada mining district, Coahuila, Mexico.

Figure 1. Location map of La Encantada mining district, Coahuila, Mexico

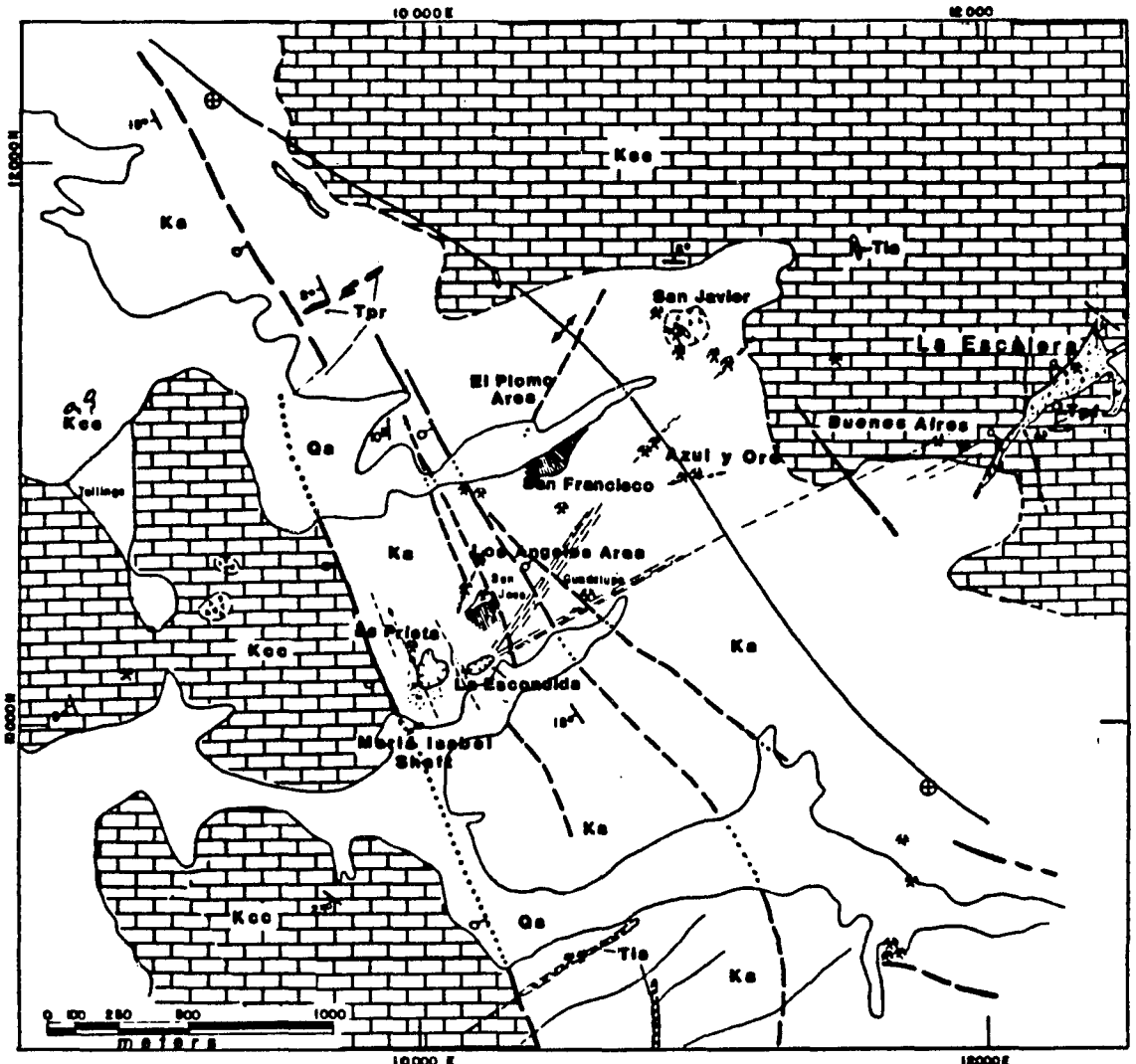

Fig.2

EXPLANATION

LITHOLOGY

QUATERNARY

Qa Alluvium

TERTIARY

Tla Andesitic porphyry

Tpf Feldespatic porphyry

Tpr Rhyolitic porphyry

Tlgd Granodiorite

CRETACEOUS

Kcc Cuesta del Cura formation. (medium bedded limestones with chert.

Ka Aurora formation Thick bedded micritic limestones.

Klp La Pena formation. Thin bedded black shales interlayered with black bituminous limestones.

STRUCTURE

Contact. Dashed where approximate.

Fault showing downthrown side Dashed where approximate, dotted where concealed, ?-? where interpreted.

Veins, fractures.

Strike and dip of beds.

Breccia zone.

Pit outline.

Figure 2. Generalized geologic map of La Encantada mining district, showing areas of study. -- Map adapted from Comaduran and Giles (unpublished data) and Solano (1985).

from 800 m up to 2350 m in elevation, with the La Prieta mine located at an elevation of 1800 m. Asymmetrical anticlines and synclines, commonly with low structural relief, have few recumbent folds. Normal faults and fewer thrust faults are common.

Unlike many mining districts discovered in the past century in Mexico, La Encantada is a recent discovery. The first discoveries were made about 1950 by local prospectors (Alvarez, 1971), followed by the discoveries of the Guadalupe, San José, La Escandida, and San Francisco orebodies by the Los Angeles Mining Company in 1956. The La Prieta chimney, the most productive orebody, was discovered in 1963; later, the contact bodies "660" and the mantos zone were discovered and put into production by the Compania Minera La Encantada in 1973.

Production from 1967 to 1983 included more than 1.8 metric tons (t) of ore with an average grade of 350 g/t silver and 5% lead (Trejo, 1983). The most important orebodies were the La Prieta chimney with 1.7 t of ore with an average grade of 646 g/t silver and 23.5% lead, and the "660" orebody with 1.3 t and an average grade of 418 g/t silver and 5.8% lead (Solano, 1985). Part of the ore at La Prieta remains inaccessible due to the collapse of the chimney. Selective mining in the mantos zone produced additional high-grade ores containing and average of 1.25 kg/t silver and 20% lead.

Records of studies before 1970 are scarce and belong mostly to private companies. Baker (1971) published an overview of regional geology and structure, and the West Texas Geological Society (1981) published a collection of papers describing stratigraphy and structure of northeastern Mexico. Humphrey (1956) described the tectonics of

northeastern Mexico. Locally the district's areal stratigraphy and structure have been studied by Hunter (1972), Sharpley (1972), Lozej and Beals (1977), and Lozano (1981). The geology of the ore deposits has been discussed by Alvarez (1971), Luján (1975), and Solano (1985).

CHAPTER 2

GEOLOGY

The La Encantada deposits lie in the Coahuila composite tectonostratigraphic terrane (Campa and Coney, 1983), paleotectonically near the edge of the Jurassic Peninsula of Tamulipas (Humphrey, 1956). The Coahuila terrane is considered a Paleozoic accreted terrane composed of metamorphosed rocks intruded by upper Paleozoic granodiorite. The oldest rocks known in the region are Paleozoic metamorphic rocks that crop out 100 km northwest and approximately 110 km south of La Encantada in Sierra Del Carmen and Sierra Del Fuste, respectively (Flawn and Maxwell, 1958; Denison et al., 1969; Cuevas, 1985). These rocks consist of Permian phyllites, marbles, and quartzites and a granite-quartz andesite igneous complex. Farther south, at Las Delicias (190 km southwest of La Encantada), conglomerates, graywackes, shales, and fossiliferous limestones are underlain by Pennsylvanian limestones. Unconformably overlying the Paleozoic rocks are redbeds and evaporites of late Triassic to middle Jurassic age (Imlay, 1943; Humphrey, 1956) assumed to be related to rifting (Coney, 1983; Coney and Campa, 1984). Overlying the basement rocks and the Mesozoic rift assemblage is a thick sequence of Mesozoic carbonate rocks, which is called an overlap assemblage, part of the marine transgression related to the opening of the Gulf of Mexico (Coney, 1983) and upper Cenomanian-Maestrichtian terrigenous sediments with minor carbonate

deposits probably related to the beginning of the Laramide orogeny in Mexico (Smith, 1981). Part of the overlap carbonate assemblage hosts the mineral deposits at La Encantada.

Silver and lead deposits at La Encantada are oxidized supergene-enriched examples of carbonate-hosted high-temperature (200-400°C) massive sulfide (60% sulfides) ores. These deposits resulted from both replacement and open-space filling (Titley and Megaw, 1985; Ruiz et al., n.d.). At La Encantada, a series of mantos, chimneys, veins, and contact orebodies were hosted in micrites of the Aurora Formation. Most orebodies occur on the west flank of a northwest-trending anticline. A 27-Ma-old granodiorite and northwest-trending fractures control the mineralization.

Surface expression of orebodies varies from none to very limited. Oxidized zones of scarce breccias or stockworks of calcite with iron and manganese oxides appear to rise above orebodies. Commonly, thin (less than 1 mm to a few centimeters) calcite-hematite-manganese oxide microveinlets make up the stockworks or are irregularly distributed above mineralized zones. The calcite veins also contain Pb, Mn, Zn, As, Sb, Cd, Bi, and Mo.

Lithology and Stratigraphy

The stratigraphy of the La Encantada mine area was described in detail by Lozej and Beals (1977), who made an intensive study of litho- and biofacies of the thick limestone package that is present in the area. They stressed the uniformity of the limestone sequence and described it as a single formation with map units based on

biostratigraphy. According with age based on fossils reported by Lozej and Beals and lithology similar to type localities, the lithologic units at La Encantada can be named in accordance with the nomenclature for northeastern Mexico into several formations.

The stratigraphic sequence at La Encantada is composed of slightly folded, faulted, and locally thrusted Cretaceous (Aptian-Cenomanian) carbonate and pelitic rocks that include, from the bottom to the top, La Peña, Aurora, Cuesta del Cura, Del Rio, and Buda Formations. Their total thickness is more than 800 m (Lozano, 1981). Underlying the La Peña and Aurora Formations is the Cupido Formation, which has not been recognized in the mine. In the vicinity of the mine the sequence was intruded by dioritic and rhyolitic dikes and a 27-Ma-old granodioritic pluton. Marble, skarn, and hornfels derived from the carbonate and pelitic rocks are locally distributed around both the granodiorite intrusion and hydrothermally altered breccia and fractures zones (Fig. 3).

Cretaceous Units

The oldest rocks in the mine region are upper Neocomian-lower Aptian massive to thin-bedded limestones and dolostones of the Cupido Formation and upper Aptian thin-bedded shales, limestones, and dolostones of the La Peña Formation. Both formations crop out in the Sierra De La Vasca 30 km northwest of La Encantada. The Cupido–La Peña contact is transitional and has not been reached at the mine. The La Peña Formation is known in the mine area from drill holes and consists of more than 130 m of thin-bedded black shales interlayered

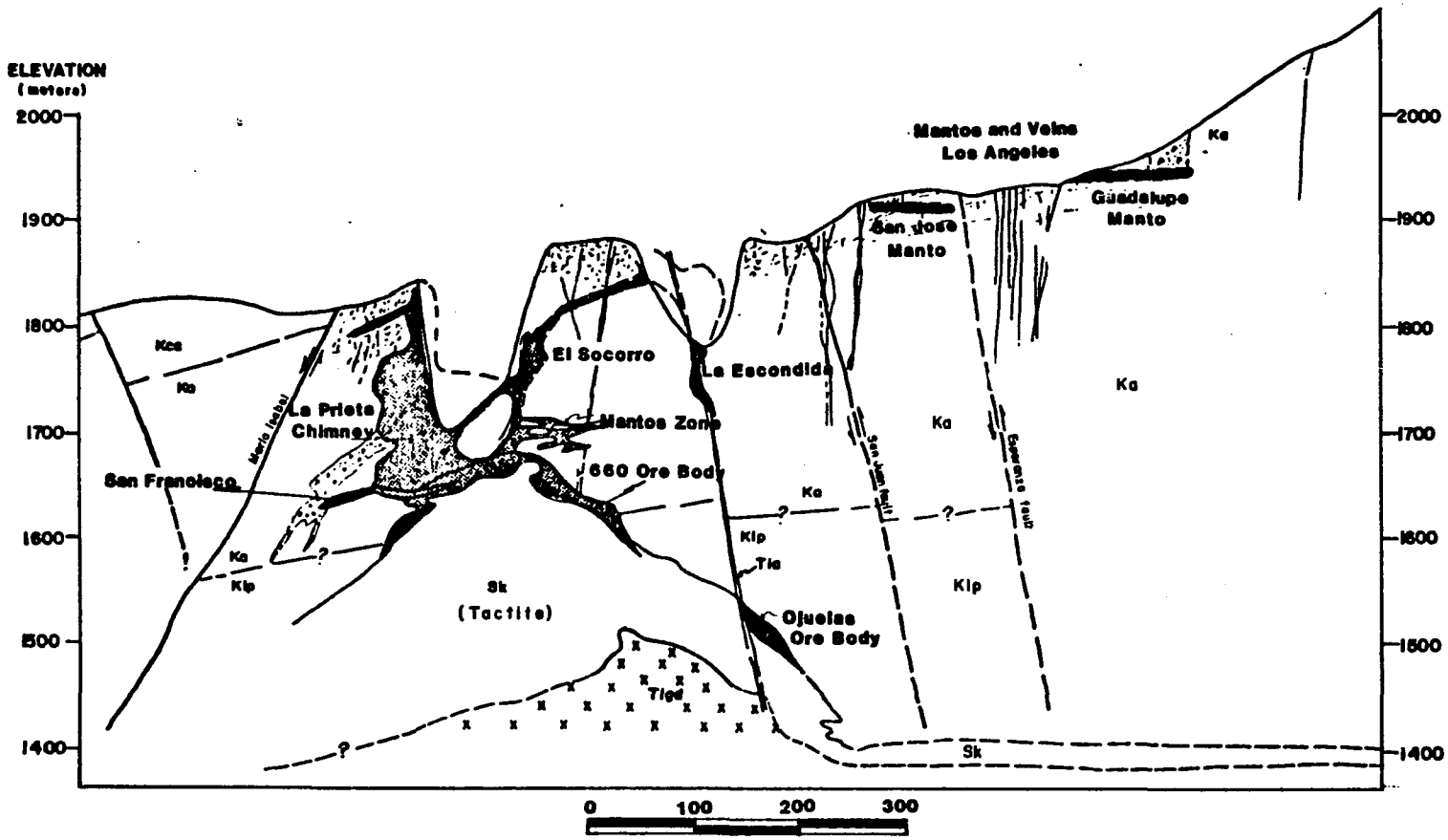

Figure 3. Longitudinal N. 47° E. section of the La Encantada district, view to the northwest. -- Adapted from Solano (1985). Symbols are the same as for Figure 2.

with black bituminous carbonaceous limestones (Lozano, 1981). The base of the limestone sequence, as described by Lozej and Beals (1977), includes micrites and biomicrites with Collomiella mexicana of late Aptian age (Bonet, 1956) and correlates in age with the La Peña Formation.

Conformably overlying the La Peña Formation is the Aurora Formation (early-middle Albian), a 452-m-thick sequence of thick-bedded to massive gray micritic limestones. Dolostones and authigenic quartz are present only in the lower portion of the limestone. This limestone is macroscopically very homogeneous and as an additional feature contains scattered chert nodules and lenses. The lower portion of the Aurora Formation locally changes facies to the near-shore pelitic-calcareous facies of the Glen Rose Formation (Lozej and Beals, 1977). Most of the orebodies occur in the lower limestone of the Aurora Formation in biopelsparites and intra-biosparrudites. However, no specific marker beds or highly favorable horizons are mappable (Lozej and Beals, 1977; Lozano, 1981).

Conformably overlying the Aurora Formation are fairly distinctive thin-bedded limestones of middle Albian-lower Cenomanian age of the Cuesta del Cura Formation. This formation consists of 250-350-m oolitic limestones with abundant chert nodules, strings, and lenses relative to the Aurora Formation. This formation becomes argillaceous upward and is distinguished by its Calcisphaerula content (Lozej and Beals, 1977).

Thin-bedded (30 cm) alternating shales and limestones correlative with the Del Rio Formation and medium-bedded (60-70 cm) limestones similar to those of the Buda Formation conformably overlie the

Cuesta del Cura Formation; their precise thicknesses in the mine area are unknown, but estimated thicknesses are approximately 45 m for the Del Rio Formation and 100 m for the Buda Formation. The Del Rio Formation is early Cenomanian in age. The lower Cenomanian Buda Formation overlies the Del Rio Formation.

Igneous Rocks

Unlike may similar districts where igneous intrusions either are absent or show no clear association with the mineralization, La Encantada offers an excellent example of carbonate-hosted, intrusion-centered system. At La Encantada, a granodiorite body and felsic-to-mafic dikes of Oligocene age intrude the sedimentary sequence. The granodiorite is of regional extent and apparently has a semi-horizontal attitude. The composition of this intrusion is shown in Table 1. It consists of feldspars, quartz, and ferromagnesian minerals with pyrite and epidote along fractures and is known in the mine from drill holes and shows alteration to sericite and chlorite. It appears to be responsible for the formation of the skarn dome and metamorphic halo. A whole-rock K-Ar date of the hydrothermally altered granodiorite yields a 27-Ma age.

The association of this intrusion with the domic skarn structures, alteration zones, zones of higher fracture density associated with mineralization, intrusion alteration itself, and close spatial relationship with orebodies provides strong evidence that this intrusion is directly associated with ore mineralization.

There are four sets of dikes in the district. They occasionally localize vein mineralization (Luján, 1975) or cut orebodies as well.

TABLE 1
Composition of the granodioritic intrusive body. -- From Trejo (1983).

Oxides, %											
Sample	SiO_2	Al_2O_3	Fe_2O_3	CaO	MgO	Na_2O	K_2O	TiO_2	MnO	P_2O_5	LOI	Total
535-10	67.87	11.74	0.75	7.79	0.26	2.9	3	0.18	0.02	0.05	2.82	97.7
535-11*	74.05	11.51	0.68	1.88	0.13	0.7	10	0.18	0.01	0.06	0.91	100.2

Elements, ppm										
Sample	Cd	Co	Cr	Cu	Ni	Mo	Pb	Sb	V	Zn
535-10	4	21	277	20	14	21	51	4	1	860
535-11	39	21	186	64	13	1	123	5	2	2080

*Strongly altered sample.

Rhyolite-porphyry dikes consist of feldspars, quartz, minor hornblende, and disseminated pyrite. These dikes generally have a N. 50° E. strike, parallel to and also within ore-controlling fractures. N. 50° W. and N. 15° W.-striking diorite and andesite porphyry dikes consist of plagioclase, Hornblende, biotite, and chlorite. These dikes are associated with the major intrusion at depth and are presumably contemporaneous. In general, the dikes are strongly hydrothermally altered and (or) weathered often having a reddish coloration due to iron oxide content. This alteration largely consists of kaolinization, chloritization, sericitization, and carbonatation (Luján, 1975). A fifth intrusive type is a set of east-west-striking aphanitic-to-porphyritic lamphrophyre dikes composed of plagioclase, hornblende, and magnetite.

In the mine vicinity, the Aurora limestone is locally metamorphosed to grayish-white saccharoidal marble. This marble is irregularly developed and is found mainly around breccia zones or hydrothermal channels. Marble and local skarn zones are also products of contact metamorphism of limestone by the granodiorite intrusion. The granodiorite–limestone contact is a dome-shaped zone surrounding the granodiorite intrusive body. This zone consists of an outer portion of a black-gray marble and an inner zone of diopside-garnet skarn. This inner skarn dome is a semi-elliptic body with a vertical extent exceeding 200 m. It is 225 m in diameter at the 630 level and tapers from 70 m to 15 m in thickness from the center outward (Fig. 3). The skarn consists of calc-silicates and is rich in fluorite (Luján, 1975).

Structures

Structurally, La Encantada lies on the southwestern flank of the northwest-trending Sierra de La Encantada anticlinorium. The beds on the flanks of the Sierra de La Encantada dip 30-40 degrees with local vertical and overturned strata (Lozej and Beals, 1977) and in the mine dip from 20° to 30° W. (Fig. 2). Guzmán (1972) noted a west bending of the La Encantada anticline. The undulation coincides with the La Encantada's mineralized trend and with minor intrusive bodies (Luján, 1975). However, the significance of these anticlinal bendings for mineralization is unknown.

Block faulting cuts the anticlinal structures of Sierra de La Encantada. A regional N. 26° W.-striking fault, traceable for 38 km, cuts the anticlinorium southwest of the mine (Baker, 1927). This fault

possibly reflects reactivation of Paleozoic basement faults during the Laramide orogeny (Smith, 1970) and may have controlled the emplacement of the granodiorite body. A similar structural setting has been invoked to explain the localization of several mineral deposits along the Chihuahua Trough (Megaw, Ruiz, and Clark, 1986; Ruiz et al., 1986).

Most of the faults are normal, and the main systems strike N. 15°-30° W. and N. 50°-80° E. Both systems postdate folding and predate mineralization, although the exact relationship between them is unclear. Northeast-trending fractures appear to be older than northwest-trending faults. Multiple phases of fracturing associated with uplift and igneous intrusions add complexity to the structural regime. With the exception of the regional La Encantada fault, the N. 14°-30° W.-striking system appears to be shallow and probably indicates separate fracturing phases that were active after folding and continued after intrusion and mineralization. In the mine area, two grabens bounded by the Romo-Maria Isabel and San Juan-San José faults contain the central orebodies (La Prieta-La Escondida) (Fig. 3). No detailed structural studies of Sierra La Encantada are available; however, the structural style of deformation of the Laramide allows us to presume that northwest-striking normal faults can be related to relaxation of Laramide stresses. Fracturing in both northeast and northwest directions is also attributed to mid-Tertiary intrusion phases that caused doming and metamorphism.

Mineralization

Description of Orebodies

Orebodies at La Encantada occur as chimneys, mantos, veins, and skarn (contact bodies) within the Cretaceous Aurora Limestone. The orebodies are part of an intrusion-centered system with crude alteration zoning and a wide spectrum of mineralization textures, varying from replacement at depth to open-space filling textures upward and away from the intrusive center. Ore zoning consists of contact bodies that lie along the skarn margins at depth and grade upward to mantos and chimneys. Veins dominate at the highest levels along the same structural trends that host the mantos and chimneys. All ores are oxidized and are supergenically enriched bodies probably resulting from deep oxidation of iron, lead, zinc, and silver sulfides and sulfosalts.

The most important orebodies are chimneys, followed by contact bodies, mantos, and veins. The chimneys are bodies with a semi-elliptic section and a vertical extension exceeding their horizontal dimension (Fig. 3 and Table 2). The La Prieta chimney, the most productive orebody, is a northeast-oriented vertical body, 160 m high with a 135 × 75 m maximum horizontal cross section. It extends from the 790 to the 630 levels and merges with the skarn at its base in the 635 level. This chimney contains a high-grade core with silver-lead grades increasing with depth and an outer, lower grade hematitic halo (Fig. 4). Silver-lead grades decrease again approaching the deep sulfide zones of the skarn. The chimney–limestone contact is generally sharp with local alteration occurring in the host rock. Host-rock alteration

TABLE 2
Characteristics, grade, and tonnages of main orebodies at La Encantada

	Dimension (meter)				Surface Elevation, m	Grade		Tonnage t	Alteration
	Top	Bottom	Height	Section		Ag, g/t	Pb, %		
Chimneys									
La Prieta La Escondida San Javier Socorro, Tiro Nuevo Del 800, 8 de Enero Los Angeles	1790 1900 1950	1630 1790 1770	160 110 180	135x75 88x33[a] 75x50 (surface)	1850 1860 2100	646	23	1.7	marmorization (silicification)
Contact									
660 Ojuelas	1680	1580	100			418	5.8	1.3	silicates marmorization at contact with limestone
Mantos									
San Jose Guadalupe San Juan Refugio Esperanza "Zona mantos"	1760	1635	125			1250	20		marmorization
Vein									
San Francisco Azul, Azul Y Oro Buenos Aires	2200	1620	580	500x1.2	2200				

a. Maximum.

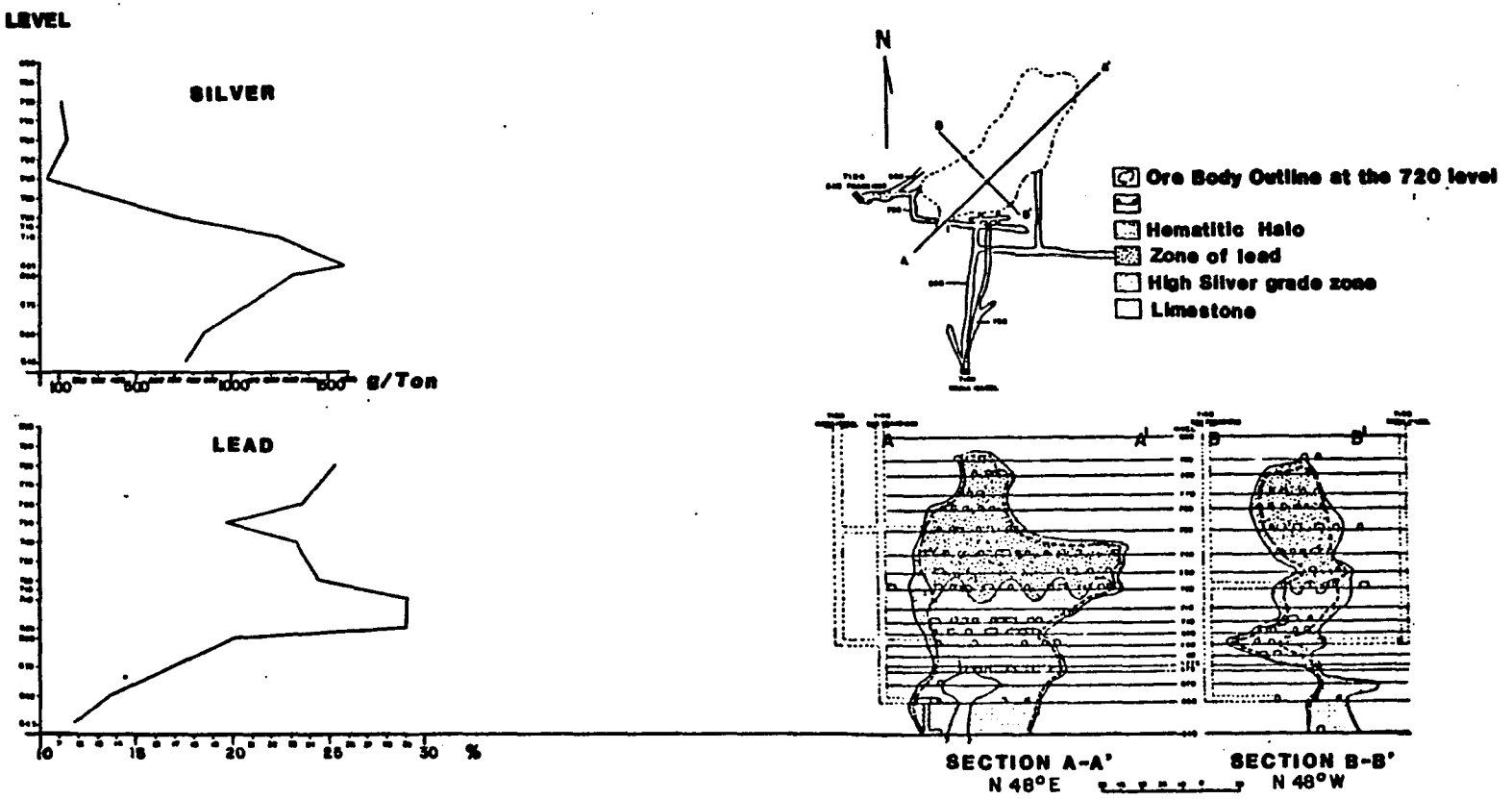

Figure 4. Vertical cross sections of La Prieta chimney showing its structure and Ag and Pb grades. -- After Alvarez (1971). Upper part of sections is predominantly lead; lower zone is high in silver and also contains lead (fine stippled pattern). Outer zone is a hematitic halo.

and contact characteristics indicate that partial replacement and mainly filling processes formed most chimneys. Massive replacement appears to have occurred in the San Javier chimney. The San Javier chimney is a poorly consolidated collapse breccia where some limestone fragments are completely replaced by iron and manganese oxides. Other limestone and matrix fragments are fresh, and everything is mixed in a fine- to coarse-grained matrix with minor cement.

Contact orebodies are developed at the granodiorite–limestone contact and are part of a skarn system. The Ojuelas and "660" orebodies are the only ones of this type. The skarn is zoned: orebodies in the outer zone consist of Pb, Zn, and Ag oxides and carbonates, which grade downward to sulfides and calc-silicates. Sulfide mineralization occurs as blebs, disseminations, and veinlets, in the calc-silicates. In general, the sulfide mineralization consists of Fe-rich sphalerite (5-7%), which replaces pyrite and arsenopyrite in addition to galena, chalcopyrite, and molybdenite. Paragenetically late fluorite mineralization replaces sphalerite (Luján, 1975). Homogenization temperatures of fluid inclusions in fluorite from the 660 orebody indicate that the fluorite formed at 360°-370°C (Kesler, cited by Luján, 1975).

Mantos are stratabound tabular bodies. The mantos are sparsely distributed from the 635 level (elevation 1635 m) up to the surface at around 1900-m elevation. Shallower mantos display strong brecciation and filling fabrics, whereas deeper mantos (e.g., Manto Zone) may have formed by more replacement of the limestone.

Veins are commonly found in the northeast part of the district (northeast of La Prieta). They are shallow tabular bodies commonly

rising from mantos and are mineralized between 1600 m and more than 2200 m in elevation (Table 2). It is not uncommon to have dike-localized veins and mantos along the trace of the same controlling structures. Mineralization in mantos and veins consists of cerussite, goethite-limonite with high silver content and minor lead and zinc sulfates and sulfides.

Ore Controls

Mineralization is dominantly controlled by N. 60° E.- and N. 30° W.-striking fractures. Major N. 30° W.-striking faults do not appear to be significantly mineralized (Lozej and Beals, 1977). Measurements of fracture density taken at the surface in the mine area show that fracturing and microfracturing are perhaps the most important controlling factors for both filling and replacement mineralization (Figs. 5 and 6). The most densely fractured areas lie above the skarn dome and coincide with chimney bodies (Fig. 5). Other mineralization controls are the intrusion dome, lithology, and fractures in the limestone and skarn. The skarn, developed along the limestone–granodiorite contact, controls the distribution of the contact orebodies. Chimneys tend to expand where fractures cut across the more favorable biopelsparite and intrabiosparrudite beds (Lozej and Beals, 1977). Mantos appear to be most abundant in these favorable zones at the base of the Aurora Limestone.

Although a stratigraphic control seems evident, there is no obvious difference between barren and host limestone. Lozej and Beals (1977) pointed out the difficulty of distinguishing different limestone

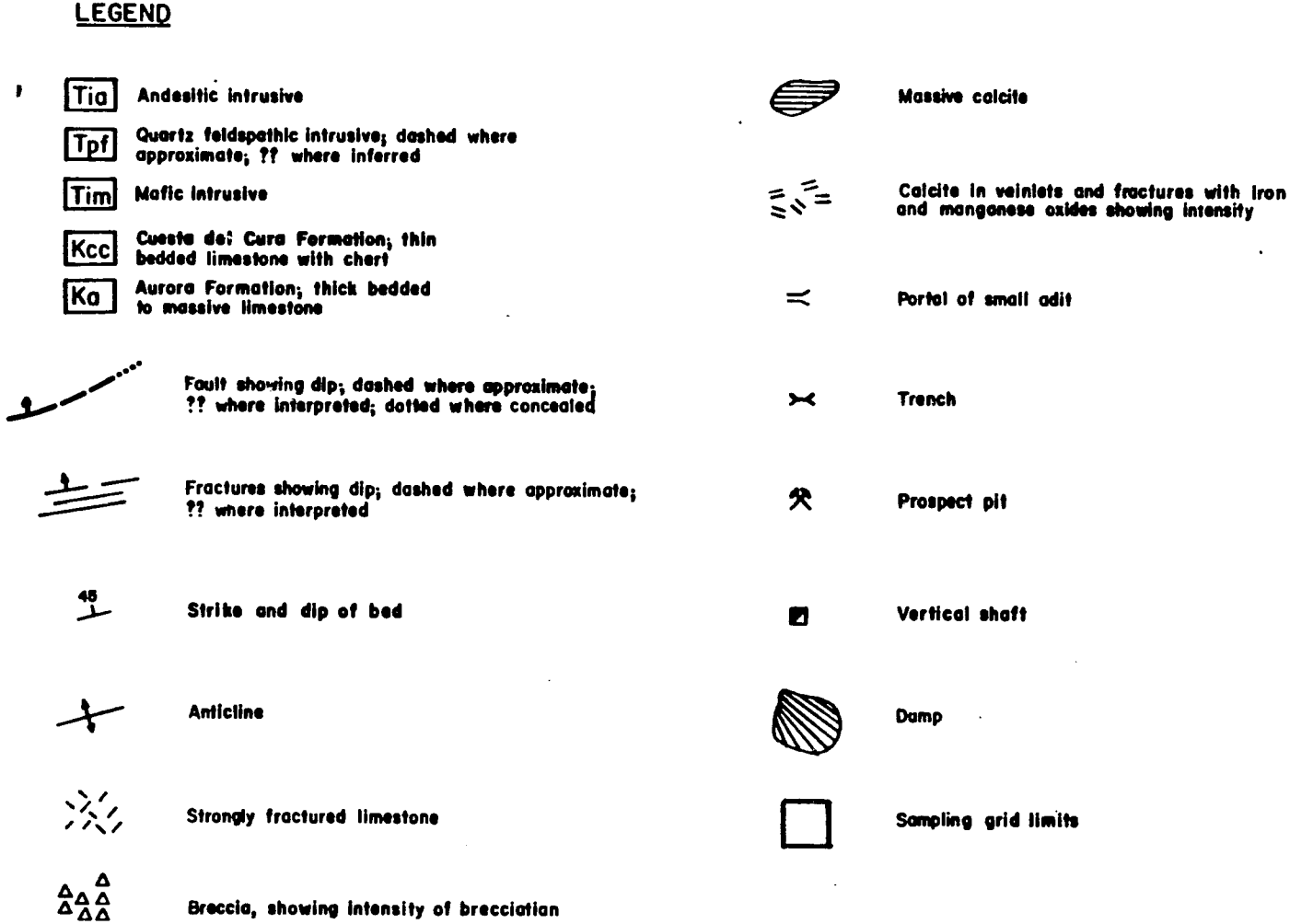

Figure 5. Geologic map of La Prieta area showing the northeast and northwest ore-controlling structural trends. -- Barbed lines are the pits of major chimneys. Tilted square inside map is the outline of the sampling grid shown for reference with fracturing and geochemical maps of the area. Map adapted from Solano and Flores (1983).

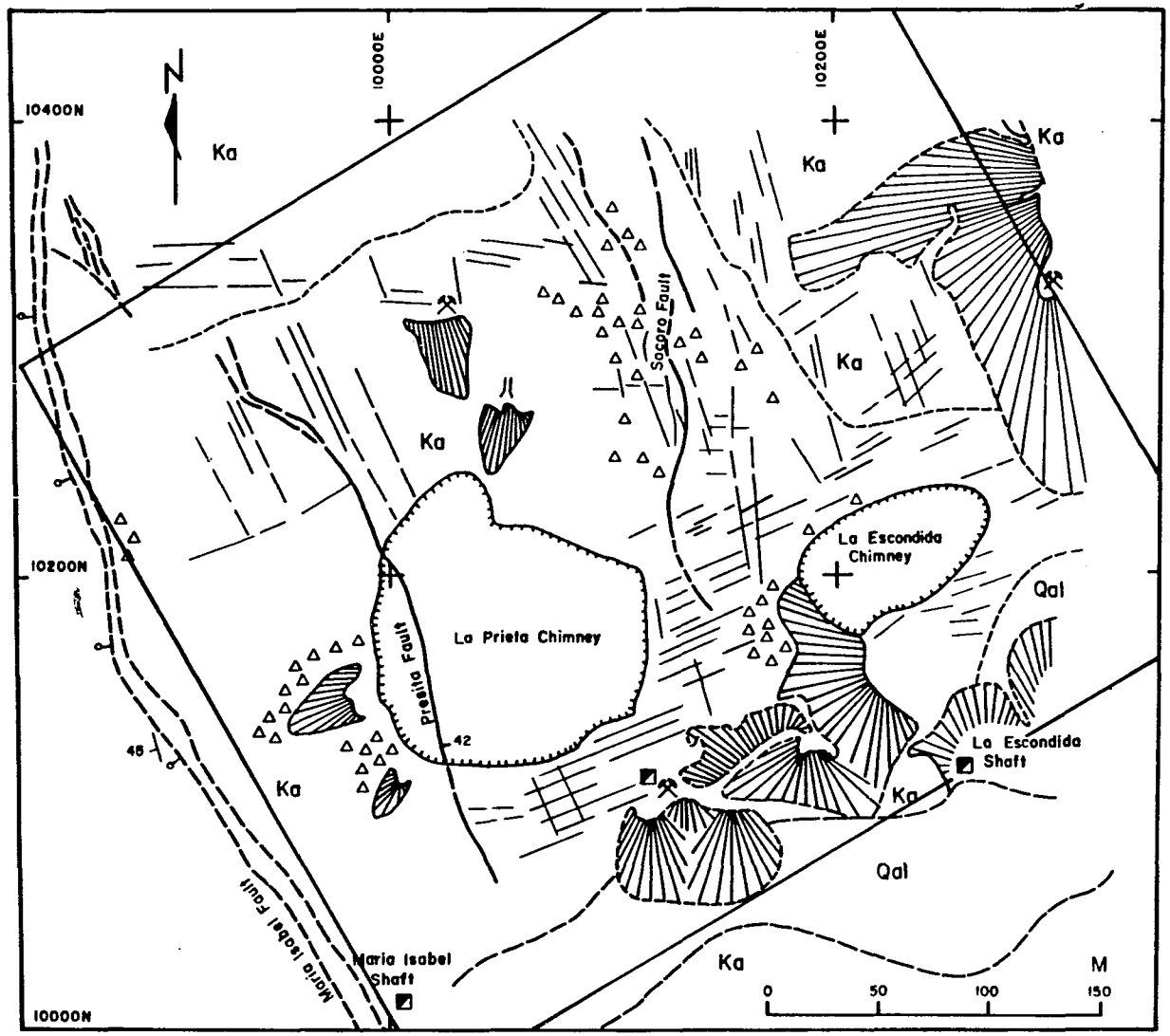

Figure 5. Geologic map of La Prieta area

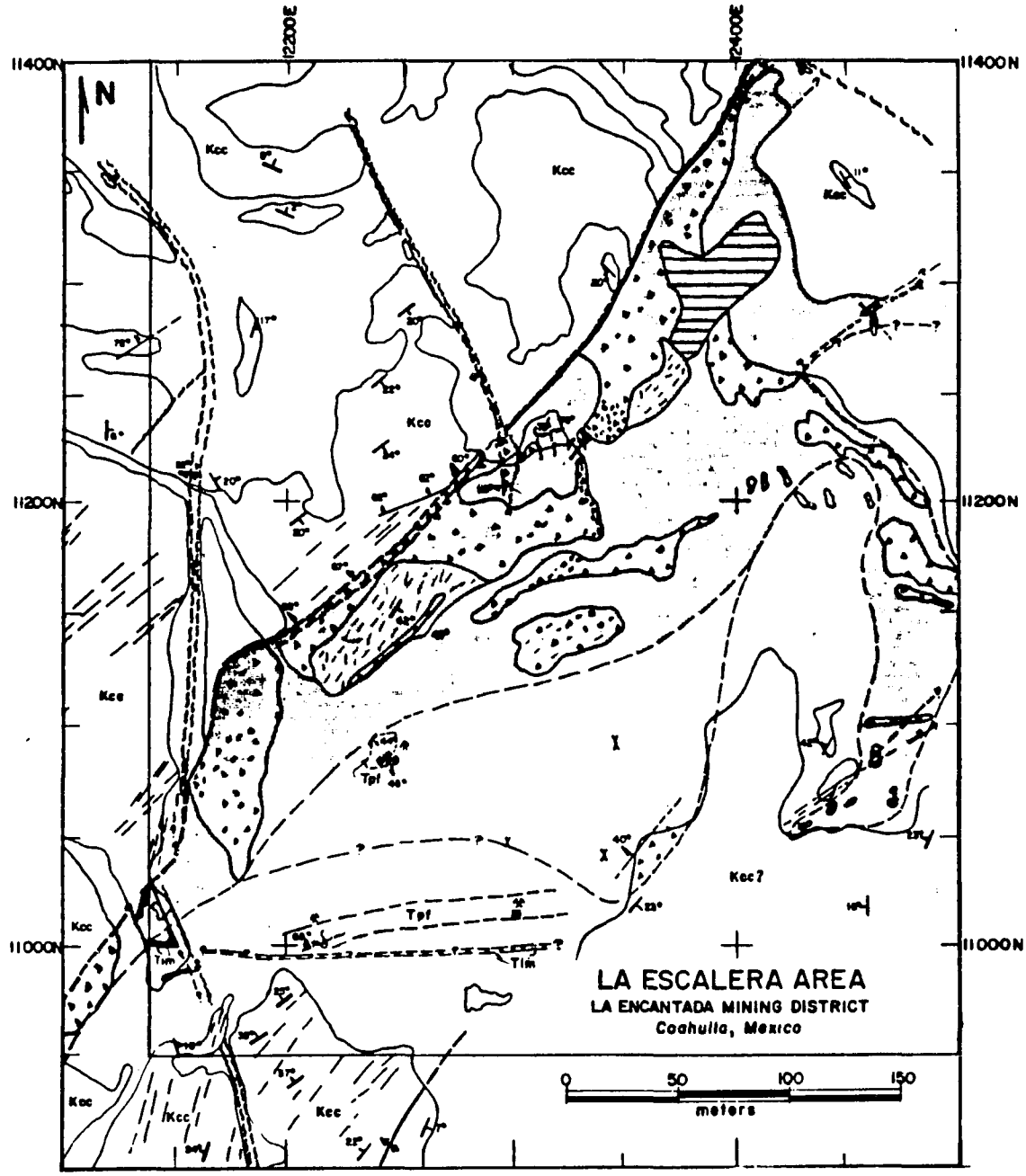

Figure 6. Geologic map of La Escalera area. -- Note the northeast- and northwest-trending structures, similar to the geologic setting of La Prieta. Symbols are the same as for Figure 5. Map adapted from Comadurán (1985, unpublished data).

horizons even microscopically. They suggested, however, that the favorability of the host-limestone is due to the readiness of the coarser grained biopelsparite and intrabiosparrudite to be fractured.

Mineralogy of Orebodies

Mineralization in orebodies consists of a complex assemblage of carbonates, sulfates, and oxidized minerals of iron, silver, lead, and zinc (Table 3). Common minerals are hematite, goethite, limonite, cerussite, minium, argentojarosite, anglesite, hemimorphite, with minor relict Fe-rich sphalerite, galena, arsenopyrite, proustite-pyrargyrite, pyrite, and lesser chalcopyrite, freibergite, cassiterite, and molybdenite. Fluorite, quartz, and calcite appear to be coeval with mineralization; they may occur replacing sulfides and filling veinlets and vugs. Calc-silicate minerals such as garnets (andradite-grossularite), diopside, tremolite, and actinolite compose the skarn and and restricted to the skarn dome area. Metal zoning occurs as a consequence of oxidation and supergene enrichment, and no primary zoning can be defined.

Alteration

Alteration consists of irregular halos of marmorization, bleaching, local silicification, and epidotization. Silicate alteration occurs in the skarn dome, and the outer skarn zone contains strong epidotization, chloritization, and lesser talc. Marmorization occurs adjacent to chimneys, dikes, the skarn body, and mineralized fractures. The dimension of its halo ranges from less than 1 cm to a maximum of a few tens of meters (60 m). Diffuse local silicification and quartz in

TABLE 3
Mineralogy at La Encantada. -- Modified from Luján (1975)

	Abundant		Common		Rare	
			Hypogene Minerals			
Silicates	andradite	$Ca_3Fe_2(SiO_4)_3$	actinolite	$Ca_2(Mg,Fe)_5Si_8)_{22}(OH)_2$	hedenbergite	$(Ca,Fe)Si_2)O_6$
	grossularite	$Ca_3Mg_2(SiO4)_3$	epidote	$Ca_2(Al,Fe)_3Si_3)_{12}(OH)$	tremolite	$Ca_2Mg_5Si_8O_{22}(OH)_2$
	diopside	$CaMg(SiO_3)_2$			vesuvianite	$Ca_{10}Mg_2A_{14}(SiO_4)_5(Si_2O_7)_2(OH)_4$
	quartz	SiO_4				
Oxides			magnetite	$FeSO_4$	cassiterite	SnO_2
Sulfides			Pyrite	FeS_2	chalcopyrite	$CuFeS_2$
			Galena	PbS	molybdenite	$Cu_{12}AgSb_4S_{13}$
Carbonates			calcite	$CaCO_3$		
Halides			fluorite	CaF_2		
			Oxidation Minerals			
Oxides	hematite	Fe_2O_3	minium	PbO	manganite (?)	MnO(OH)
			pyrolusite	MnO_2		
Hydroxides	goethite	FeO(OH)				
	limonite	$FeO(OH)nH_2O$				
Carbonates	cerussite	$PbCO_3$	smithsonite	$ZnCO_3$	malachite	$Cu_2(CO_3(OH)$

TABLE 3
Mineralogy at La Encantada--Continued

Abundant	Common		Rare	
		Oxidation Minerals--Continued		
Sulfates	anglesite	$PbSO_4$	plumbojarosite	
	angento-jarosite		gypsum	$CaSO_4nH_2O$
Silicates	willemite	Zn_2SiO_4		
	hemimorphite	$Zn_4SiO_7(OH)_2.2H_2O$		
Halides			cerargyrite	AgCl
Native			copper	Cu
			silver	Ag
Sulfosalts			proustite	Ag_3AgS_3
			pyrargirite	Ag_3SbS_3

fractures are abundant near the ore. With the exception of marmorization and bleaching, alteration halos are so local and narrow that they are of little use as ore guides.

Calcite Types and Their Relation to Paragenesis

Figure 7 shows both the succession of identified calcite types and a preliminary paragenetic sequence. Sulfide paragenesis is defined from a few samples taken from skarn and from sulfide relicts at the roots of the La Prieta and El Socorro chimneys. Elsewhere, sulfides are scarce.

Four stages of calcite mineralization were identified and sampled using field criteria. The field criteria were based on surface and underground observations and include: (1) mineral assemblages, (2) crosscutting relationships, (3) empirical criteria such as color of calcite, and (4) iron and manganese oxide content. Further microscopic analysis distinguished three varieties of calcite stage I. Because these substages are local variations within the skarn and are specific to one stage of mineralization, they are therefore irrelevant in this discussion and will not be emphasized. Five calcite stages were recognized:

1. Stage I. Clear calcite, which is primarily associated with skarn mineralization, is paragenetically related with fluorite and perhaps late galena stages. It was observed only underground in skarn samples from La Prieta and in veinlets below the San Javier body where it is associated with galena (Fig. 8). Fluid-inclusion temperatures from fluorite associated with this calcite

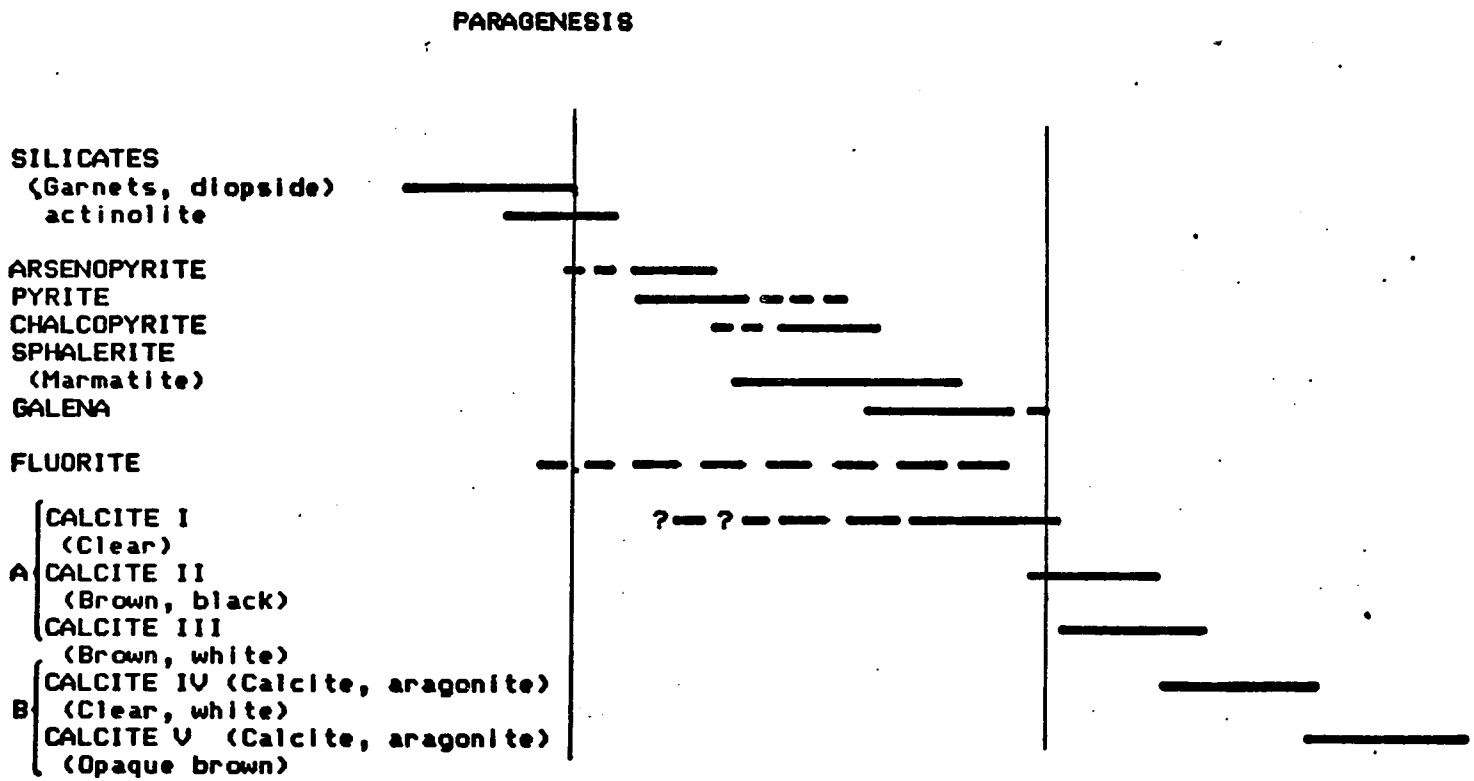

A Not all necessarily present in an area.
These calcites are referred as to ore related calcites

B Referred to as late calcites.
Cut calcites I-III or fill breccia. The white calcite may be late part of the calcite IV.

Figure 7. Preliminary paragenetic sequence and succession of calcites at La Encantada mining district

stage indicate a temperature of formation of 360°-370°C (Kesler, cited by Luján, 1975).

2. Stage II. Black-brown calcite and brown-zoned calcite. These calcites are abundant in veinlets at surface and also filling vugs in breccia in the La Prieta mine. The brown-black color is produced by the iron and manganese content that exists in the calcite or replacing it (Fig. 9). Iron oxides range from less than 1 to greater than 50 percent. Samples almost totally replaced by iron and manganese oxides are included in this stage as long as calcite structures and crystal faces are recognized.
3. Stage III. White, brownish, and white with black-brown calcite. Calcite III is undistinguishable from calcite II when the two are not in contact with it. This calcite stage is also very abundant at the surface in veinlets and breccia and can be easily recognized adjacent to brown calcite II and also when located between this (calcite II) and clear calcite IV. Clear calcites within this stage are undistinguishable from other stages of clear calcite in the absence of crosscutting relationships between them.
4. Stage IV. Includes three substages of calcite, all of them with clear crosscutting relationships with earlier calcite stages. They are found in veinlets, filling breccia, or massive. Calcite substage IVa is a milky-white calcite common in veinlets and may overlap with or be part of late calcite III or may turn brownish and become undistinguishable from white-brownish calcite II. Substage IVb is a clear calcite and clear-yellowish

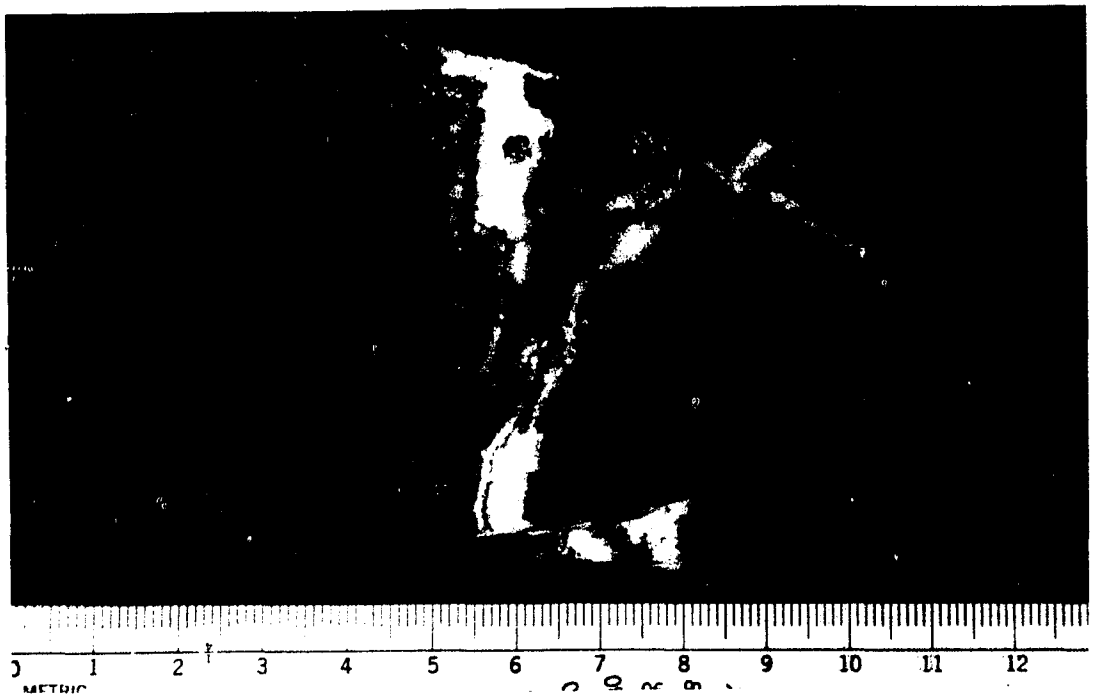

Figure 8. Clear calcite I

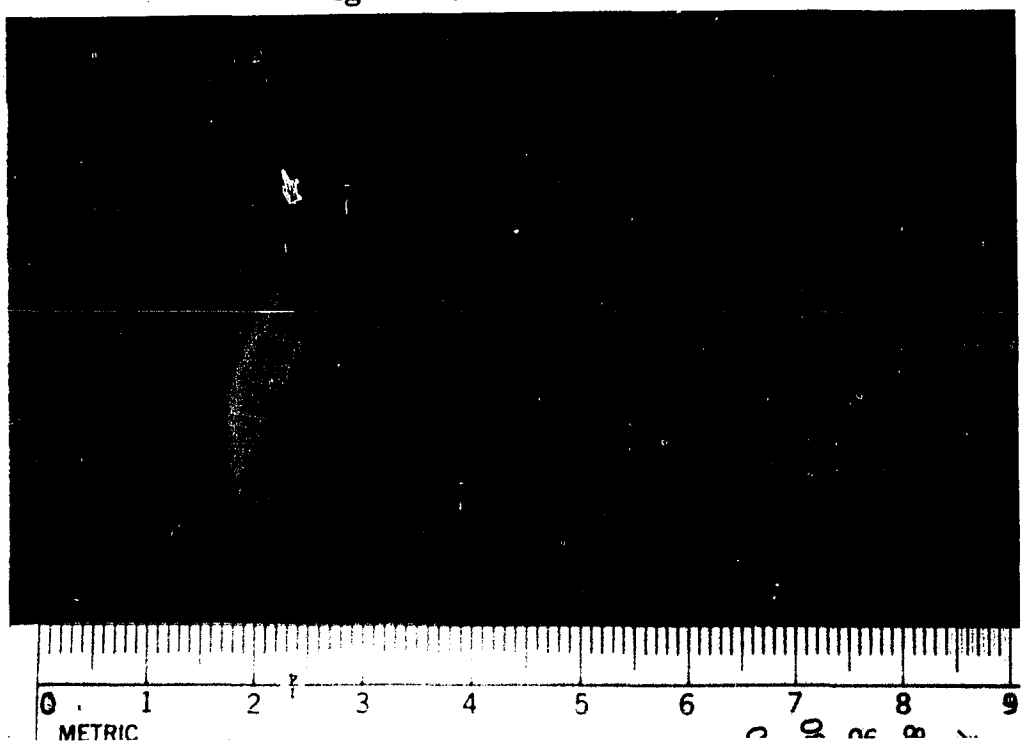

Figure 9. Black and brown calcite II

calcite-aragonite found as a late stage in many veins district-wide but is particularly abundant at La Escalera and outside known mineralized areas. Further isotopic analysis distinguished the calcite IVc from this stage, justifying a calcite V.

5. Stage V. Massive, light-brown, opaque calcite with local aragonite.

Calcite Stockworks as a Surface Expression of Orebodies

"Calcite stockwork" is a general term used to describe an irregular network of calcite veinlets, stringers, or long veinlets. These stockworks commonly contain Fe-Mn oxides with other trace elements if found in mineralized zones such as La Encantada. Similar stockworks exist in barren carbonate terranes. It is therefore significant in exploration to determine how these stockworks relate to mineralization. At La Encantada, calcites overlap at least partially with mineralization stages, and ore-associated calcites have a wide spectrum of trace-element content not found in common calcites in barren terranes (Table A-1, Appendix A; Fig. 3).

The stockworks are composed mainly of brown and black, thin, calcite veins (1 mm to a few cm thick) with or without a diffusion halo of oxidized elements that extends up to tens of centimeters wide into the host limestone (Fig. 9) and containing manganese and iron oxides and variable trace-element content, mainly Ag, As, Pb, Zn, and Cu. The stockwork outcrops range in extension from a few to hundred of meters (500 × 150 m at La Escalera). These calcite veinlets may exist as a long belt of short discontinuous parallel veinlets that run for

kilometers; Individually, the veinlets range in length from tens of centimeters up to tens of meters. The length of the belt of veinlets at La Encantada has been recognized for a distance of 3 km. For comparison, in larger districts such as Mapimí in Durango, the trends of stockworks or veinlets extend for more than 10 km. High fracture density and calcite filling are centered above the skarn dome and above orebodies; calcites of the second stage are in the center of the area shown in Figure 2 (La Prieta) and grade outward toward white calcites until they disappear. Calcite veinlets at La Escalera are pervading the limestones forming a breccialike structure but unlike the La Prieta chimney, textures in this breccia do not show evidence of collapse. Oxides content in La Escalera calcites is relatively less than that of La Prieta; in contrast, calcite often extensively pervades the limestone and in the process formed blocks of massive calcite that may exceed tens of meters in length (Fig. 6).

Fluorescence in Calcites and Limestone

Many calcites and limestones at La Encantada show red fluorescence under short- and long-wave ultraviolet (UV) radiation. This fluorescence appears to form a halo around the ore zone. To investigate the extension of this halo and its possible causes, observations were made on approximately 150 calcite and limestone samples from surface and underground, in addition to field observations.

The precise cause of fluorescence halos is still unknown; however, my interpretation based on field observations and assay data is that fluorescence is related to recrystallization in limestones and a

"moderate" manganese and iron content in calcites. Additional causes of fluorescence may be the presence of willemite and fluorite, but these minerals are not as widespread as the fluorescent halo and have typically green and blue fluorescence, respectively.

Calcite veinlets show fluorescence perhaps due to Mn in the lattice. Fluorescence has been linked with lattice disturbances, which are a result of foreign ions in the mineral's structure, which function as activators. In calcite, the activating ion is Mn (Mason and Berry, 1968). Fe-Mn-replaced opaque calcite, however, does not fluoresce. In limestone, the fluorescence may be related to decarbonation and the introduction of Mn and Mg. At the La Prieta and San Javier areas, most of the calcites and recrystallized limestone show intense red to pink fluorescence under short- and long-wave UV light. These calcites and limestones have higher than average manganese and magnesium contents (0.7% Mn, 0.9% Mg, 0.01% Fe) or are recrystallized. This recrystallization halo and manganese background decrease away from ore mineralization and is linked with a decrease in fluorescence, that is, fluorescence appears to extend as far as the recrystallization halo and perhaps was developed where Mn background values are above 0.2% (Tables A-1 and A-2, Appendix A). For example, average Mn concentration in calcites at the La Escalera area are below 0.2%, and coincidently, fewer samples show fluorescence than in the La Prieta area.

At a local scale, fluorescence is no more useful in exploration than other methods such as determining oxidized outcrops, recrystallization, or marbleization. But on a regional scale, this property may indicate a promising exploration tool for remote-sensing techniques.

According to this idea, fluorescent areas in carbonates may indicate recrystallization halos that may be associated with intrusive-centered systems and carbonate-hosted deposits.

This regional approach is limited by the randomness of Mn substitution into calcite lattices. Although this substitution commonly takes place in association with ore deposits, it is also present in barren terranes. Therefore, the presence of manganese oxides alone does not prove the existence of ore mineralization.

CHAPTER 3

FRACTURE DENSITY ANALYSIS

The importance of the structural control of a variety of mineral deposits has been stressed extensively in the literature (Conolly, 1936; Bateman, 1985; Titley et al., 1986) emphasizing that fracture patterns frequently reflect intrusive centers or mineral bodies, hence are important for exploration. At La Encantada, unpublished studies have shown that there is a strong control of the mineralization and that the most fractured zones coincide with mineralized areas. However, a quantitative measure of fracturing that relates mineralization with fracturing does not exist.

Traditionally, a "more fractured" area is subjectively delineated and then assumed prospective. Yet this method does not allow an equal comparison of areas at different elevations or locations. Accordingly, this study includes fracture-density measurements (length of fractures-sample area) in three areas at different elevations in the district, the purpose being to evaluate objectively the structural control and determine a quantifiable fracture density associated with mineralization.

Method

Fracture-density (fracture length/sample area) (Titley et al., 1986) maps were made from data located at sample locations and additional stations at the La Prieta and La Escalera areas (Figs. 10 and 11). Total fracturing was used because most fractures predate mineralization;

in addition, total fracturing represents the overall structural control that channeled mineralization. Alteration criteria cannot be used at La Encantada to distinguish stages of fracturing due to the supergene effects that have spread out oxides into postmineralization fractures.

Raw data were plotted and contoured by using linear interpolation between adjacent points. Values of fracturing are in units of ℓ^{-1} and are expressed in cm^{-1}, the result of fracture length measured in meters divided by the area (m^2), which in this example was 20 × 20 cm.

Results

This fracture analysis method provides a good picture of the actual unsmoothed fracture distribution and structural pattern of the area; the relative small variability within the data favors the use of this simple method. Factual data from the raw-data contours are:

1. Fracture density decreases upward. Fracture density of 0.725 and 0.48 cm^{-1} taken from the topographically lower La Prieta and San Javier, respectively, decreases to 0. 365 cm^{-1} at La Escalera (Table 4).

2. The shape of fracture contours at the La Prieta area shows a northwest and northeast trend that indicates the orientation of the main faults and fracture systems.

3. The overlay of the geologic map of La Prieta with the orebodies' location and fracture-density map shows that contours peak above orebodies and above the intrusive center.

There are at least three stages of fracturing in the district that account for heterogeneities in fracture density. These stages may not

TABLE 4
Fracture densities at La Prieta, San Javier, and La Escalera areas.

	Surface Elevation, m		Fracture Density, cm^{-1}	
	Range	Avg.	Range	Avg.
La Prieta	1830-1860	1850	0.412-1.11	0.73
San Javier	2070-2120	2100	0.325-0.75	0.46
La Escalera	2230-2290	2260	0.050-0.80	0.36

be present, or if they are present may not be identified over the entire district. These multiple stages of fracturing have added structural complexity to the region and thwarted the attempt to separate different fracturing stages. The investigation of the evolution of fractures is then beyond the scope of this thesis. It is clear, however, that multistage fracturing is a variable that affects differently the fracture-density measurements.

Variables that affect the fracture-density measurements are the replacement and pervasive filling of breccia zones; fracturing within breccia fragments and within the matrix; postbreccia fractures; and in some places collapse. Despite the variations caused by these variables, fracture-density measurements offer clear trends that can be an important tool in interpreting ore distribution and location.

Fracture contour maps (Figs. 10 and 11) revealed six structural anomalous areas at La Prieta and five at La Escalera. At La Prieta three densely fractured zones are above known orebodies; three

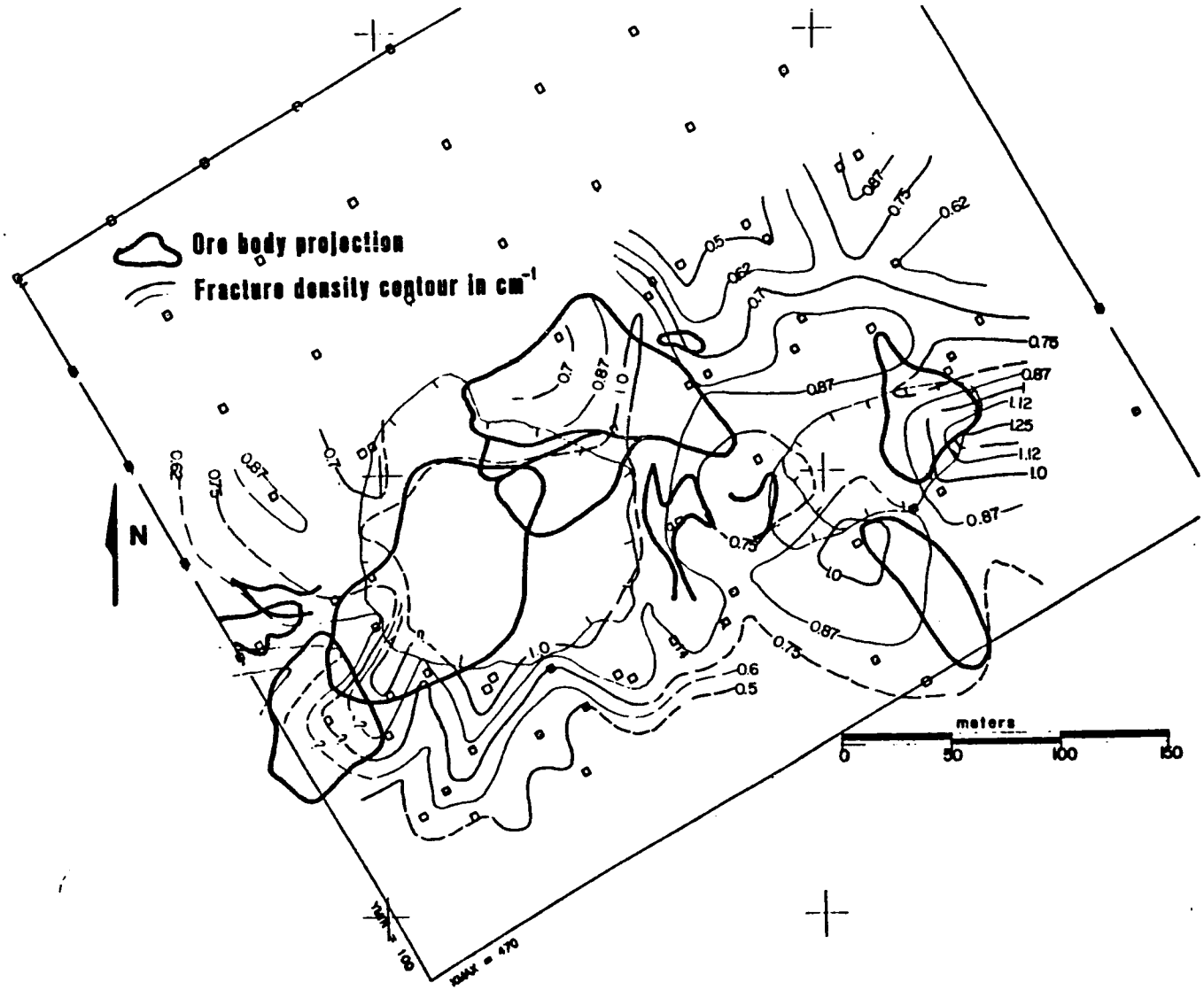

Figure 10. Fracture-density map of La Prieta area

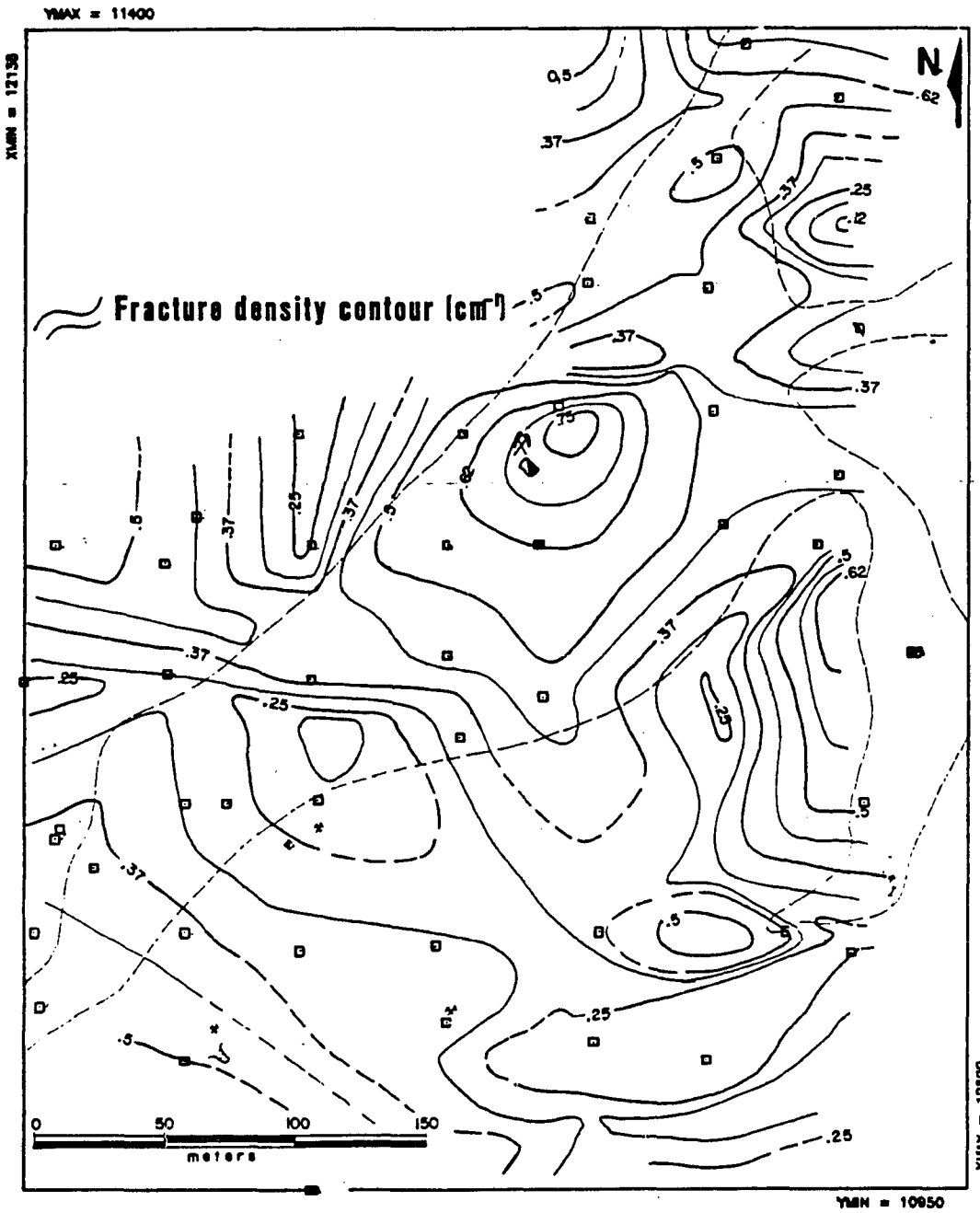

Figure 11. Fracture density map of the La Escalera area. -- Dashed line is the outline of the breccia shown in Figure 6.

additional zones of intense fracturing are unexplored. In both areas the contours exhibit clear northeast structural trends, although at La Escalera the interpretation is not as straightforward as at La Prieta. Interestingly, both areas show high fracture densities that correlate with molybdenum anomalies that, in turn, are associated with an intrusive body. These relationships suggest that the intrusion is responsible for the generation of northeast-striking ore-controlling fractures and mineralization.

CHAPTER 4

GEOCHEMISTRY OF CALCITE STOCKWORKS

The passage of hydrothermal solutions through carbonate rocks is manifested as alteration, which if measurable becomes an important ore guide. These hydrothermal solutions may cause a recrystallization, leave a trace-element halo, or develop diagnostic alteration mineral assemblages in the rocks. In addition, during recrystallization and fluid circulation, a carbon and oxygen isotope halo develops.

Among a variety of exploration methods for carbonate-hosted deposits, the use of the geochemical signature associated with these deposits appears to be a promising exploration tool. In view of the strong alteration imprint that is spatially associated with mineralization, I also conducted: (1) geochemical sampling to determine the chemical characteristics of calcite stockworks and to investigate the use of trace elements as geochemical indicator elements and (2) stable isotope analysis of calcites to define the isotopic changes associated with mineralization and to evaluate the use of carbon and oxygen isotopes in exploration.

The study of calcite stockwork geochemistry instead of traditional rock geochemistry stemmed from the fact that the host limestones in carbonate-hosted deposits do not typically have good, detectable geochemical halos. In contrast, extensive leakage halos develop far from the mineral deposits, as will be described. I used both volatile

elements such as As, Hg, and Sb to investigate if epigenetic halos are imprinted in the veinlets and elements such as Pb, Zn, Ag, Mo, Bi, and Mn associated with Pb-Zn skarns and base-metal deposits as geochemical indicator elements of orebodies in leakage anomalies. Additionally, isotopic halos are paragenetically and structurally related to ore deposits. These halos depend on the original isotopic content of the forming fluids, temperature-dependent fractionation factors, and original isotopic composition of the rocks and have the advantage that they are unaffected by metamorphism and perhaps also oxidation, thus being excellent hypogene indicators of the mineralization.

Procedures and Areas Sampled

Calcite stockworks were sampled at surface at the La Prieta and La Escalera areas for geochemical assays; surface and underground samples from La Prieta were taken for isotope analysis. At La Prieta, extensive underground workings provide the correlation with surface data which one can be used to extrapolate to unexplored, potentially mineralized areas in the district such as the La Escalera area.

Ninety-eight samples for chemical analysis were collected from surface veinlets within a rectangular grid shown in Figure 12. La Prieta includes assays for 47 additional samples provided by the La Encantada mine staff. Sampling was made at intervals of 25 and 50 m in a circular area 5 m in diameter. Calcite veinlet material was attempted at all times; however, where veinlets were too thin, some host limestone was included in the sample. No sample contains more than 35

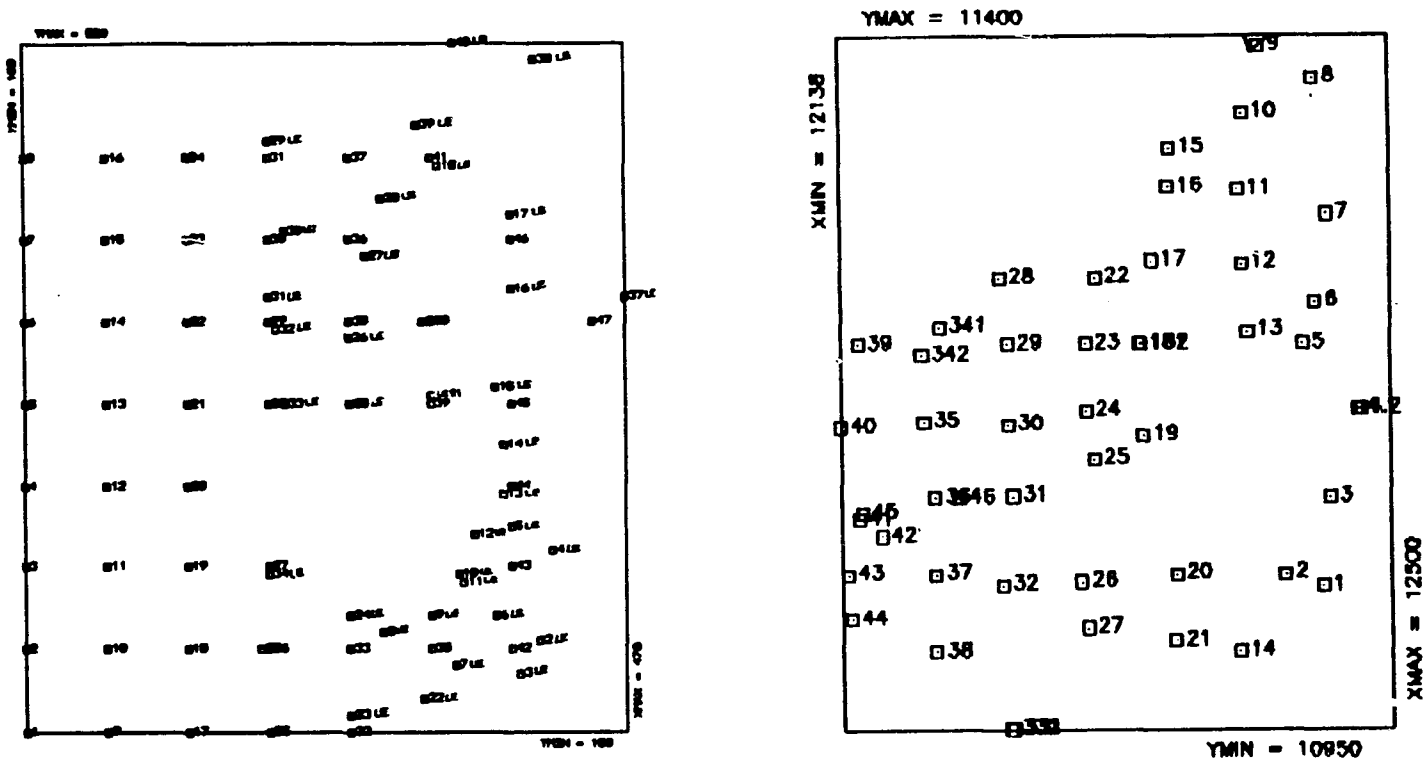

Figure 12. La Prieta and La Escalera study areas showing sample locations. -- The boundaries of the grid are outlined in the geologic, fracture, and geochemical contour maps.

percent limestone. All calcite stages were included in the sample (to evaluate the leakage halo in calcites).

Samples were analyzed by atomic absorption for Ag, Pb, Zn, As, Mn, Hg, Mo, Sb, and Bi, and SIPSA DE CV provided Cd, F, Cu, and $BaSO_4$ assays from nine calcite samples from the La Prieta area.

Calcite samples for isotope analysis were selected from two traverses across the La Prieta chimney and from a vertical section underground. Selected calcite samples were analyzed for C-O isotopes at The University of Arizona.

Data Processing and Contouring Method

The data acquired were subjected to statistical analysis and tested for different contouring methods. Analysis consisted of basic statistics with the BSTAT program developed by Y. C. Kim of the Department of Geological Engineering, University of Arizona, and contouring of values with the Plot Call program from Golden Graphics Software, Golden, Colorado, 1985 version.

The data show a good geochemical contrast between high and low values so that no other statistical analysis other than basic statistics was required for background-threshold separation. However, because the data are occasionally multimodal, different criteria for separation of background from anomalous populations were analyzed, including histograms and cumulative plots for normal (untransformed) data and data transformed to logarithm.

In general, based on the distribution type, number of populations, and significant anomalies, it was observed that background

threshold separation using 75 percent of the population (Parslow, 1974) or the break between first and second populations (Sinclair, 1974; Rose Hawkes, and Webb, 1979) usually coincide and represent the best criteria for separating anomalous populations. The 84th percentile of the log-data distribution was selected as a separating criterion in a few cases.

In regard to the plots, the values were contoured with the mentioned gridding and plot programs; raw data were also contoured. A subjectively chosen grid spacing proved to be the best among multiple possible combination of grid sizes. It was noted that the greater the grid size, the more accurate and smooth the curves produced by the plot program are.

The algorithm the program uses is weighted average inverse distance squared using all data points. This method has the advantage of reducing noise from sample variability and analytical error, thus enhancing regional trends. The disadvantage is that extreme smoothing in a highly variable dataset can obscure the location of significant anomalies.

Despite the drawbacks, anomalies obtained by the weighting algorithm closely reflect the location of the orebodies.

Elemental Geochemistry

Considering the mechanisms of epigenetic emplacement of elements and the mobility of elements, it is clear that the diffusion in limestones is not enough to provide detectable geochemical halos. In contrast to diffusion anomalies, which are limited to about 30 m, leakage

anomalies can extend for hundreds of meters (Rose et al., 1979). Geochemical anomalies can be developed as a result of hypogene or primary processes or as a result of oxidation or secondary factors. Primary anomalies provide in situ information, whereas secondary anomalies can be transported large distances depending on the environment. Hence, it is important to distinguish the processes that have taken place in the studied area for the correct interpretation of the anomalies.

Mechanisms of transport of solutions in both primary and secondary environments depend largely on permeability, porosity, and fracturing (in addition to mobility of the elements and chemistry of the solutions). This dependence emphasizes that leakage halos are major factors to consider in geochemical studies. Accordingly, the idea was to sample veinlets above orebodies and use the extended method as a geochemical technique districtwide. In the past, the search for leakage anomalies in calcite veins has been successful in the Michigan copper district (Routsala, Nordeng, and Lweege, 1969) where anomalies around the native copper deposits are not detectable in the basaltic host rocks. At La Encantada, results indicate that Pb in veinlets is enriched an average of 26 times relative to the regional background in limestones (from 40 to 500) or 800. Arsenic is enriched 800 times and Sb 950 times the average abundance of those elements in average limestone (Turekian and Wedepohl, 1961; Rose et al., 1979). Such enrichment (Fig. 13) exemplifies the potential of veinlet geochemistry as an ore guide.

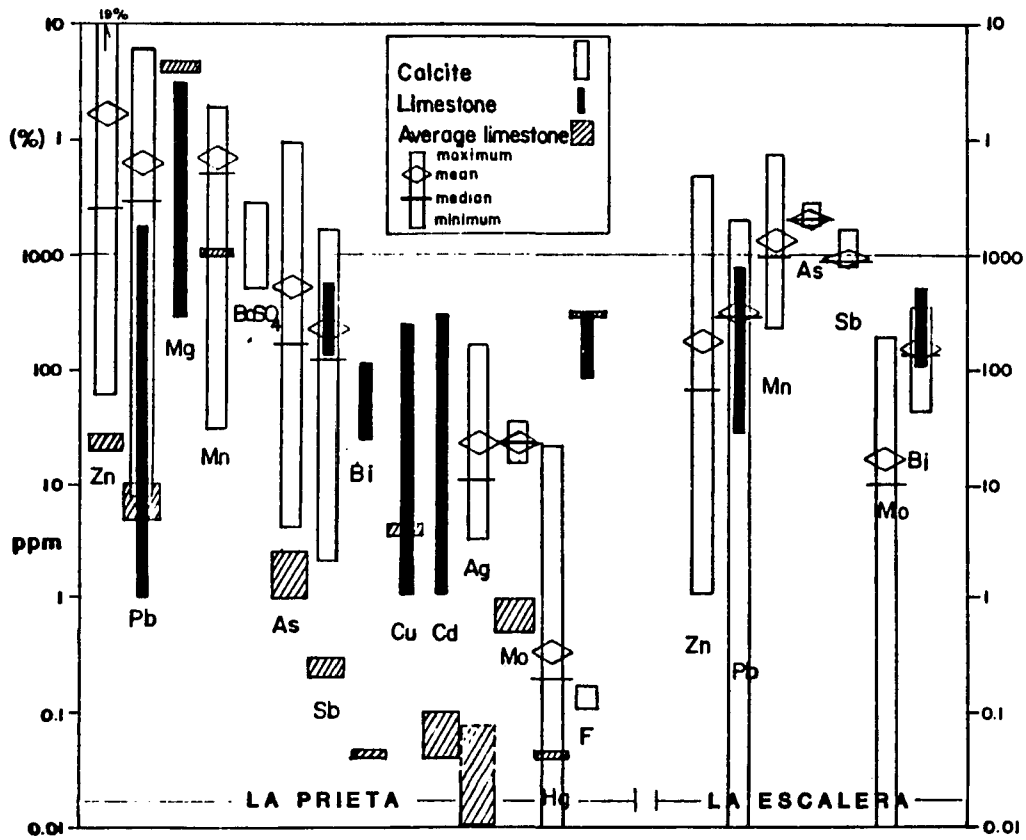

Figure 13. Concentration of elements in calcites compared to local and average limestone. -- Number of assays per area: calcite. La Prieta, 85; La Escalera, 50; limestone. La Prieta, 116; La Escalera, 142. Crustal averages from Turekian and Wedepohl (1961).

Elemental Geochemistry Results

The two areas, La Prieta and Escondida, plus a traverse connecting them, were selected to investigate the properties of the calcite stockworks and the behavior of the elements in different environments.

The most important ore-indicator elements common in all samples are Ag, Pb, and As, although Mo, Bi, Mn, Sb, and Zn are also abundant and are excellent aids in the interpretation of geochemical anomalies. Figure 13 shows the elements assayed for the La Prieta and La Escalera areas and their concentrations and contrast with limestones in the district and in the earth's crust.

Six facts useful for exploration stand out from the geochemical results: (1) the distribution of the elements, which cluster above ore bodies and primarily along structural trends; (2) the clear association of Ag, Pb, As, and Mo with orebodies and their source; (3) the potential use of Hg and Sb as geochemical indicator elements of deep orebodies; (4) the vertical zoning from Pb, Zn, and Ag at ore levels to Sb and As increasing markedly upward (400 m above the top of known orebodies); (5) the striking uniformity of Mo content through more than 500 m of vertical section and its close association in space, shape, and grade with the skarn dome and granodiorite intrusion; (6) the association of manganese (and iron oxides) with mineralized zones.

The correlation coefficient between elements was calculated for all samples with two main purposes: (1) optimization of the subsequent number of elements assayed and (2) assessment of the potential migration of elements relative to Mn. No good correlation was found to exist

among elements from the La Escalera samples, and a poor correlation exists among elements from the La Prieta samples (Table 5).

TABLE 5

Correlation matrices for the elements assayed in veinlets from the La Prieta and La Escalera areas

La Escalera Area

	Pb	Zn	Mn	Mo	Sb	As	Bi
Pb	1						
Zn	-0.003	1					
Mn	-0.087	+0.012	1				
Mo	-0.0757	+0.065	-0.016	1			
Sb	-0.0418	-0.0418	+0.352	-0.152	1		
As	+0.169	-0.105	-0.092	-0.122	-0.218	1	
Bi	-0.192	+0.305	+0.136	-0.098	+0.199	-0.221	1

La Prieta Area

	Ag	Pb	Zn	As	Hg	Mn	Mo	Sb
Ag	1							
Pb	0.47	1						
Zn	0.20	0.49	1					
As	0.089	0.62	0.57	1				
Hg	0.50	0.69	0.06	0.022	1			
Mn	0.094	0.006	0.22	0.022	0.11	1		
Mo	0.032	0.06	0.054	0.32	0.187	0.044	1	
Sb	0.50	0.79	0.280	0.22	0.717	0.207	0.084	1

The best correlations are from rock sampling at La Escalera that were calculated from rock data for Pb, Cd, Bi, Ca, and Mg provided by the La Encantada mine staff: Pb-Cd (0.424 - 18% fit) and Ca-Mg (0.59 - 35% fit). The best correlations in veinlets from La Prieta are Pb-Sb (0.79 - 63% fit), Hg-Sb (0.717 - 51% fit), Pb-Hg (0.69 - 48% fit), and Pb-As (0.62 - 39% fit). Despite the poor correlations when

the weighted data are plotted, the crude correlation of some of the elements' anomalies suggest that fewer elements can be used to obtain the same amount of information, as will be described. In regard to the migration of elements, it is possible that a decoupled migration from iron and manganese oxides existed due to the lack of correlation between the trace elements and manganese. It is assumed that the Mn is directly associated with the iron oxides, which tend to migrate with metal ions in transported anomalies.

La Prieta. Figures 14, 15, and 16 show the geochemical traverses and the composite maps of anomalies and orebodies at La Prieta. From the figures it is evident that Pb, Ag, and As are important elements. The anomalies of these elements peak above major orebodies and define a strip that encompasses all known orebodies present in this area. Additionally, these elements define three more zones, the significance of which has not yet been tested.

Figure 14 shows that Ag, Pb, and As yield prominent positive anomalies approximately above the La Prieta and La Escondida chimneys. The peaks of Ag and Pb anomalies are displaced about 30 m downslope relative to the position of the outcrops of the orebodies. The peaks of As are displaced 30 m and 60 m downslope from their corresponding La Prieta and El Socorro outcrops, respectively (Fig. 15).

In general, Ag, Pb, As, and to some extent, Zn exhibit similar behavior and distribution. They were leaked along northwest-dipping fractures and are found downslope approximately parallel to the NE. 60°-70° trend of the orebodies; their actual northeast-east-trending

Figure 15. Composite contour map of Ag, Pb, Zn, and As for La Prieta area. -- Outer shaded pattern shows values above threshold. Inner patterns show medium and high anomalies, which are set as multiples of the threshold, except for Pb set as mean plus increases by one standard deviation. Note the northeast orientation of anomalies parallel to and above orebodies.

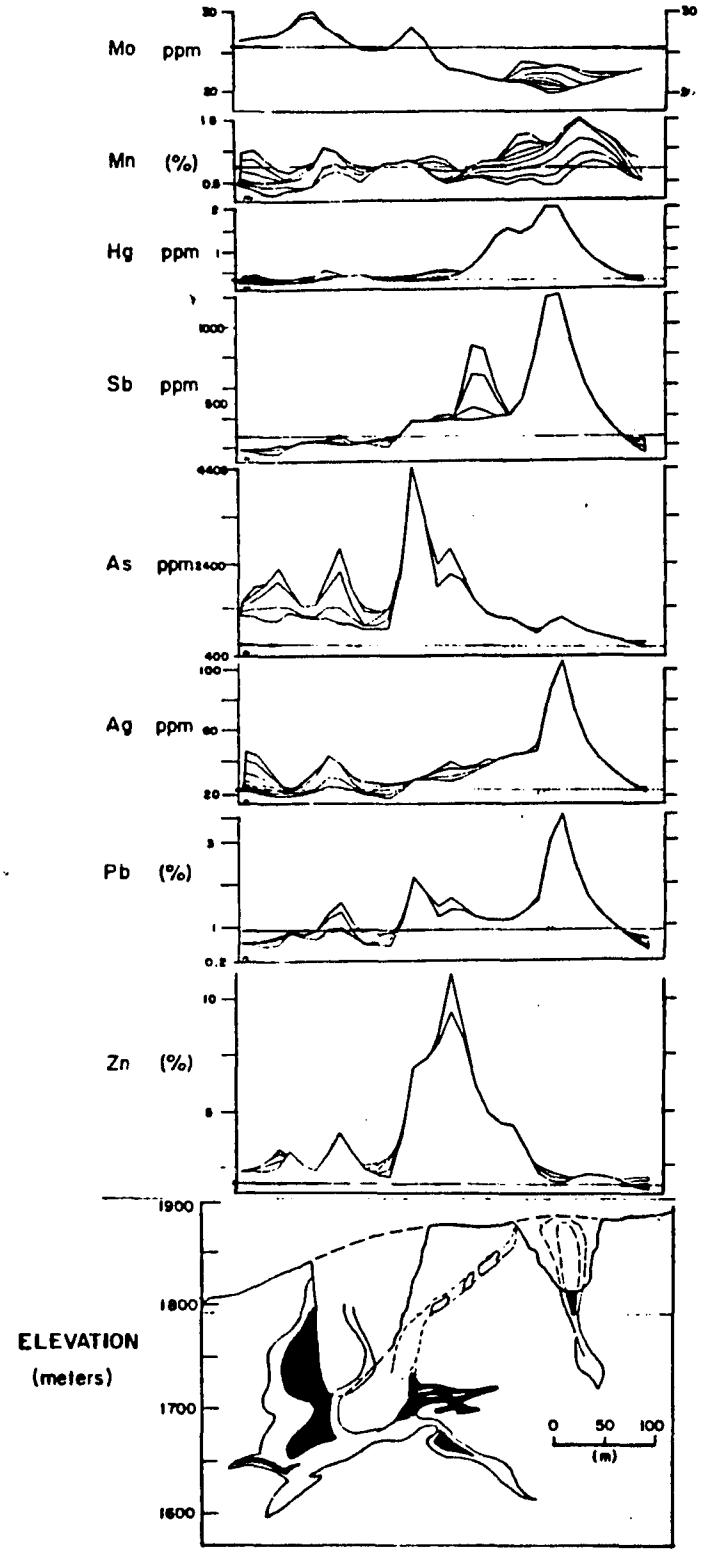

Figure 14. Concentrations of elements along eight N. 60° E. traverses from gridline 300 to 400 of the La Prieta area

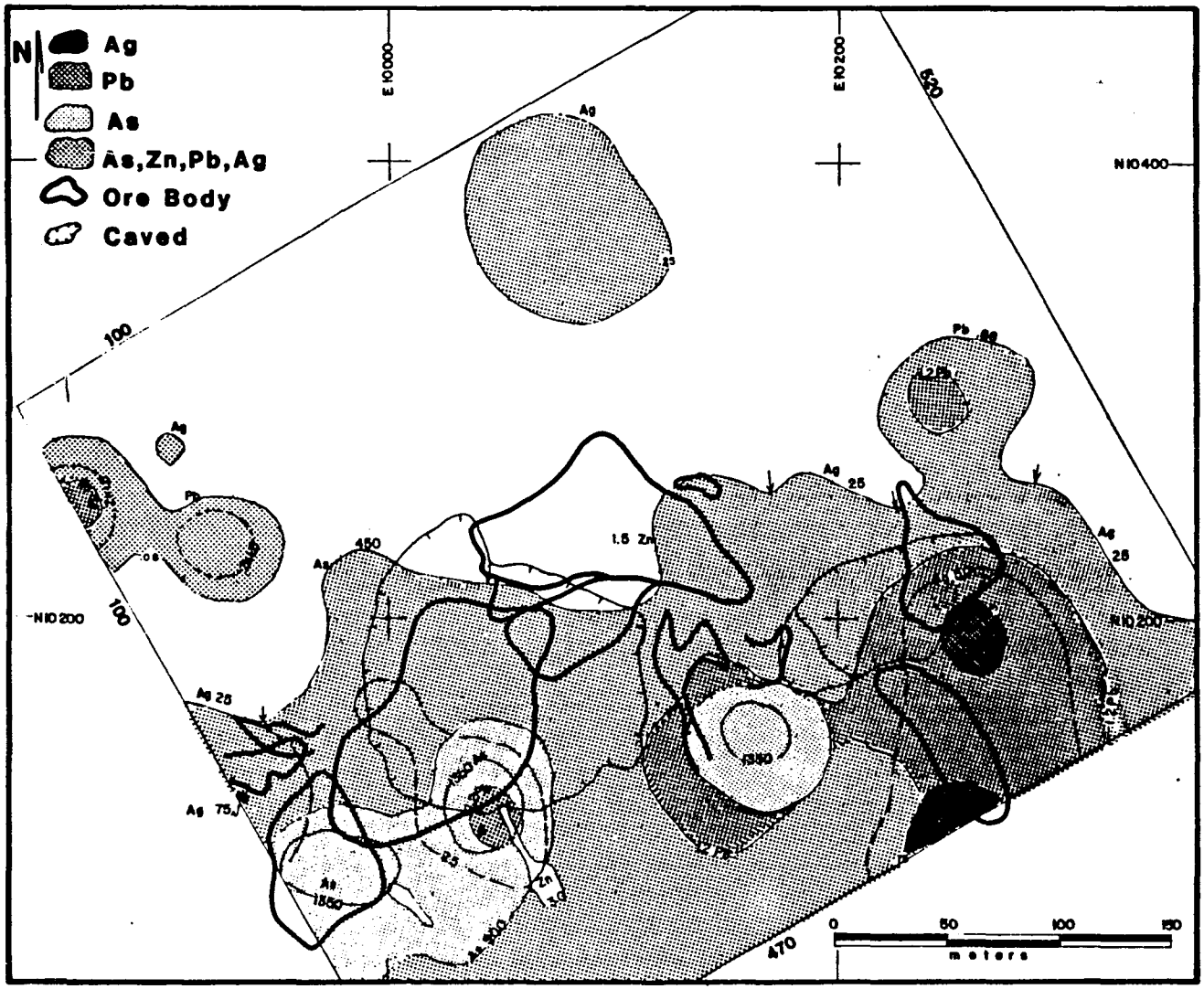

Figure 15. Composite contour map of Ag, Pb, Zn, and As for La Prieta area.

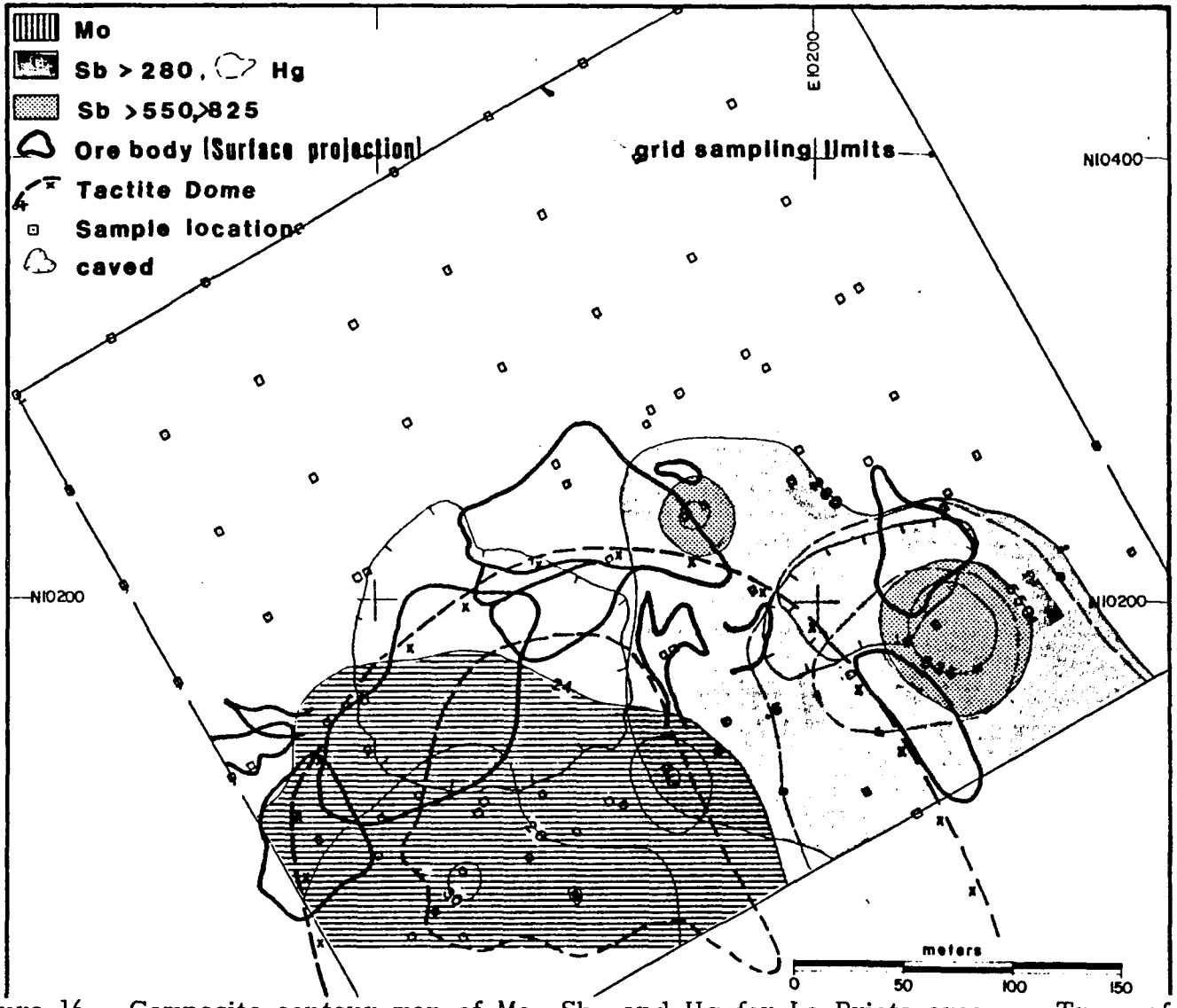

Figure 16. Composite contour map of Mo, Sb, and Hg for La Prieta area. -- Trace of skarn dome at 1600 and 1630 m of elevation is in dashed line. Average surface elevation is 1840 m.

distribution reflect strong structural control. On the other hand, Sb, Hg, and again to some extent, Zn have similar patterns. Their anomalies trend east-west-southeast forming another strip from the La Escondida chimney to the mantos zone (Fig. 16). Prominent Sb and Hg anomalies exist only above the La Escondida and Ojuelas orebodies, in addition to a Sb peak above the mantos zone (Fig. 14). The antimony is distributed along the northern portion of the strip and may be one of the best examples of an epigenetic anomaly; The Hg and Zn are in the central and southern portion of the strip, respectively, and indicate perhaps greater mobility for the Zn. Due to mobility, it is possible that As and Hg anomalies are the manifestations of deep orebodies; these elements have leaked more than 200 m and 350 m above the mantos and skarn bodies.

Molybdenum anomalies are especially important because they are centered around the skarn dome and the productive granodiorite intrusion. No similar Mo anomalies seem to exist around other nonproductive intrusions. Peripheral to the Mo anomalies are both the orebodies and the ore-metals and trace-elements anomalies. Maps of these are in Appendix B.

La Escalera. Geochemical sampling at La Escalera was made to test the effectiveness of veinlet geochemistry in this area where no underground data are available. The interpretation of the results is based on the experience from La Prieta, approximately 2.3 km to the southwest. Elements analyzed at La Escalera were Ag, Pb, Zn, Mn, Sb, Mo, and Bi.

Nearly the whole breccia at La Escalera (Fig. 6) is anomalous in Pb, Zn, As, Mo, Bi, Mn, and Sb, whereas north-south-trending structures and veinlets in fractured or fresh limestone are low in these elements (Fig. 17). A vertical zoning is also apparent; Pb and Zn are higher at La Prieta (1850 m of elevation) and As is low, whereas at La Escalera (2250 m) Pb and Zn are lower than at La Prieta, but the As is remarkably high (>2200 ppm). Because the top of known economic mineralization in chimneys ranges from approximately 1790 to 1900 m, it is evident that these anomalies may indicate deep mineralization at La Escalera.

By overlaying the composite map of geochemical anomalies (Fig. 17) on the geologic map of the area (Fig. 6), the geologic-structural control of the anomalies becomes apparent. Although the metal distribution is complex, a north-south and northeast-southwest orientation of the anomalies is clear. Note that there is a distribution from northeast to southwest of the Pb, As, Mo, Zn, Bi, and Sb anomalies; Sb, Mn, and Bi are also in the westerm portion of Figure 17 but have a north-south orientation. These anomalies are parallel to and also within the northeast- and northwest-striking fracture systems, respectively. It is worth noting that the Mo concentrations are remarkably high (20-40 ppm) relative to the average concentration in normal limestone (Fig. 13). Threshold Mo concentrations in calcites are identical to those recorded for the deep granodiorite body of La Prieta.

Geochemical anomalies at La Escalera do not follow a regular geochemical pattern: Bi (high-temperature element) coincides with As and Zn distributions (lower temperature). No logical zoning can be

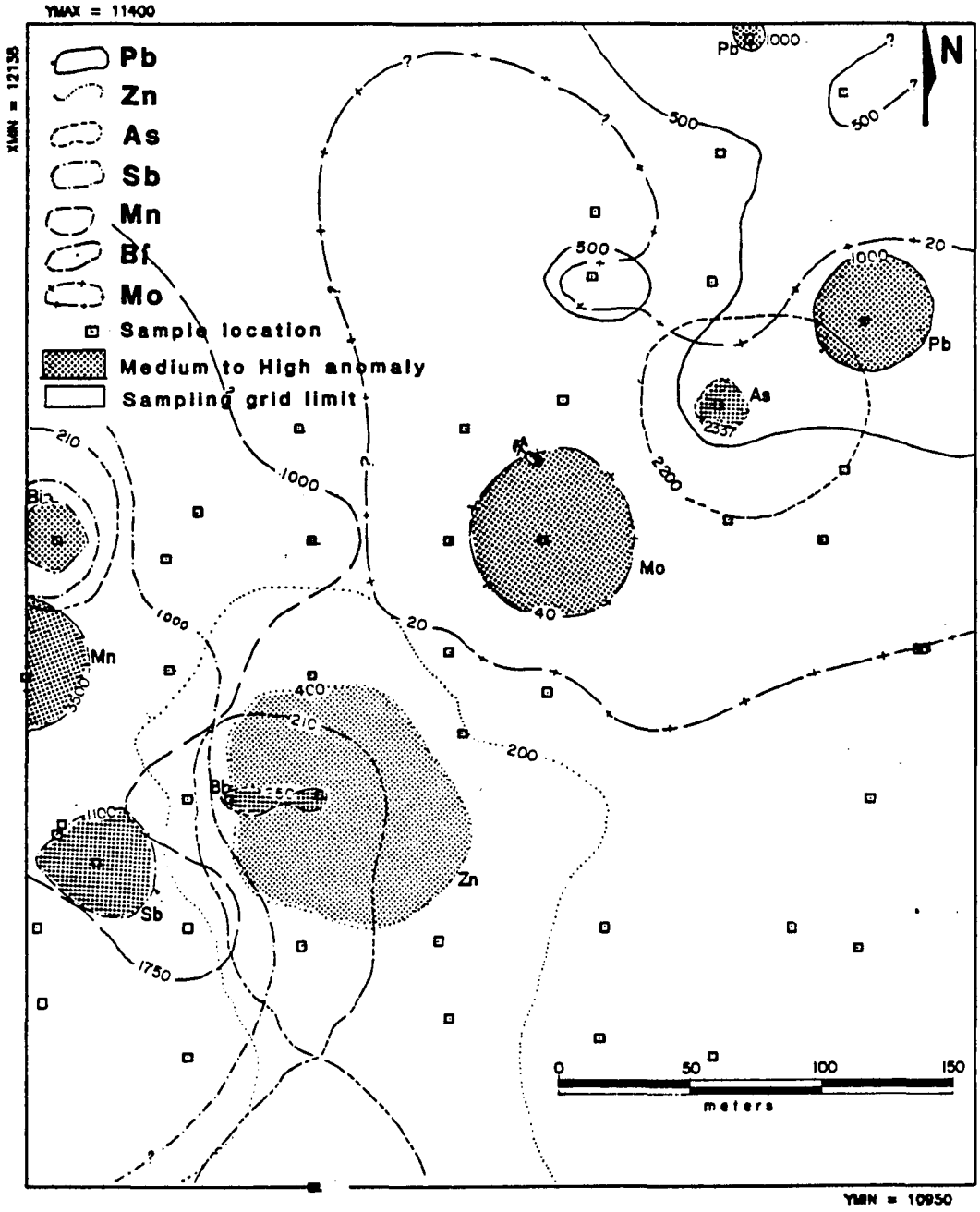

Figure 17. Composite geochemical contour map of La Escalera area. -- First contour is threshold value; successive contours are multiple of mean plus one standard deviation. Both Sb contours are threshold values set with normal and log data.

defined. Arsenic, a highly volatile element, is very homogeneous over the entire area and only one anomaly exists, which is located northeast of the Mo anomaly. A Pb anomaly is found in the opposite extreme away from elements with which it is usually associated such as Zn. These complexities can be explained as independent stages of mineralization; however, this is speculative.

Although there is an excellent contrast between background and anomalies, it is noticeable that a closely spaced grid is required because many anomalies are defined by few samples.

In summary, geochemistry results at La Escalera are complex but indicate excellent trends. As at Prieta, the most important fact is that metal anomalies clearly define the ore-controlling structures and also discriminate barren from ore-bearing structures.

Metal Ratios. In view of the irregular geochemical distribution of elements at La Escalera and despite the homogeneity of the geology, it is difficult to define a reasonable zoning from a single heat source. Accordingly, several metal ratios were tested to provide insight into the definition of regular geochemical trends.

If the anomalies at La Escalera are assumed to be primary, i.e., they do not represent significant postemplacement transport, they may reflect the original behavior of elements. If that assumption is correct, metal ratios should provide trends according to their chemical behavior. Hence, the ratios of metals widely separated in the zoning sequence are useful in identifying zoning and trends. Vertical zoning in Pb-Zn deposits in skarn is Sb, Cu, As, Ba, Ag, Pb, Zn, Cu and lateral

zoning is Ba, Zn, Pb, As, Ag, Cu, Sb (from top to bottom and in decreasing order of width of its halo, respectively) (Ovchinnokov and Grigorian, 1971). The Pb-Bi and As-Zn ratios proved to be useful in the interpretation of anomalies. The Pb-Sb and Pb-As ratios of averaged data from the N. 60° E. traverse from La Prieta to La Escalera shows a relationship between these ratios and elevation. This relationship may also be a function of the depth of the orebodies.

Lead/bismuth contours are remarkably regular, with values increasing gradually toward the southeast and northeast of the area (Fig. 18). Because Pb and Bi are lower and higher temperature elements, respectively, in a normal zoning sequence, the Pb-Bi ratio indicates a temperature gradient: a decrease in the ratio indicates higher temperature and an increase lower temperature. If this observation is correct, the Pb/Bi contours indicate that the direction of flow was from southwest toward northeast and therefore the lower temperatures were in the three eastern arms of the breccia (Fig. 18). This interpretation is consistent with a potential zone in the western portion of the breccia where the rest of the anomalies are clustered.

Lead-antimony and lead-arsenic ratios vary as a function of elevation and perhaps also with distance from orebodies. These ratios tend to decrease with increasing elevation from above ore levels and outward and decrease with a decrease in elevation from ore levels and below. Figure 19 shows the plot of the ratios of the averaged Pb, As, and Sb values for the areas indicated. These areas increase in elevation and also have variable distances to orebodies. According with existent traverse sections, the distance to the orebodies also increase

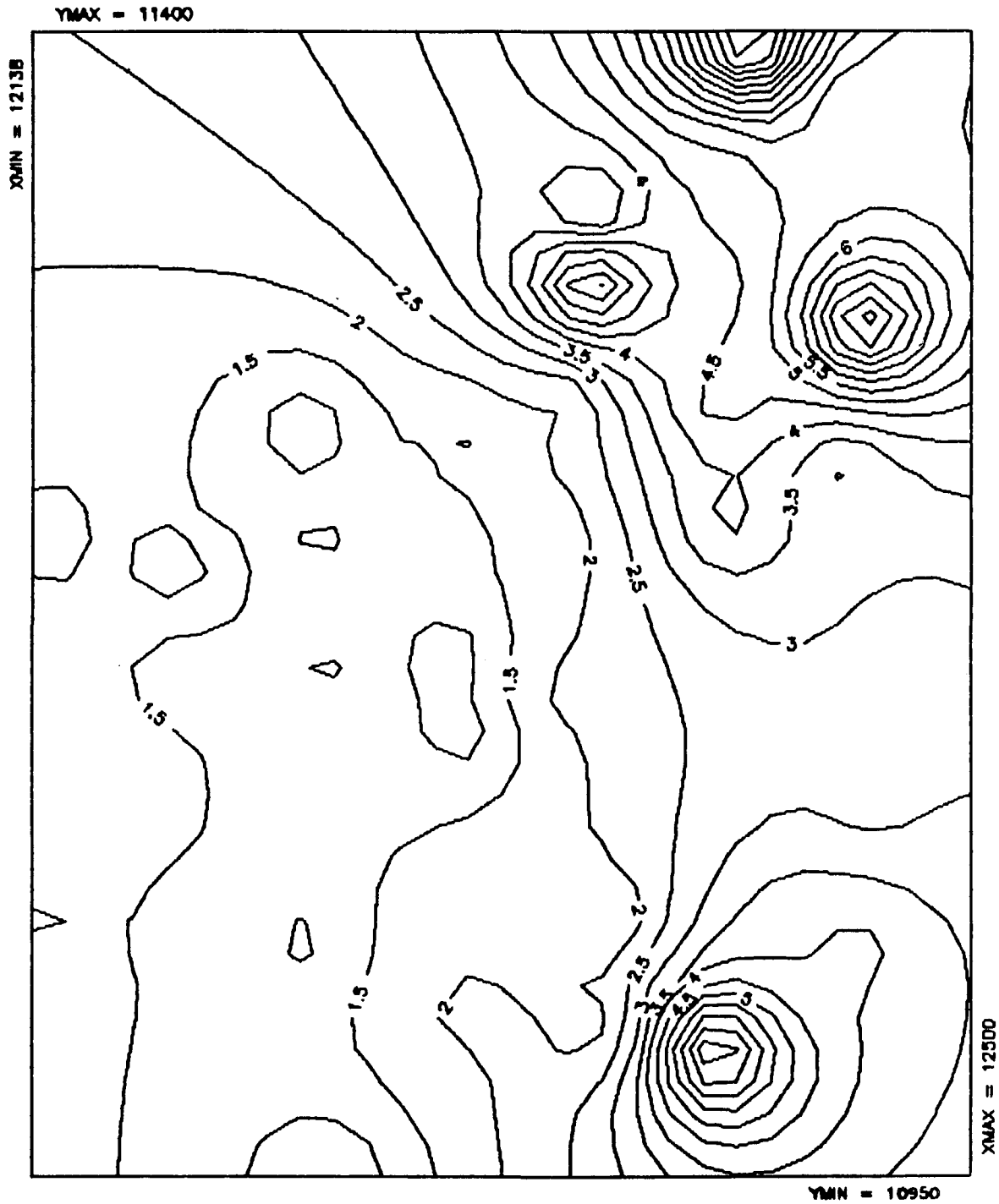

Figure 18. Lead/bismuth contours for La Escalera area

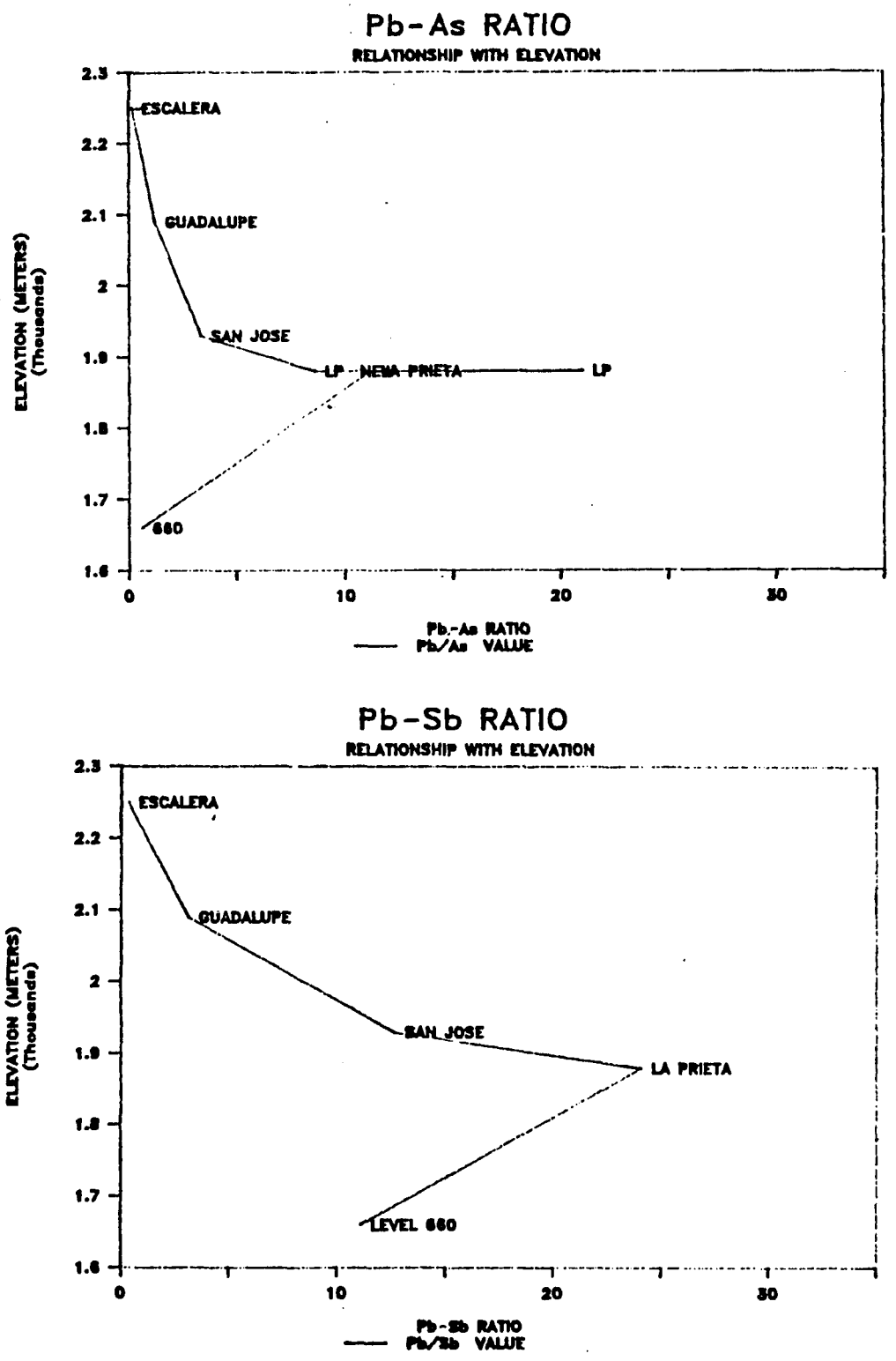

Figure 19. Lead-arsenic and lead-antimony ratios showing their relationship with elevation at La Encantada

varying from outcrops at La Prieta to shallow mantos in San José and Guadalupe. These values can provide an estimation of the depth of the mineralization and indicate the position within the mineralized system and the direction toward orebodies.

Stable Isotope Geochemistry

Many contact metamorphic aureoles and alteration halos around ore deposits vary systematically and show a decrease of carbon-13 and oxygen-18 toward the intrusive center or toward the orebodies (Engel, Clayton, and Epstein, 1958; Deines and Gold, 1969; Hall and Friedman, 1969; Pickney and Rye, 1972; Valley, 1986).

Isotope halos around ore deposits are useful exploration guides for hydrothermal mineral deposits. Green et al. (1983) pointed out that in contrast to elemental halos (e,g., Na, K, Mg, Zn) an isotope halo may extend to much larger areas, is less variable on small scale, and may persist through regional metamorphism, although Fleck and Criss (1985) and Munskgaard and Zeck (1984) showed systematic decreases in ^{18}O with increasing grade of regional metamorphism. Engel et al. (1958) reached conclusions similar to those of Green et al. (1983) in their study carried out in the Gilman mine area and noted that Cu, Pb, Zn, Mn, Sr, Ti, Al, and other elements indicate no systematic trends relative to ore, whereas the ^{18}O values of the hydrothermal dolomites decrease systematically toward ore zones.

The study by Engel et al. (1958) was the first comprehensive study of oxygen and carbon isotopes, and at the time of publication of their data the potential use of oxygen and carbon isotopes in mineral

exploration became apparent. Subsequent studies of ore deposits, however, did not confirm this (Fritz, 1969). It is evident then that a good geologic background is needed to interpret and understand the significance of this and any other method of exploration.

Literature review showed that not all of the low ^{18}O halos are associated with ore mineralization. Valley (1986) presented a compilation of studies of metamorphic aureoles that exhibit coupled O-C depletions relative to the unmetamorphosed rocks. His compilation shows that isotopic O-C trends are characteristic of contact metamorphism aureoles.

Table 6 shows a brief compilation of data of C-O isotope halos around ore deposits and data of similar C-O depletions caused by other processes. From Table 6 it is apparent that, although there is a clear contrast between isotopic values reached due to mineralization-associated processes in this context (hydrothermal alteration and mineralization per se) and non-ore-generating processes, there exists an interval within which C-O isotope values do not indicate whether these values are a result of hydrothermal processes and metamorphism or a product of diagenesis. By mineralization processes in this context, I mean magmatic-meteoric hydrothermal processes thought to be responsible for the mineralization at carbonate-hosted deposits such as La Encantada.

Note that the C-O isotopic composition of syntectonic calcites, produced, for example, by dissolution due to increased overburden pressure, a result of tectonic emplacement of overlying rocks, is very close to that of its matrix (i.e., host rock). The reason is that increased pressure solution tends to establish equilibrium at the same temperature

TABLE 6

Isotope data from hydrothermal alteration halos and from nonore-related samples in carbonate rocks

	$\delta^{18}O^{o}/oo$ (SMOW)	$\delta^{13}C^{o}/oo$ (PDB)	Reference[a]
Nonore-related Samples			
Calcite in syntectonic veins (nappes of Switzerland)			
Oxfordian	25.7 to 27.3	2.18 to 2.69	
Kimmeridgian	24.9 to 26.4	0.98 to 2.04	1
Portlandian	25.5 to 27.1	0.55 to 1.85	
Marine inorganic limestones	22 to 35	-7	2
		-3 to 3	3
Unaltered Leadville Limestone	21 to 25.2	-3.9 to +0.8	4
Unaltered limestone (St. Eulalia)	21.8 to 22	-0.7 to -0.9	5
Fine-grained dolomite (Leadville)	20.1 to 28.6	-4.5 to 2.0	4
Early jasperoid (Leadville)	-5 to -18[b]		
Late Golden barite	-18[b]		
Ore-related Samples			
Phylically altered porphyries	4.5 to 7.5[b]		4
Metal-rich quartz veins above ore	+3.4 to 11.3[b]		4
Leadville ore-related dolomite	13.4 to 22.7	-5.3 to -0.5	4
Mt. Sherman dolomite	9.3 to 10.8	-3.4 to +2	
Gilman dolomite	16.4 to 23.6	-4.9 to +1	4
Calcite I, Providencia	11.2 to 13.0	-8.2 to -6.2	6
Pearly calcite	13.9 to 18.5	-6.2 to -3.3	6
Calcite II	17.5?	-8.1? to +0.7	6
Calcite III	18.2 to 19.4	-7.2 to -1.0	6
Marble (Leadville)	15.9 to 22.8	-4 to -1.5	4
Calcite veinlets (Leadville)	6.9 to 22.7	-4.6 to 0.7	4
Calcite in ore (St. Eulalia)	12.7 to 15.42	-1.6 to -10.1	5

TABLE 6
Isotope data--Continued

	$\delta^{18}O^{o}/oo$ (SMOW)	$\delta^{13}C^{o}oo\%$ (PDB)	Reference[a]
Manganese limestone (St. Eulalia)	16.25 to 21.66	-3.9 to -0.2	5
Ore limestone (0 to 50 m) skarn contact	13.49 to 18.53	2.3 to 2.7	5
Limestone (0 to 230 m from one contact)	14.27 to 24.26	1.2 to 3.04	5
La Encantada			
Calcite from manto near contact with ore)	17.10 to 17.98	-3.17 to -2.91	
Calcite from surface (associated with mineralization)	18.96 to 22.15	-3.3 to -6.48	
Late calcite (surface)	22.6 to 24.75	-7.05 to -8.69	
Altered limestone (surface) (with 10% calcite)	24.75	-5.45	

a. Key to references:
1. Dietrich, McKenzie, and Song (1983)
2. Fritz (1979)
3. Rye and Ohmoto (1974)
4. Beaty (1985)
5. Megaw (1986)
6. Rye (1966)

b. Values for fluids in equilibrium with the minerals referred.

between matrix and dissolved carbonates. Precipitation in disequilibrium would still lead to small isotopic differences that are unlikely to overlap with values similar to those produced by the interaction of magmatic or meteoric waters with limestones. On the other hand, note that, although there exists a clear interval of $\delta^{18}O$ values originated by magmatic-hydrothermal alteration between 7 and 23 per mil ($^{o}/oo$), the upper range of these values ($20^{o}/oo$-$23^{o}/oo$) overlap with those that correspond to unaltered limestone or dolomite at Leadville.

This overlap unables one to distinguish with C-O data the significance of ^{18}O isotopic halos at ranges that are feasible to reach with magmatic-hydrothermal alteration (such as 20 per mil SMOW) but that are also common as a result of diagenesis and common in dolomites. These facts restrict the use of ^{18}O isotopes in exploration, as will be discussed later, because only large depletions can be considered with certainty as being associated with mineralization processes.

Stable Isotope Results

Twelve samples for isotope studies were selected from the underground and surface from the La Prieta area. The samples depict two plan sections and a vertical section along the La Prieta chimney and were taken from calcite veinlets and stockworks. One sample of the host limestone was included for comparison with the calcites and to investigate possible extension of the isotopic halo into the rock.

Calcite samples were separated by breaking the calcite samples and then grinding them in a silica plate. Carbon and oxygen isotope analyses were made at the Laboratory of Isotope Geochemistry,

University of Arizona. The results have a repeatability within +0.25% and are reported in the PDB and SMOW standard notation for carbon and oxygen, respectively, where:

$$\delta^{o}/oo = \frac{(R \text{ sample})}{(R \text{ standard})} - 1 \times 10^{3}$$

where $R = {}^{13}C/{}^{12}C$ or ${}^{18}O/{}^{16}O$. The results are reported in Table 7 and displayed in Figure 20.

It is worth noting that no attempt was made to characterize isotopic variation from a single orebody or to establish detailed variations within calcite stages. Rather, the main purpose was to investigate the variation or trends of isotope values away from ore mineralization. In this sense, distance measured from any orebody and general trends can be defined and used for exploration purposes, although I recognize that there may exist a local variation within single orebodies.

Carbon and Oxygen Isotopic Variations in Calcites. The results of 13 carbon and oxygen isotope analyses of the five stages of calcites, including one sample of host limestone from La Prieta, show two noticeable variations: (1) variation within individual calcite stages and (2) variation in successive calcites. Both appear to vary also as a function of distance from orebodies. The total variation in calcite ranges in $\delta^{18}O$ from 17.98 to 24.44°/oo and in $\delta^{13}C$ from -2.91 to -8.7°/oo. Altered host limestone has a value of $\delta^{18}O$ of 24.75°/oo and $\delta^{13}C$ of -5.45°/oo. Table 7 shows the C-O isotope results of analyzed samples

TABLE 7

Carbon and oxygen isotope data in calcites and limestones from La Prieta area

Level	Sample Number	Calcite Type	Description	$\delta^{18}O$	$\delta^{13}C$
670	670-1	1	clear calcite from skarn, La Prieta halo	22.8	-7.36
635	635-2	2	white and clear calcite	17.10	-2.91
	695-2	2	white- and brown-zoned calcite	17.98	-3.17
Surface	LE-8	2-3	brown (2) and white (3) 50 m above orebody	18.96	-4.24
Surface	LE-36	2	black, brown calcites, NO_x 30 m from orebody	19.53	-3.33
Surface	LE-6		White calcite with FeO_x 52 m from orebody	20.06	-4.86
Surface	LE-3	2-3	brown (2) and white (3) calcites 70 m from orebody	21.30	-4.63
Surface	LE-40	4	late clear calcites (aragonite yellowish)	22.66	-7.33
	LE-15-1	4	clear late calcites (aragonite yellowish and clear translucent	23.44	-8.69
	LE-34	5	beige late calcite and clear brownish aragonite	24.44	-7.05
Surface	LE-10		altered limestone with brown calcite #2 (20% rock)	22.15	-6.48
	LE-9		altered limestone with FeO_x	24.75	-5.45

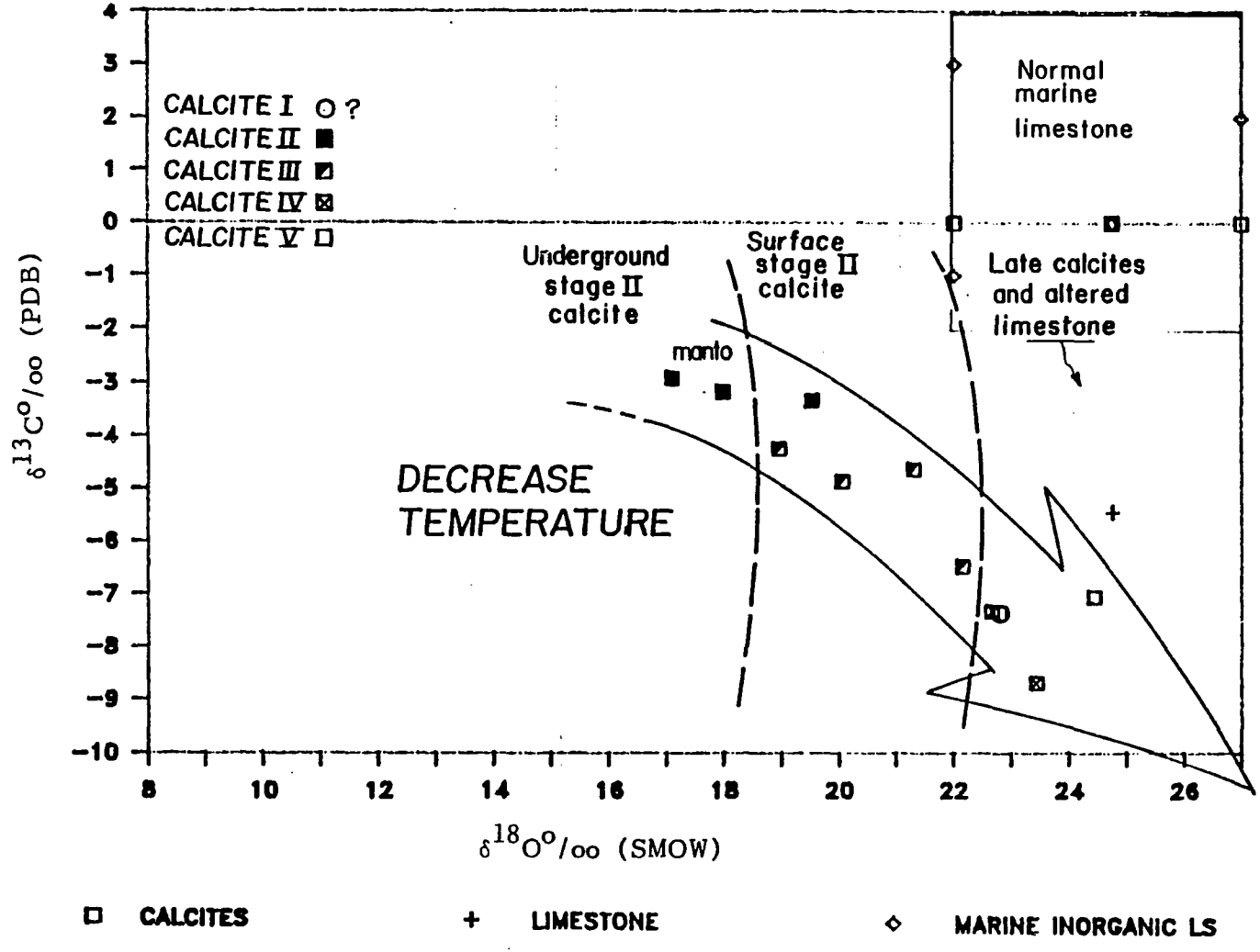

Figure 20. Carbon and oxygen isotope compositions of calcites and limestones at La Encantada

from the La Prieta area; these values indicate calcite stage and distance from orebodies when these calcites are ore associated.

Variation within single calcite stages is poorly supported due to the limited number of samples from individual stages. However, in calcites stage II, the manto calcites (from underground, near the contact with manto orebodies) show an increase in $\delta^{18}O$ values from depth upwards. The exposure of manto mineralization is in the 635 level (Sample 635-2) and has a value of $17.10^{o}/oo$. This value increases to $17.98^{o}/oo$ in the 695 level (60 m above) in a calcite of the same stage. Calcite II at surface increases to a $\delta^{18}O$ value of $19.53^{o}/oo$. The $\delta^{13}C$ values in calcite II show, accordingly, an increase with increasing depth; $\delta^{13}C$ decreases as distance from the orebody increases. Calcite II at surface has a $\delta^{13}C$ carbon composition of $-3.33^{o}/oo$ and the underground manto samples 695-2 and 635-2 have $\delta^{13}C$ values of $-3.17^{o}/oo$ and $-2.9^{o}/oo$, respectively (Fig. 20).

Similar C-O variations in calcite III apparently exist (Table 7), but the three samples available are not enough to support this presumed trend. Late-stage calcites IV and V appear to be unrelated to mineralization and show no regular variation with distance from orebodies. In general, with successive stages of calcites, $\delta^{18}O$ values approach those of the host limestone.

Carbon and Oxygen Isotopic Trends for Successive Calcites. Figure 20 shows a distinctive trend of $\delta^{13}C$ and $\delta^{18}O$ values that indicates a progressive increase in $\delta^{18}O$ composition and a decrease in $\delta^{13}C$ composition in successive calcite stages. This trend appears to

correlate roughly with increasing distance from orebodies, although more samples would be required to prove this observation.

Table 7 shows a list of values per calcite stage and distance from orebodies. In keeping with the paragenetic order of calcites, note that there is a clustering of $\delta^{13}C$ and $\delta^{18}O$ values of ore-related calcites II and III clearly distinguishable from non-ore-related calcites IV. In addition, calcites II from manto mineralization show $\delta^{18}O$ values of 17.1 to 17.98°/oo, lower than those for equivalent stages of calcites at surface, 30 to 70 m away from their closest orebodies, which range from 18.96 to 21.3°/oo. Similarly, $\delta^{13}C$ values in manto calcites (2.91-3.17°/oo) decreases in the equivalent calcites at surface (-3.33 to -4.6°/oo). Later calcites (calcites IV and V) show $\delta^{18}O$ values above the range of that for calcites II and III. These calcite values range in $\delta^{18}O$ from 22.66 to 24.44°/oo and its corresponding $\delta^{13}C$ values decrease relative to calcites II and III showing values of -7.05 to -7.3°/oo.

Temperature of formation for successive calcites I to III are estimated to decrease progressively from 360°C, the temperature at which calcite I is in equilibrium with fluorite in the skarn, to temperatures perhaps around 200°C. Actual temperature of individual calcite stages at La Encantada were not possible to determine; the few fluid inclusions present in calcites II and III are too small and their bubbles are poorly visible. However, abundant iron and manganese mineralization associated with different stages of ore mineralization present in calcites I to III suggests that these calcites belong to a sequential and progressive cooling from the same fluid source. It is possible then that

temperatures at the time of calcite II and III deposition may have ranged between 300°C and 200°C.

According with the estimated temperatures of formation of calcites, the $\delta^{18}O$ variation in calcites can be explained as due to increased isotopic fractionation with decrease of temperature from calcites I to V. Table 8 shows the possible compositions of fluids from which calcites originated as a function of temperature. Different water-to-rock ratios in open and closed systems are another variable considered in the estimations of the higher temperature calcite I, where the isotopic fractionation does not explain the composition of the only sample of calcite I (Table 9).

Thus, the heavy oxygen isotopic composition of the 360°C calcite I ($\delta^{18}O$=22.8) in the skarn could have been precipitated in a closed system with water-rock ratios of approximately 0.1 from a hydrothermal solution having a $\delta^{18}O$ value of +6 to 7°/oo similar to that of magmatic waters.

If fluids exceeded a water-rock ratio of 0.1, it is possible that only one fluid, similar in composition to magmatic water, was responsible for the formation of the calcites in skarn. But considering that natural closed systems do not exceed 0.02 to 0.1 for the oxygen system (Ohmoto, 1986), it is possible that some mixing with meteoric waters occurred. Note from Table 9 that meteoric waters with similar water-rock ratios and similar temperatures yield ^{18}O isotopic compositions such as the ones observed in the calcite I from the skarn. Note also that isotopic values reached in an open system are not as likely to form isotopic compositions as those actually found in the skarn. Water-rock ratios

TABLE 8

Estimation of possible isotope composition of the hydrothermal fluids determined from calcites. -- Modeling with different temperatures based on isotopic fractionation[a]

(level)	Sample Number	Calcite Type	^{18}O	250°C	225°C	200°C	175°C	150°C	100°C	20°C
Manto Calcites							^{18}O fluids			
635	635-2	2?	17.10	10.3	9.3	8.10	6.6	5.00	0.5	
695	6955-2	2	17.98	11.18	10.18	8.98	7.5	5.88	1.4	
Surface Calcites										
				200°C	175°C	150°C	124°C	100°C	50°C	20°C
	LE8	2-3	18.96	9.96	8.46	6.9	4.76	2.36		
	LE6	3	20.06	11.06	9.56	7.96	5.86	3.46		
	LE36	2	19.53	10.53	9.03	7.4	5.33	2.93		
	LE3	2-3	21.30	12.30	10.8	9.2	7.1	4.7		
	LE15	4 3	23.44	14.44	12.94	11.34	9.24	6.84		-6.06
	LE40	4	22.66	13.66	12.16	10.56	8.46	6.06		-6.84
	LE34	5	24.44	15.44	13.94	12.34	10.24	7.84		-15.06
	LE10		22.15	13.15	11.65	10.05	7.95	-5.55		-7.35
	LE9		24.75	15.75	14.25	12.65	10.55	8.15	7.65	-4.75

a. $\Delta = \delta^{f}_{rock} - \delta^{f}_{H_2O}$ (Friedman and O'Neil, 1977).

TABLE 9
Estimation of final isotopic values for the case of skarn

T°C	Δ		Water-Rock Ratio 0.001	0.01	0.1	1	10
			Closed System				
a. Case Magmatic Water Origin							
350	3.8	δ_r^f	25	24.85	23.66	17.4	11.2
300	5.1	δ_r^f	25	24.8	23.7	18.0	12.4
b. Case Meteoric Water							
350	3.8	δ_r^f	25	24.7	22.4	10.9	-0.6
300	5.1	δ_r^f	25	24.7	22.6	11.6	0.5
			Open System				
a. Magmatic Water							
350	3.8	δ_r^f	25	-24.7	-21.7	-3.0	9.8
300	5.1	δ_r^f	25	-24.6	-21.6	-2.2	11.1
b. Meteoric Water							
350	3.8	δ_r^f	-25				-3.2
300	5.1	δ_r^f	-25	-24.7	-22.8	-10.4	-1.9

Variables: initial δ_{fluids} meteoric water = $-7^o/oo$ (Sheppard, 1986)
magmatic water = $6^o/oo$

initial δ_{rock} average limestone = $25\text{-}28^o/oo$
Cretaceous limestone = $27^o/oo$ (Veizer, 1983)

a. Δ is the isotope fractionation factor.

b. δ_r^f is the final isotopic composition of the rock.

greater than 10 in an open system tend to yield final $\delta^{18}O$ values in the rock of $\delta^{i}_{w} + \Delta$ where δ^{i}_{w} is the initial isotopic composition of water and Δ is the water-rock fractionation factor. The fractionation factor between calcite and water is 1000 ln α $CaCO_3$-H_2O = $2.78(10^6T^{-2})$ - 2.89 (Friedman and O'Neil, 1977). The equations of conservation used for open and closed systems are from Taylor, 1979).

It is worth noting that the paragenetic situation of this calcite I is not very clear and that it is possible that late calcites IV (also present cutting the skarn) are involved in this sample. Nevertheless, if heavy ^{18}O compositions were present during the skarn formation, it is feasible that the gangue and ore formed via a closed system with water-rock ratios between 0.01 and 0.1.

Alternatively, calcite II, which is likely to have been formed at 200°C, equilibrate with fluids having compositions similar to those of magmatic waters (Table 9). Calcites II and III at surface could have formed from magmatic waters between 100 and 150°C. Small depletions (1-9°/oo) due to diagenesis or decarbonization may have been responsible for the ^{18}O composition of late calcites IV.

In regard to carbon isotopic values, the trend observed at La Encantada ($\delta^{13}C$ decreasing with a decrease in temperature) may reflect oxidizing conditions of deposition (Sassano, Fritz, and Morton, 1972). Normal C-O isotopic halos exhibit a coupled C-O decrease toward the mineralization centers or plutons. Examples of such "normal" trends are the calcites at Providencia (Rye, 1966). At Providencia, however, calcites stage III show a C-O trend similar to the one observed at La

Encantada. This similarity indicates that these trends are not rare in hydrothermal systems.

The carbon depletion observed at La Encantada could have originated from magmatic carbon species. However, the variations found cannot be explained as a function of isotopic fractionations. It is possible, then, that carbon in carbonates did not evolve in equilibrium (CO_2 with $CaCO_3$) and that the large ^{13}C depletion was externally controlled in oxidizing conditions where lower ^{13}C would prevail (Sassano et al., 1972). In addition, depletions in ^{13}C at La Encantada may be due to decarbonation. Such large ^{13}C depletions were reported by Nabelek et al. (1986). The ^{13}C depletions by decarbonation at La Encantada are feasible and consistent with a decrease of calcium in limestone from 39 to 26.7 percent reported by Rosas (1983).

CHAPTER 5

DISCUSSION

Summary of Anomalies and Geochemical Model

Silver, lead, and arsenic are the best geochemical indicator elements as they account for 11 out of 12 known orebodies at the La Prieta area. They also show remarkably similar trends that closely reflect those of mineralization. In addition to their coincidence with the already known orebodies, Ag, Pb, and As point to three anomalous zones.

Zinc also appears to be a good geochemical indicator, but it does not provide information in addition to that gained with Pb, Ag, and As, and due to its mobility, it is usually displaced much farther than Pb and Ag, or moreover it can be leached away.

Volatile elements such as Hg and Sb appear to be excellent indicators of deep orebodies. Near-surface orebodies (less than 100 m deep) exhibit very low Hg or Sb anomalies, perhaps due to its vertical zoning. However, from the data presented here, Sb and Hg are estimated to appear in anomalous quantities approximately 100 m above orebodies. Yet this cannot be asserted, because no underground Sb and Hg geochemical data are available. The orebodies detected by the Hg and Sb anomalies are the Ojuelas and the Manto Zone, 200 and 350 m deep, respectively. In the La Prieta area, Hg and Sb are very accurate geochemical indicator elements, but their use is not quite efficient;

their anomalies have a one-to-one correspondence with orebodies, but similar deep orebodies do not show Hg or Sb anomalies at all. In this sense, the use of only Hg and Sb as a pathfinder would tend to miss potential orebodies.

Molybdenum anomalies alone do not locate orebodies, but conversely, they define the heat source and the center of mineralization. Molybdenum is an important element, because orebodies and their ore-metal anomalies are located peripheral to Mo anomalies. Molybdenum is also important in the definition of the model described hereafter where significant anomalies develop around the Mo anomaly.

The La Escalera area appears to be a geological and geochemical analog of La Prieta but at a higher elevation. As in the La Prieta area, the La Escalera area contains a northeast-trending breccia structure with a north-northwest-striking fault located in the west side of the breccia and northeast-striking faults and joints converging along the breccia zone. The geochemical anomalies are peripheral to a Mo anomaly, which is interpreted as a heat center, but unlike at La Prieta, the distribution of the anomalies does not indicate regular zoning around a single heat source. The values for elements shown on Figure 17 clearly indicate a structurally and geochemically anomalous area that deserves to be tested by drilling on the best possible targets defined under the available model. This is around the edges of the molybdenum anomalies in the overlap of ore metal anomalies with Mo anomalies. Particularly important are the structurally and geologically favorable areas with geochemical anomalies such as the intersection of the

north-south-striking fault with the breccia (11100 N, 10200 in Figs. 6 and 17).

Geochemical Model

According to the geological and geochemical data available at La Prieta, the distribution of anomalies fits into a model where the molybdenum anomaly represents the center of mineralization with the orebody's trace- and ore-element anomalies distributed peripherally to this center. Variables such as topography, secondary environment, leaching, and mobility of elements are considered in the model.

Figure 21 shows a generalized picture of the model. Molybdenum anomalies are centered above an intrusive center with the Pb, Ag, As, and Zn anomalies around it and an outer layer of Sb and Hg anomalies. This distribution would approximately represent typical periplutonic zoning.

The geochemical anomalies in calcite veinlets are primary. However, because sampling included total fracture material, it also records secondary processes. The present location of the anomalies is then primary but includes secondary effects. Oxidation and leaching may have affected the original distribution of anomalies and caused a variable downslope migration of elements, which is a function of the chemical environment, mobility of the elements, topography, and iron and manganese oxides content in its path. Accordingly, a larger displacement of Zn anomalies relative to Pb and Ag anomalies is observed. Antimony and mercury, due to their high volatility and normal zoning, are farther away from the center and remain in their original position due to a

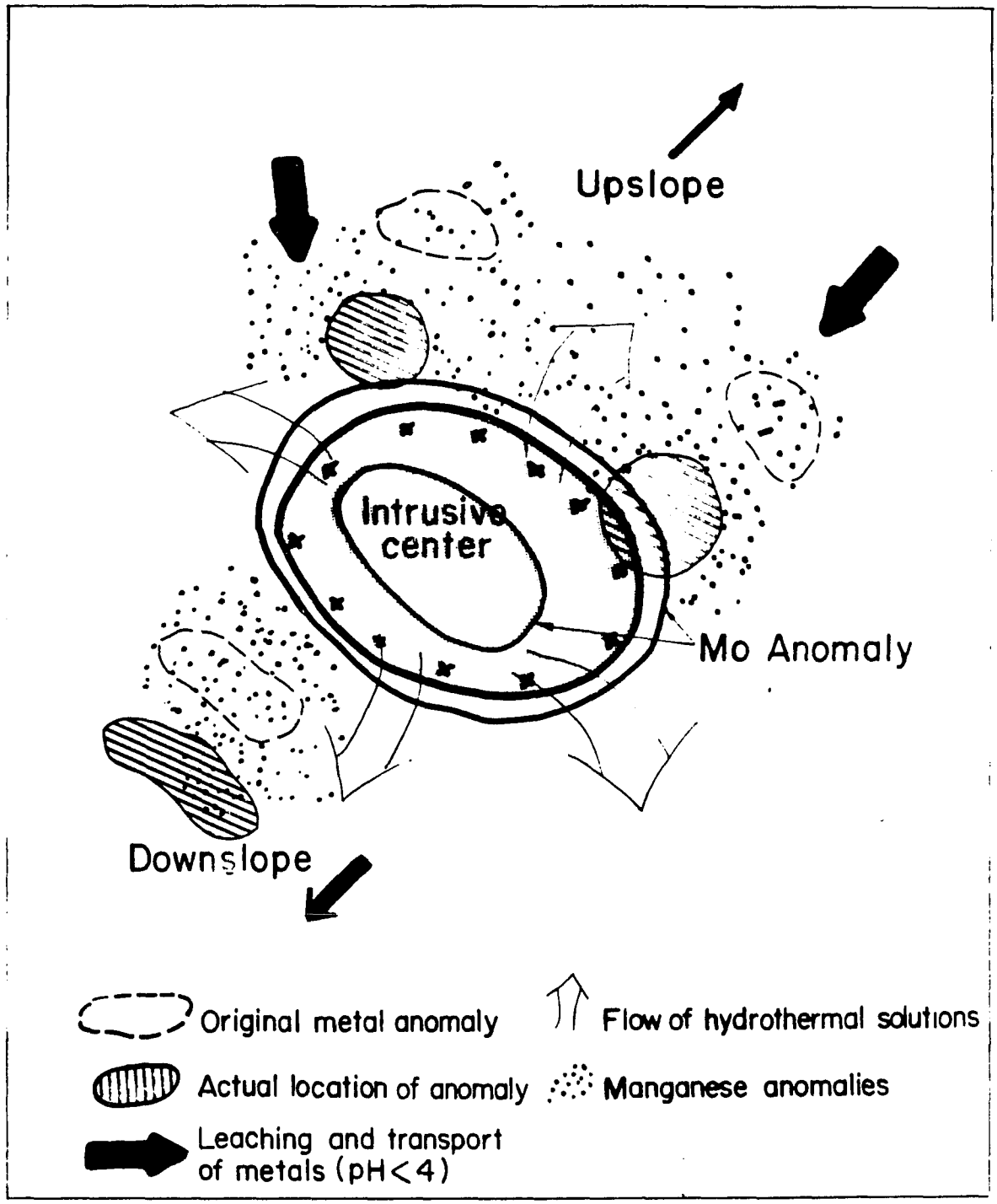

Figure 21. Ideal geochemical model of the La Encantada district

decoupled migration from oxides that make them relatively independent of the chemical environment and migration.

The interpretation of the model is in keeping with the geology and the underground data available on the area. The presumed center of mineralization indicated by the Mo anomalies is indeed coincident with the skarn dome as defined from underground and geophysical data. Additionally, the orebody's location supports the interpretation of the distribution of metal anomalies.

Figure 21 shows the elements considered in the model. The open arrows indicate the flow of solutions as they formed the original anomalies; closed arrows indicate the direction of transport due to oxidation and leaching. Note in stippled pattern the distribution of Mn, which remained immobile, a behavior that agrees with the prevailing oxidation and acid environment. The ore and trace-metal elements that existed did not depend on mobility with iron oxides other than in primary calcites (e.g., sulfides in fractures). Acid leaching removed metal ions from the original location, and these elements were precipitated shortly afterwards in a less oxidizing environment. The host limestone provided a quick restoration of balance in pH, which permitted reprecipitation of the metals. Metals can also be coprecipitated or adsorbed by iron and manganese oxides. The balance in pH and oxidation conditions occurred up to 50-100 m away from the orebodies. Because Mn is present as oxides, it is assumed that most of it is associated with iron oxides and that the Mn assays should provide an approximate estimation of the correlation between iron oxides and

elements, thus helping to estimate the mobility of iron oxides with trace and ore elements.

Isotope Model and Its Use in Exploration

Figure 22 shows a plot of C-O stable isotope trends with data from selected ore deposits, contact metamorphic aureoles, and standard isotopic values of carbonate rocks reported in the literature that were plotted to provide a general framework for the isotope results at La Encantada. The purpose is to compare isotopic trends and offer an application for mineral exploration. Table 6 presents a partial list of isotopic values at the localities included. The plot is based on data from Providencia, Mexico (Rye, 1966), Santa Eulalia, Mexico (Megaw, 1986), Gilman, Colorado (Engel et al., 1958; Beaty, 1985), Trenton Limestone, Quebec (Deines and Gold 1969), and Weolag, Korea (So, Rye, and Shelton, 1983).

The halos discussed range in size from 3 m to 3 km (Valley, 1986). Specifically of interest are isotopic halos of systems such as at La Encantada. At Santa Eulalia and Providencia, $\delta^{18}O$ halos in limestone extend from 25 to 90 m. At La Encantada an incomplete section indicates that the isotopic halo in calcite veinlets extends for more than 70 m; the halo in limestones was not measured but appears to be at the scale of centimeters (Fig. 22).

The most significant features from Figure 22 are a domain with two isotopic trends associated with magmatic hydrothermal "alteration" and three other distinctive domains separated from the former. The line $\delta^{18}O=21^{o}/oo$ is of particular importance because it separates fields

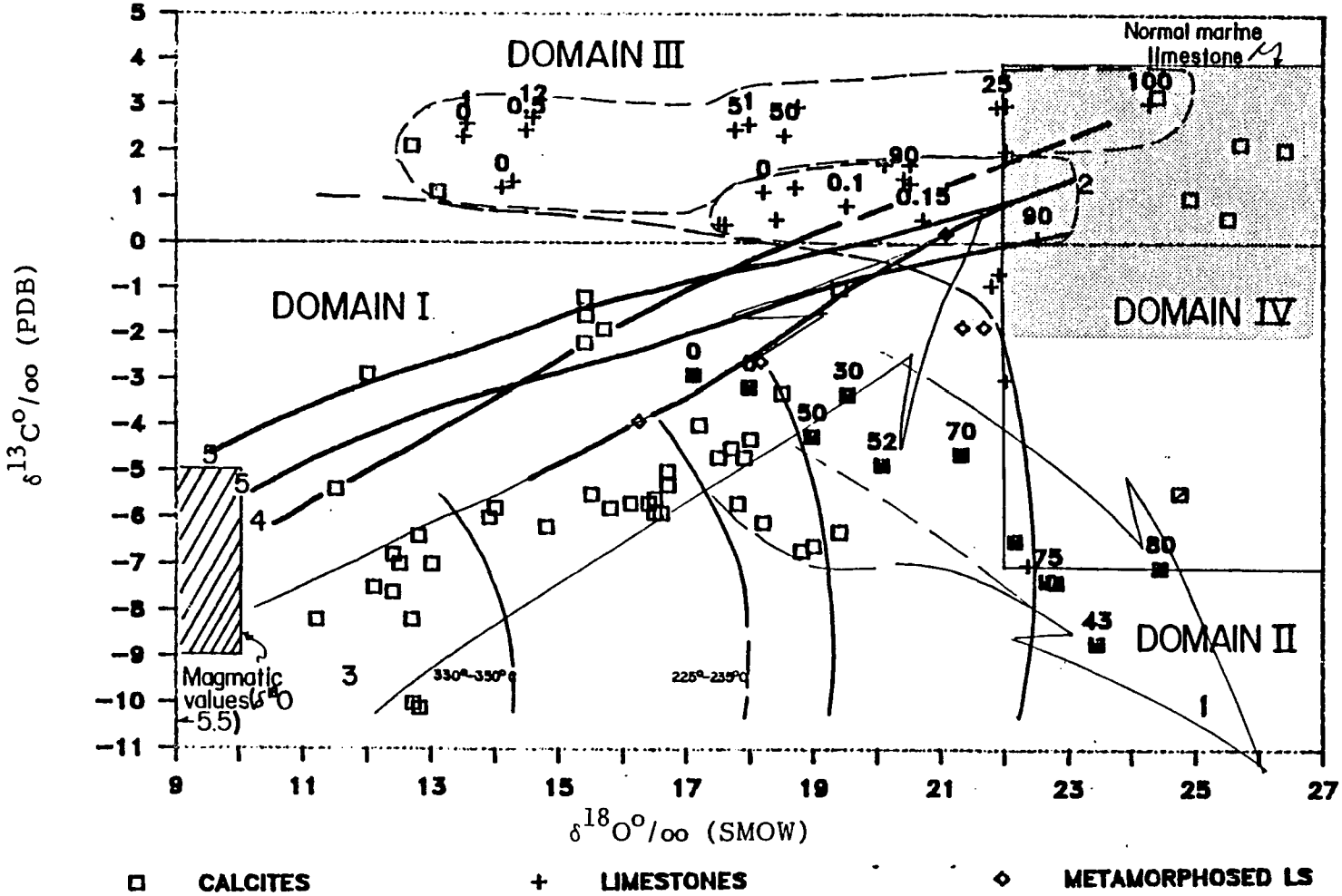

Figure 22. Carbon and oxygen isotope aureoles around plutons and orebodies. -- Data compiled from sources cited in text and in Table 6. Trend 1 is from La Encantada, 2 from Santa Eulalia, 3 from Providencia, and 4 from Trenton Limestone. Temperatures indicated are from Providencia; isotherms from other deposits mimic this pattern. Note the trends as function of temperature and distance from orebodies.

of magmatic-hydrothermal alteration in both limestone and calcites from other isotopic effects (perhaps diagenesis or metamorphic volatilization). The four domains are:

I. Magmatic-hydrothermal (>100°C) calcite and limestone domain ($\delta^{18}O < 21^{o}/oo$, $\delta^{13}C < 0^{o}/oo$). Typically associated with ore.

II. Low-temperature (high $\delta^{18}O$, low $\delta^{13}C$), hydrothermal?, non-ore-related calcites and limestones.

III. Hydrothermally altered limestones (low $\delta^{18}O$, high $\delta^{13}C$).

IV. Unaltered limestones.

Domain I – Magmatic-hydrothermal

The magmatic-hydrothermal domain is defined by two trends: Trend a is a coupled isotopic C-O depletion with increasing temperature, and Trend b is a $\delta^{18}O$ decrease and a $\delta^{13}C$ increase with increasing temperature (approaching orebodies or plutons). This domain, limited by the line of "magmatic" calcites ($\delta^{18}O = 21^{o}/oo$), is named after the predominance of calcites that define these trends. Anything beyond this line is not significant to mineralization.

Trend a exemplifies "normal" trends around plutons (Valley, 1986) and is present in calcites at Providencia and Naica.

Trend b is observed in calcites III at Providencia, the calcites at La Encantada and possibly also calcites at Santa Eulalia show the same behavior. As in Trend a, $\delta^{18}O$ in Trend b decreases with increase in temperature, but unlike in Trend a, $\delta^{13}C$ in Trend b increases with increase in temperature.

1. ^{13}C Variation – Trend b may reflect special characteristics of the hydrothermal system that indicate perhaps oxidation conditions alternating during ore deposition (Sassano et al., 1972). The ^{13}C composition in Trend b cannot be explained by isotopic fractionation and it is suggested that deposition occurred in disequilibrium from magmatic carbon in solution. Because fractionation factors of carbon species at hydrothermal temperatures are small ($\delta^{13}C$ ~2°/oo at >200°C) (Emrich, Ehhalt, and Vogel, 1970; Deines et al., 1974), then it is unlikely that the carbon from Trend b is derived entirely from the host limestone. Similarly, isotopic fractionation would require that the $\delta^{13}C$ composition in the fluid (as CO_2) decreased from -3 to -17°/oo in successive period of time and temperature drop, which is also unlikely.

Worth noting in the carbon variation is the fact that most "magmatic-hydrothermal" calcites fall below a $\delta^{13}C$ composition of 0 to 0.5°/oo, marking a clear difference with the $\delta^{13}C$ composition of the limestones of Providencia and Santa Eulalia, which is above 0°/oo.

2. Oxygen Trends – Very important in both trends is the $\delta^{18}O$ composition, because it will help discerning ore-related isotopic compositions from non-ore-associated ones.

The $\delta^{18}O$ compositions of Trends a and b are easily explained as a result of increased isotopic fractionation with decrease in temperature. Thus, note that the dashed lines within Domain I approximate isotherms, which may vary from deposit to deposit. In some deposits, associated with the decrease of temperature is an increase of distance

from the orebody (La Encantada, Trenton Limestone aureole (Deines and Gold, 1969)).

Using the fractionation factor equation from Friedman and O'Neil (1977), 1000 ln $\alpha = 2.78(10^6T^{-2}) - 2.89$, and assuming that the lowest temperature of hydrothermal calcites is 100°C, I estimate that the maximum $\delta^{18}O$ of magmatic hydrothermal calcites is 23°/oo. $\delta^{18}O = 23°/oo$ is the theoretic ceiling value that can be associated with magmatic signature; however, because the values for unaltered limestones lower down to 21°/oo, a more practical $\delta^{18}O$ ceiling value should be lowered to between 21 or 22°/oo.

If it is considered that 21.5°/oo is the ceiling $\delta^{18}O$ value of magmatic hydrothermal compositions, the size of the halos can be estimated, as was described (Fig. 22).

Domain II – Low-temperature Hydrothermal Calcites

Domain II is beyond the "magmatic" calcites line $\delta^{18}O >$ 21.5°/oo. Although the calcites in this field are clearly out of the significant isotopic range of Domain I, its carbon composition suggests that they may have formed from a magmatic source. This suggestion makes the name "magmatic" calcites exclusive of calcites of Domain I inappropriate. Calcites IV and V at La Encantada fall in this field and could have formed from magmatic waters at 80°C or from meteoric waters at <20°C. Decarbonation is also feasible as having been responsible for small depletions (4-2°/oo) (Valley, 1986). Calcites within this domain are of little use for exploration.

Domain III – Hydrothermally Altered Limestones

The hydrothermally altered limestones show striking differences in $\delta^{18}O$ and $\delta^{13}C$ compositions from those of "magmatic" calcites, with $\delta^{13}C$ values consistently higher than 0-0.5°/oo. Their $\delta^{18}O$ values, which fall the within <21.5°/oo range, are also significant for exploration.

These differences have implications for the source of carbon. Whereas in calcites a decrease in $\delta^{13}C$ values was noted, the values become steadily uniform in limestones. This finding means that within the limestones the carbon composition is buffered by the limestones and the carbon in the limestones is derived from the matrix. Accordingly, a similar process is proposed for the high carbon calcites ($\delta^{13}C$ > 0°/oo) that transgress into Domain II. Thus with time and with decrease in temperature, the source of carbon from limestone became more important, whereas at early stages of mineralization the main source for oxygen-18 and carbon-13 was magmatic water.

Domain IV – Unaltered Limestone

Domain IV shows the C-O isotopic values for limestones reported by Rye and Ohmoto (1974), Veizer (1983), and Valley (1986). The lower $\delta^{18}O$ values overlap approximately in the range 21-23°/oo with the domain assigned to hydrothermally altered limestone and magmatic calcites. This overlap creates uncertainty as to whether to assign the ceiling magmatic values to Domain I or Domain IV. Thus significant (hydrothermal-magmatic) isotopic values may be misclassified.

Fritz (1969) reported $\delta^{18}O$ values for inorganic marine limestones of $22^{o}/oo$ and $\delta^{13}C$ values of $-7^{o}/oo$. As has been discussed, low $\delta^{13}O$ values can be reached due to diagenesis and low $\delta^{13}C$ values due to acidic solution flushing the rock (Beaty, 1985); however these values are unrelated to mineralization.

CHAPTER 6

SUMMARY AND CONCLUSIONS

The combined use of calcite veinlet stockwork geochemistry, isotope data, and structural analysis proved an excellent exploration tool at La Encantada, and it is suggested that the model be extended to other carbonate-hosted deposits. Use of these data, interpreted and integrated with a good geologic background of any prospective area in carbonate terranes, enhances the probability of success in exploration at any level of exploration in grass-roots as well as in detailed exploration.

Calcite veinlet geochemistry, detailed fracturing analysis, and sampling of oxidized outcrops are to carbonate-hosted deposits what alteration, fluid inclusions, and structural studies are to epithermal veins. The comparison is crude but emphasizes that the alteration in carbonate-hosted deposits is erratic to none, that structural control need not be tremendously evident but microfracturing may be important, and that their geochemical signature in rock is usually extremely limited. The inclusion of more meaningful methods such as sampling veinlets or stockworks in search of leakage anomalies, the careful analysis of the significance of anomalies within a complete geological framework, and the more careful analysis of selected calcite samples for ^{18}O isotopes is emphasized. These methods, combined with microfracture

analysis, are excellent tools in the exploration for carbonate-hosted deposits.

I should point out that veinlet geochemistry can be done in any prospective area almost without being selective. Oxidized outcrops are certainly more geologically attractive; veinlets with iron and manganese oxides and other trace-metal contents also enhance the probability of success in exploration. However, oxygen isotopes analyses should be made from carefully selected material with care being taken to separate different phases of gange and sampling its host rocks to look for a possible $\delta^{18}O$ halo in the rock. Because the ^{18}O isotope is very sensitive, it can be an excellent guide and indicator—yet a wrongly selected sample could yield misleading results.

Sampling unaltered rock may be important to establish ^{18}O isotope "background," to estimate ^{18}O isotope diffusion in the host rock, and to estimate the $\delta^{18}O$ ceiling value, either in calcites or limestones, which can be associated with certainty with mineralization.

The most important conclusions are:

1. Veinlet and stockwork geochemistry is an excellent exploration tool. It forms easily contrastable anomalies, and its values are enhanced from 5 to 26 times the concentration in local limestones.

2. Lead, arsenic, and silver are the best geochemical indicators and combined account for 100 percent of known orebodies.

3. Molybdenum anomalies indicate a deep heat source; ore-metal anomalies located around it are thus significant.

4. Mercury and arsenic are good geochemical indicators of deep (perhaps >100 m) orebodies and are known to indicate orebodies deeper than 350 m.

5. The dip of fractures and possible leaching should be considered in the interpretation of halos. Manganese and iron oxides form a halo above orebodies. Trace- element and ore-metal anomalies show decoupled, small (30 to 90 m) migrations away from the projection of the orebody to surface.

6. Vertical zoning from Pb, Zn, and Ag to Sb-As from bottom to top is present.

7. Lead-antimony ratios may help determine vertical location within the hydrothermal system and crudely estimate depth of orebodies.

8. Lead-bismuth ratios help indicate hydrothermal direction flow in little-oxidized areas such as La Escalera.

9. Lead-antimony and lead-bismuth ratios also clearly separate the barren from mineralized sectors.

10. A low ^{18}O isotope content halo is present in calcite veinlets above orebodies. This halo is independent of alteration and oxidation, hence provides an excellent hypogene signature of orebodies.

11. The $\delta^{18}O$ values equilibrate with fluids having compositions similar to those of magmatic waters. However, it is proved also that similar values are reached with meteoric waters. A magmatic-hydrothermal source influenced by meteoric waters is suggested.

12. An ^{18}O isotope genesis reinforces the significance of calcite veinlets as ore associated.

13. Highly fractured (microfractured) Cretaceous limestones that overlie a metamorphosed Paleozoic basement intruded by mid-Tertiary granodiorites provide an excellent geological environment for carbonate-hosted deposits such as La Encantada.

14. Fracture density decreases upward from orebodies; its measurement offers a quantitative estimator element useful to contrast and establish an order of priority for different prospective areas.

15. Fluorescence can be used as an aid to recognize hydrothermally altered areas where the alteration and recrystallization are too subtle to be recognized in the field. In large-scale exploration, i.e., remote sensing, fluorescence is another piece of information to consider in target selection.

16. Paleozoic faults appear to be important structural features. Metals could be leached from Paleozoic basement and channeled through Cretaceous reactivated Paleozoic faults.

17. The heat source that activated the hydrothermal system appears to be a 17-Ma granodiorite. This age is consistent with ages of the mineralization for similar deposits such as the Naica and Santa Eulalia deposits.

18. The most important suggestion for exploration is to look for Fe-Mn-calcites stockworks and their Ag, Pb, and As anomalies, particularly those near molybdenum anomalies, looking for the orebodies in the direction of the dip of the structures.

APPENDIX A

GEOCHEMICAL DATA FOR LA PRIETA AND LA ESCALERA AREAS

TABLE A-1
La Prieta veinlet geochemical assays

SAMPLE	X	Y	Ag	Pb	Zn	As	Hg	Mn	Mo	Sb
			ppm	%	%	ppm	ppm	%	ppm	ppm
MEAN VALUES			23.13294	0.651587	1.785012	572.2941	0.870263	0.712526	22.83783	231.3421052
1	100	100	3.8	0.0166	0.006	30				
2	100	150	3.3	0.044	0.0146	14				
3	100	200	14.3	0.11	2.58	47				
4	100	250	4.2	0.0297	0.021	23				
5	100	300	6.1	0.0386	0.0437	24				
6	100	350	16.5	0.0646	0.0417	25				
7	100	400	4	0.11	0.0182	4				
8	100	450	7	0.0603	0.0528	24				
9	150	100	28.8	2.09	2.72	580				
10	150	150	34.2	0.17	0.66	275				
11	150	200	8.8	0.0636	0.0533	24				
12	150	250	9.5	0.12	0.1	190				
13	150	300	15.4	0.27	0.13	54				
14	150	350	178	0.16	0.0862	22				
15	150	400	4.2	0.1	0.0244	13				
16	150	450	11.2	0.16	1.33	77				
17	200	100	5.2	0.17	0.1	83				
18	200	150	5.4	1.43	2.83	1340				
19	200	200	5.2	0.0604	0.0238	29				
20	200	250	9.6	0.0762	0.063	210				
21	200	300	4.9	0.0297	0.0232	148				
22	200	350	23.4	0.55	1.42	48				
23	200	400	27.1	0.0752	0.0283	18				
24	200	450	19.5	0.15	0.13	70				
25	250	100	20	0.46	0.63	105				
26	250	150	10.8	0.27	0.21	90				
27	250	200	6.3	0.11	0.0366	23				
28	250	300	6	0.12	0.04	23				
29	250	350	7.4	0.0697	0.0213	19				
30	250	400	6.3	0.0844	0.0635	21				
31	250	450	4.9	0.4	10.7	295				
32	300	100	55	0.48	0.61	310				
33	300	150	6	0.14	0.0607	29				
34	300	300	3.6	0.0217	0.0086	12				
35	300	350	14.7	0.41	1.56	180				
36	300	400	4.6	0.22	0.16	200				
37	300	450	12.3	2.4	0.0542	48				
38	350	150	12.5	1.34	1.81	740				
39	350	300	20.7	0.62	0.82	250				
40	350	350	35.9	0.93	2.97	200				

Table A-1--Continued

41		350	450	15	1.23	1.91	400				
42		400	150	13.7	1.4	4.82	1400				
43		400	200	16.1	1.21	6.43	550				
44		400	250	7.7	0.13	0.57	25				
45		400	300	25.9	0.73	8.03	320				
46		400	400	18.2	0.88	1.11	275				
47		450	350	19.1	0.73	8.07	180				
LE2	1810	417	155	9	0.44	0.88	719	0.3	0.23	29	235
LE3	1808	405	135	12	0.14	1.1	405	0.2	0.11	27	41
LE4	1815	425	210	17	0.38	0.23	360	0.6	0.99	31	57
LE5	1830	400	225	12	0.4	1.81	425	0.5	0.22	25	230
LE6	1825	390	170	7	0.29	0.24	495	0.1	0.029	34	228
LE7	1820	365	140	7	0.89	4.78	3800	0.05	0.52	27	194
LE8	1840	320	160	5	0.12	0.018	16	0.05	0.064	24	7
LE9	1838	350	170	39	0.52	1.57	213	0.2	0.55	27	38
LE10	1842	367	195	26	3.4	5.72	6900	0.3	0.94	29	337
LE11	1840	370	190	89	0.93	0.29	175	1	1.91	28	167
LE12	1845	377	220	8	0.044	0.14	42	0.1	0.58	22	10
LE13	1830	395	245	11	0.4	0.25	50	0.2	0.95	25	72
LE14	1838	395	275	33	4.1	11.6	9700	0.2	1	31	425
LE15	1853	390	310	17	2.42	19.3	4400	0.2	0.27	22	382
LE16	1868	400	370	44	1.15	5.01	1100	1.8	0.35	21	353
LE17	1868	400	415	175	6.2	0.62	1400	21	0.26	19	1600
LE18	1886	355	445	41	1.11	0.68	374	0.6	1.92	18	327
LE20	1885	345	350	54	0.85	0.91	192	0.4	0.91	19	88
LE21	1875	350	305	61	2.11	4.3	701	0.6	0.21	19	429
LE22	1820	345	120	19	0.21	0.99	2600	0.2	0.34	26	75
LE23	1810	390	110	50	0.42	0.47	310	0.5	1.23	22	130
LE24	1840	300	170	47	0.42	1.05	1200	0.5	1.06	25	104
LE25	1905	333	300	9	0.16	0.073	46	0.4	1	20	70
LE26	1915	300	340	10	1.66	5.6	272	0.2	0.21	15	1300
LE27	1915	310	390	53	0.8	2.32	383	0.4	1.58	25	336
LE28	1920	320	425	8	0.24	0.25	111	0.2	1.1	24	37
LE29	1958	250	460	8	0.31	0.19	536	0.1	0.68	24	132
LE30	1950	260	405	25	0.033	0.21	148	0.4	1.71	20	13
LE31	1946	250	365	6	0.22	0.18	148	0.5	0.16	21	97
LE32	1937	255	345	4	0.035	0.03	12	0.3	0.22	18	176
LE33	1910	260	300	10	0.036	0.051	29	0.05	1.86	23	7
LE34	1870	253	195	12	1.42	4.55	987	0.05	0.03	16	253
LE35	1863	245	150	13	0.23	0.24	151	0.1	0.54	23	25
LE36	1828	250	100	32	0.49	0.36	107	0.2	1.18	22	13
LE37	1845	470	365	173	1.71	14	867	0.5	0.38	19	274
LE38	1822	415	510	10	0.16	0.11	60	0.05	0.38	23	30
LE39	1900	342	470	9	0.4	0.19	190	0.01	1.4	0	72
LE40	1910	365	520	7	0.002	0.017	4	0.01	0.003		2

TABLE A-2
La Escalera veinlet geochemical data, in ppm

SAMPLE	EAST	NORTH	Pb	Zn	Mn	Sb	As	Mo	Bi
MEAN VALUE----------			320	166.2	1366.6	954	2102	17	160.8
1	12455	11042	400	100	400	900	2000	0	90
2	12430	11050	400	150	1710	1000	2000	0	100
3	12460	11100	400	140	1700	1000	2000	10	150
A4	12478	11158	400	70	540	800	2000	20	190
B4	12480	11155	400	80	1750	1000	2200	20	130
5	12442	11200	300	70	1630	1000	2200	30	90
6	12450	11227	300	50	2700	900	2200	30	140
7	12458	11264	1900	80	410	900	2200	30	170
8	12450	11373	400	70	550	1000	2000	0	90
9	12414	11394	1200	100	280	900	2000	10	90
10	12403	11350	400	90	500	900	2100	0	90
11	12400	11300	400	80	240	900	2100	10	100
12	12402	11252	700	90	470	800	2800	20	130
13	12406	11208	400	50	220	1000	2200	0	80
14	12400	11000	400	70	490	1000	2200	10	40
15	12355	11327	100	70	430	900	2200	40	100
16	12354	11302	900	60	1280	900	2200	10	90
17	12343	11254	100	60	3000	900	1900	40	90
A18	12335	11200	200	60	1290	800	2000	10	120
B18	12336	11200	100	70	1080	800	1900	190	80
19	12337	11141	200	70	880	800	2200	10	80
20	12359	11050	100	50	730	1000	2000	0	110
21	12357	11007	100	60	680	900	2100	10	90
22	12316	11243	100	50	820	600	2200	20	100
23	12300	11200	100	50	1270	900	2100	30	100
24	12300	11157	0	10	1040	1000	2000	10	170
25	12305	11125	0	40	820	900	2100	10	200
26	12296	11045	400	300	730	800	2200	20	190
27	12300	11015	400	200	910	1000	2000	10	180
28	12243	11243	0	20	1100	800	2200	10	290
29	12242	11200	100	110	2560	800	2200	10	240
30	12246	11145	100	110	580	900	2200	10	200
31	12251	11101	300	4750	1380	800	2000	30	290
32	12244	11043	100	90	720	1000	2200	30	290
A33	12250	10950	100	450	470	1000	2200	10	290
B33	12248	10950	100	40	400	1000	2100	30	270
A34	12204	11211	200	60	1680	900	2100	0	210
B34	12192	11193	500	80	4970	900	2000	0	140
35	12195	11150	200	40	2480	1100	2100	10	210
36	12200	11100	300	40	1060	1100	2100	20	150
37	12200	11050	200	50	3300	1100	2100	0	200
38	12200	11000	200	50	360	1000	2000	0	160
39	12150	11200	300	600	3110	1400	2000	20	320
40	12138	11147	300	70	7500	1100	2200	0	150
41	12150	11086	300	60	2600	1300	2000	0	210
42	12145	11075	300	50	2250	1500	2000	30	180
43	12142	11050	300	30	1490	900	2100	10	260
44	12144	11021	300	40	760	1000	2000	10	140
45	12152	11090	300	30	390	800	2000	10	120
46	12218	11100	300	100	1330	900	2000	10	340

APPENDIX B

GEOCHEMICAL CONTOUR MAPS FOR LA PRIETA AND LA ESCALERA AREAS

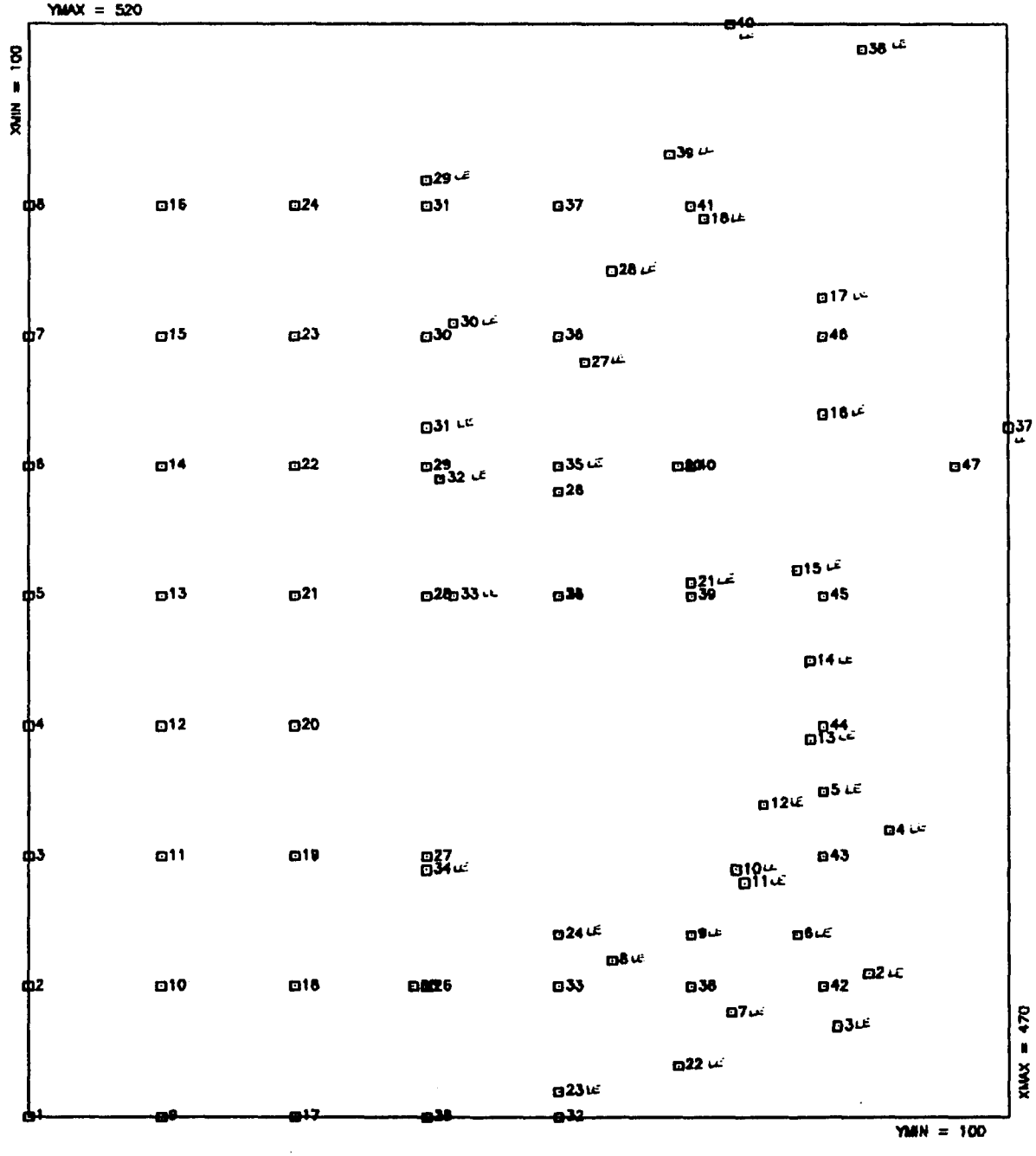

Figure B-1. Sample locations, La Prieta area

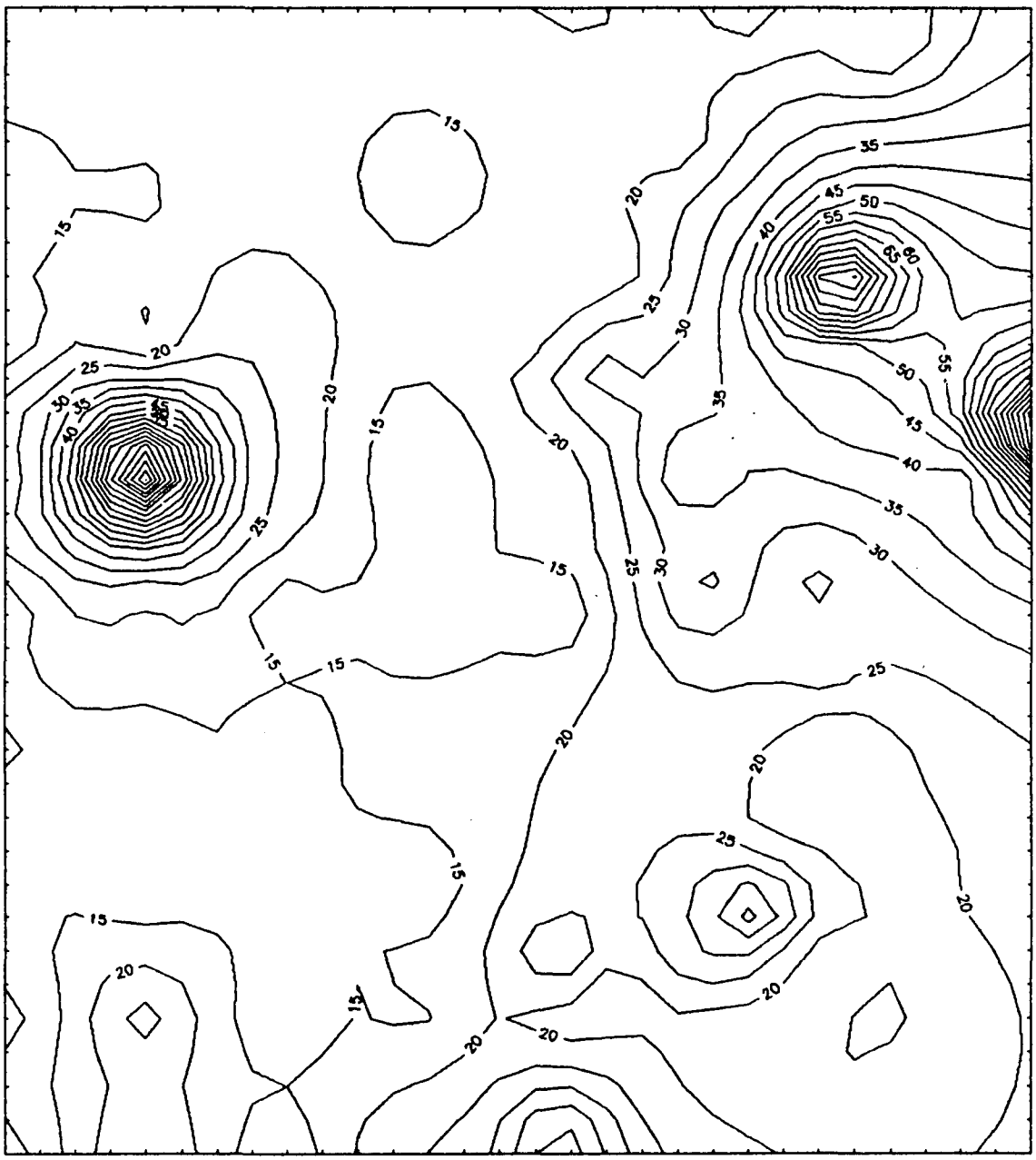

Figure B-2. Silver veinlet geochemistry, La Prieta

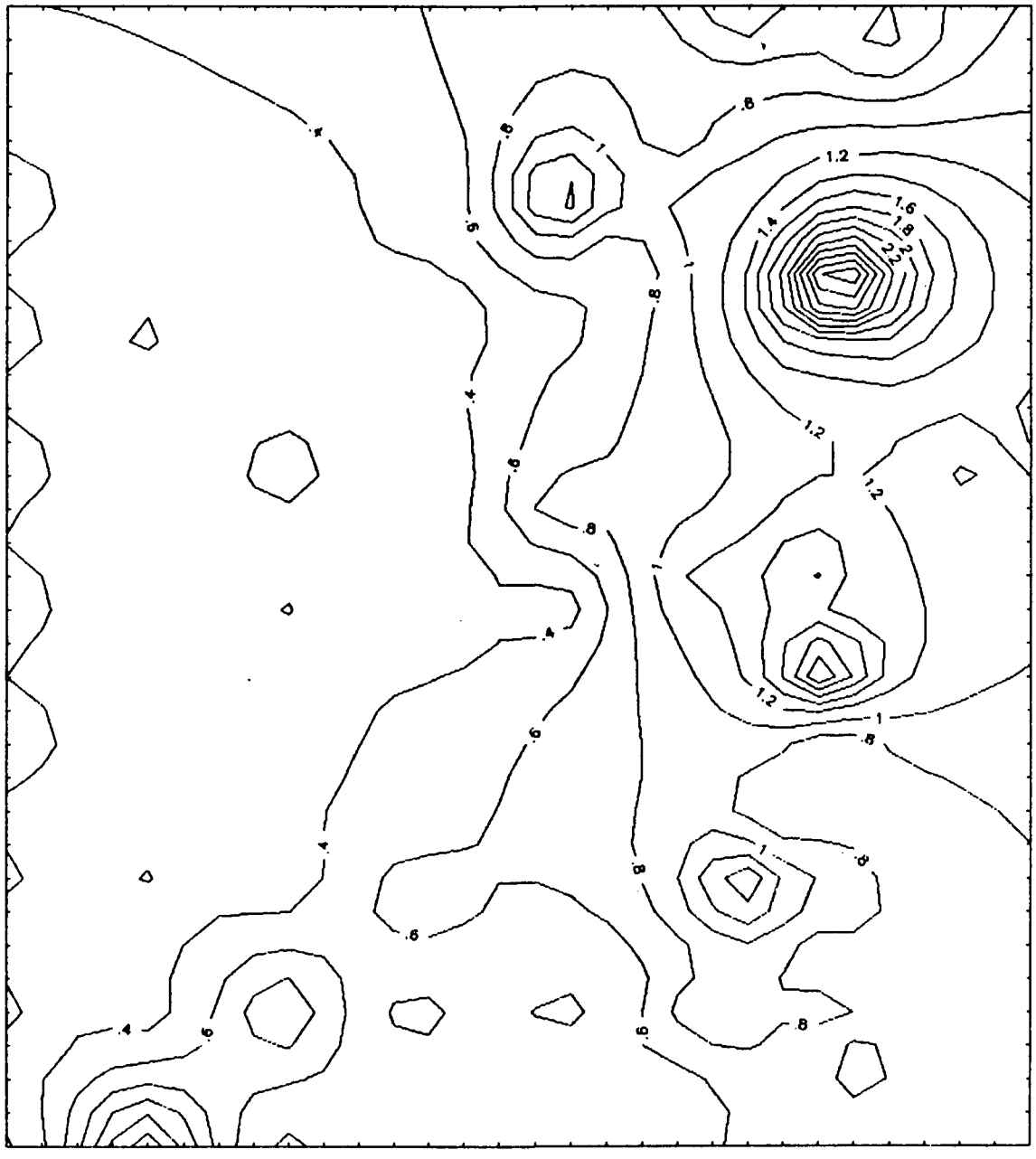

Figure B-3. Lead veinlet geochemistry, La Prieta

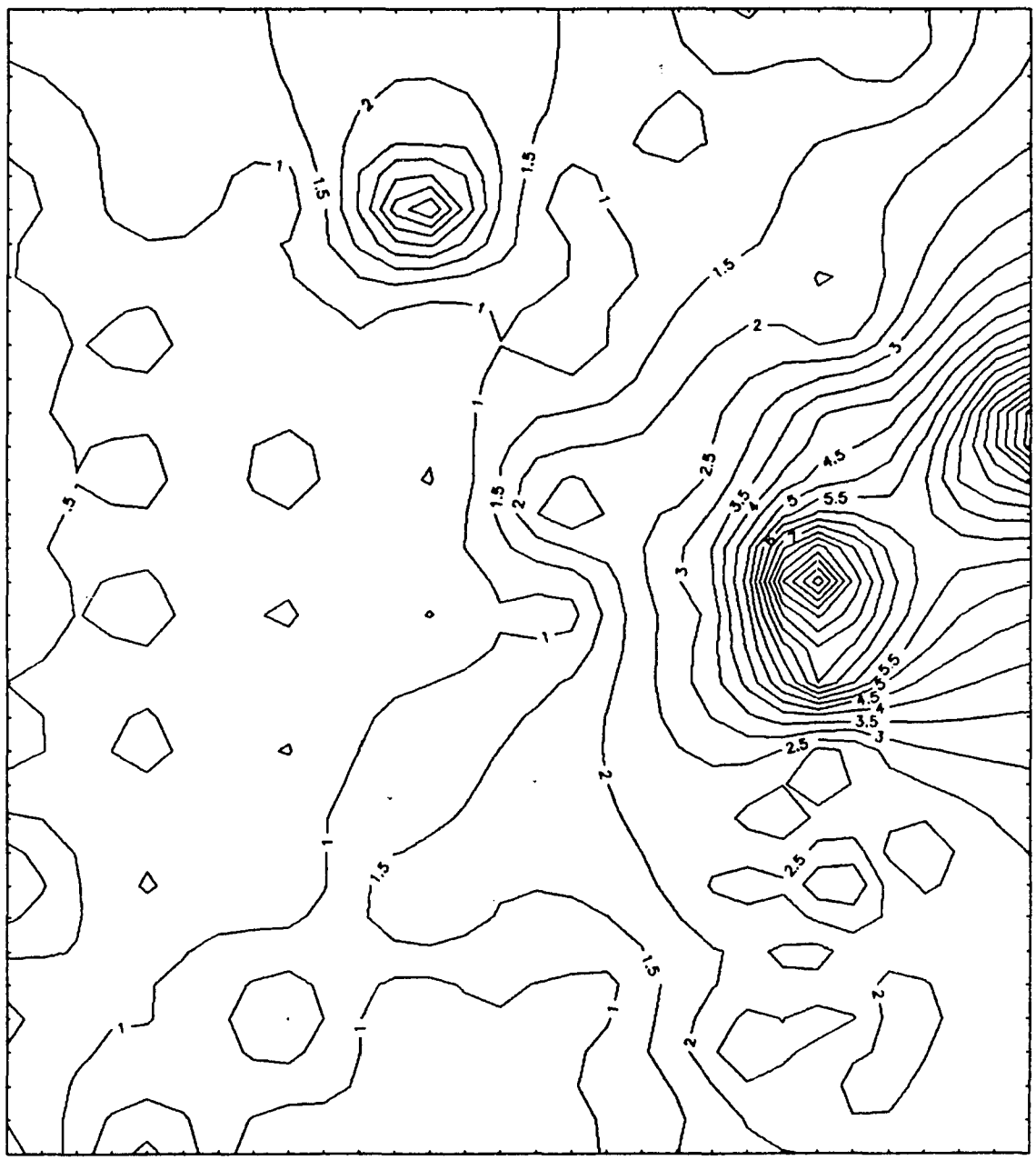

Figure B-4. Zinc veinlet geochemistry, La Prieta

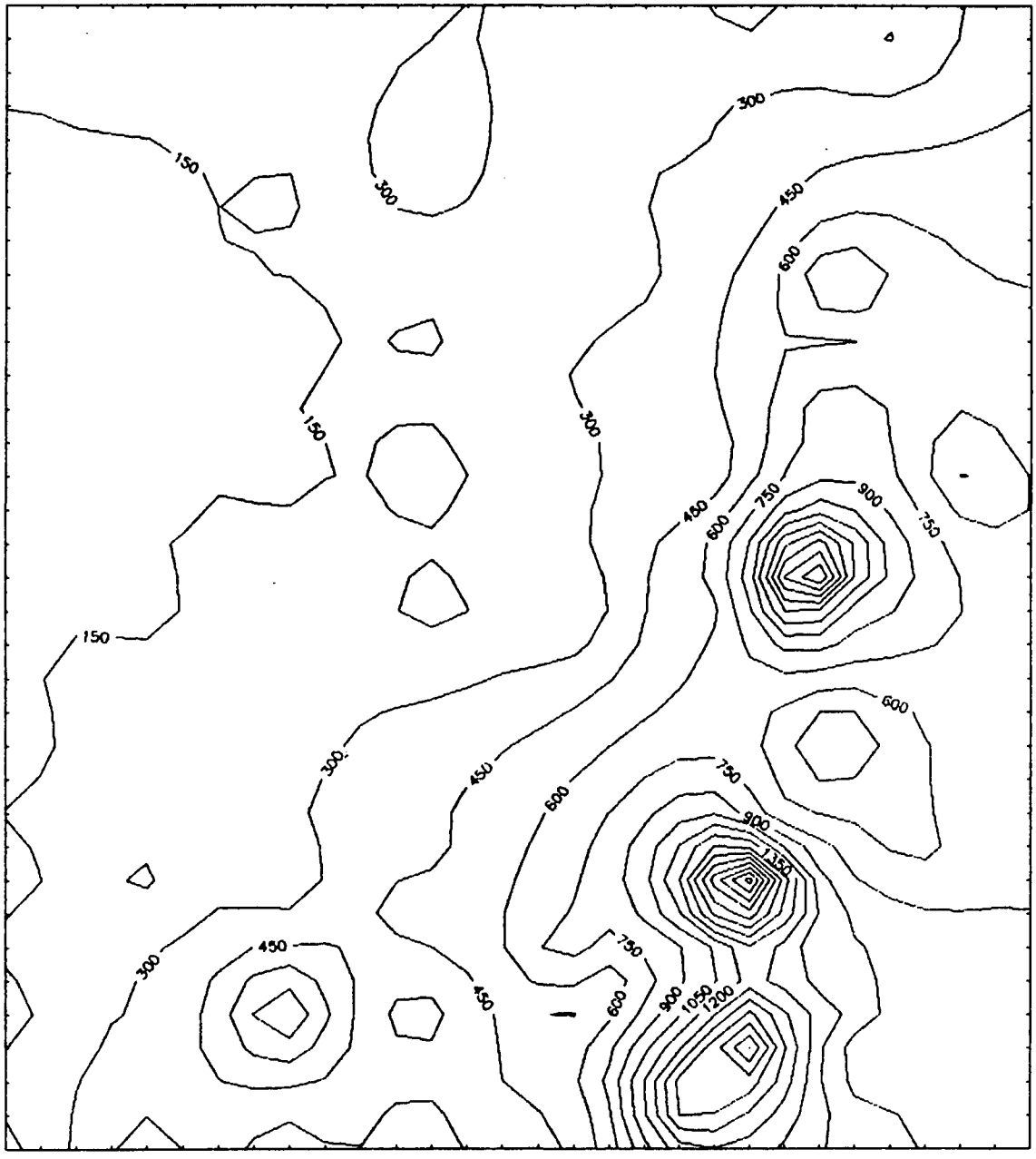

Figure B-5. Arsenic veinlet geochemistry, La Prieta

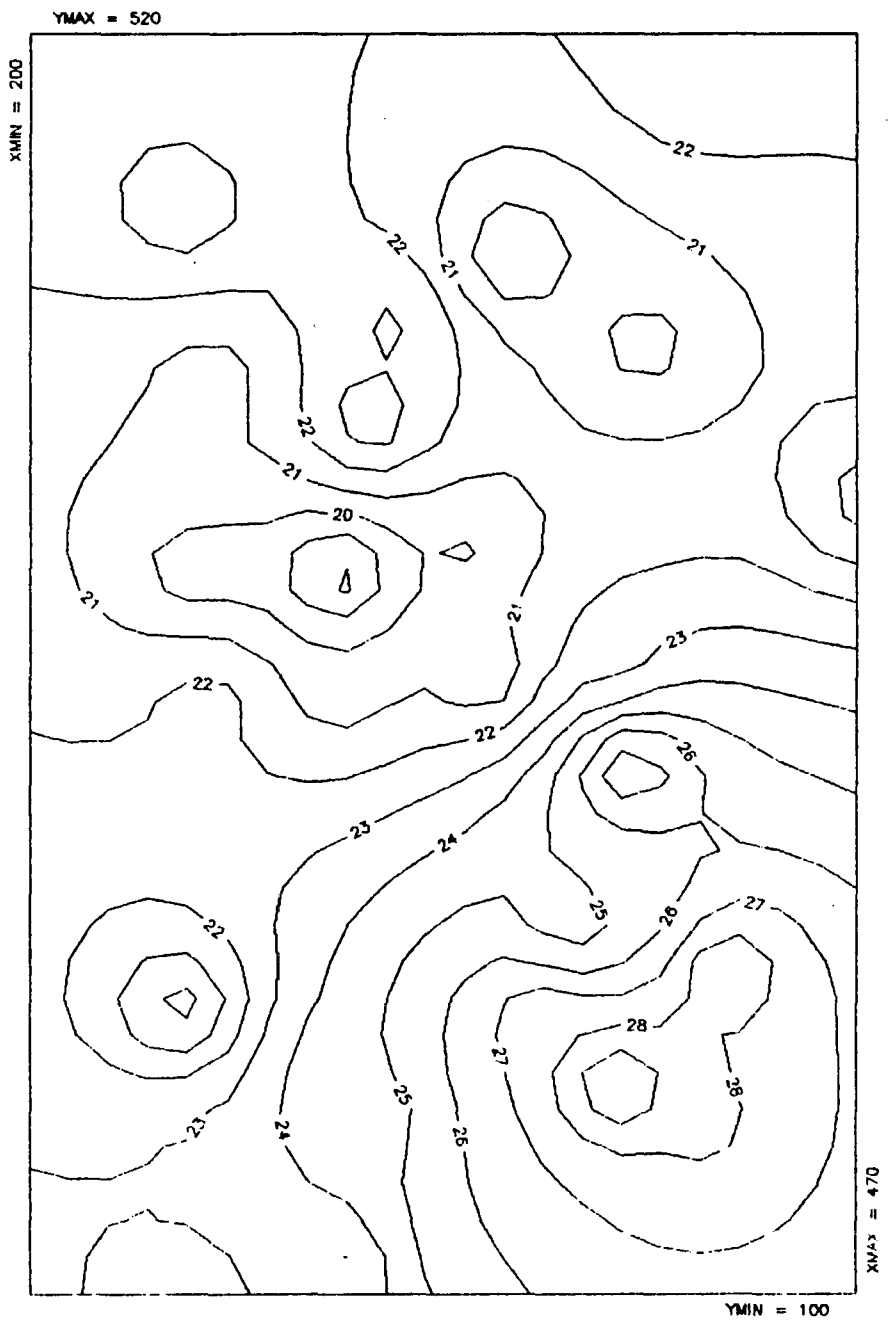

Figure B-5. Molybdenum veinlet geochemistry, La Prieta

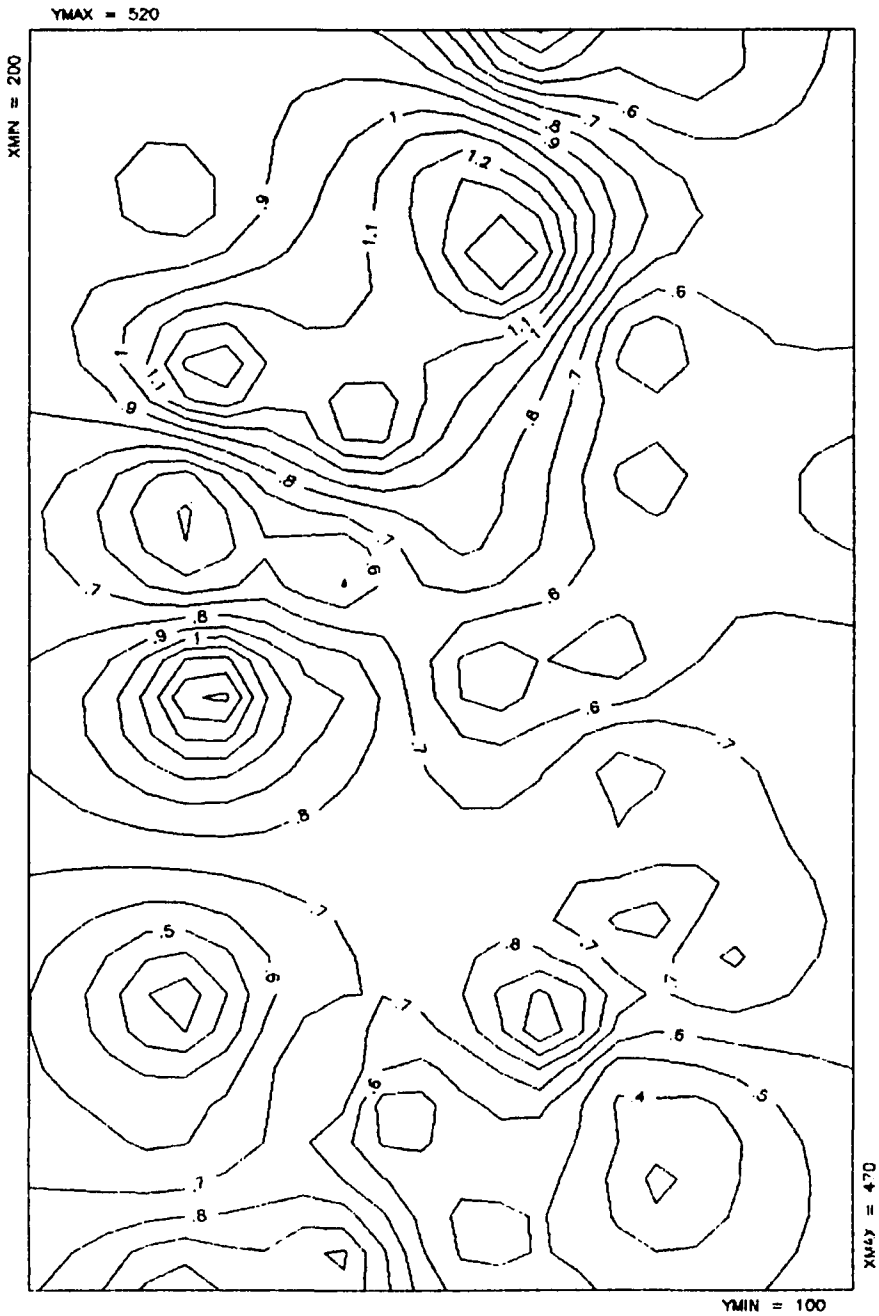

Figure B-6. Manganese veinlet geochemistry, La Prieta

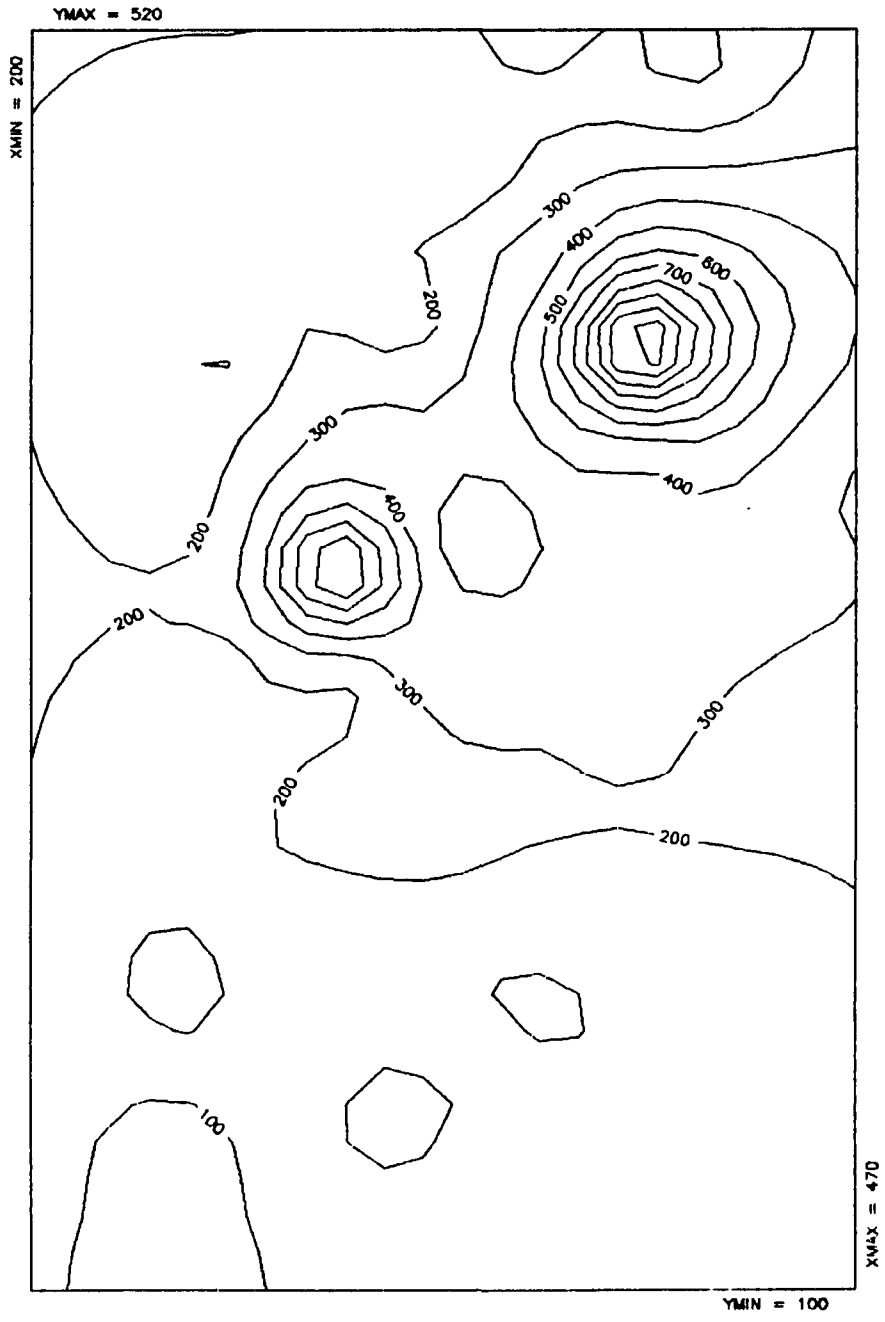

Figure B-7. Antimony veinlet geochemistry, La Prieta

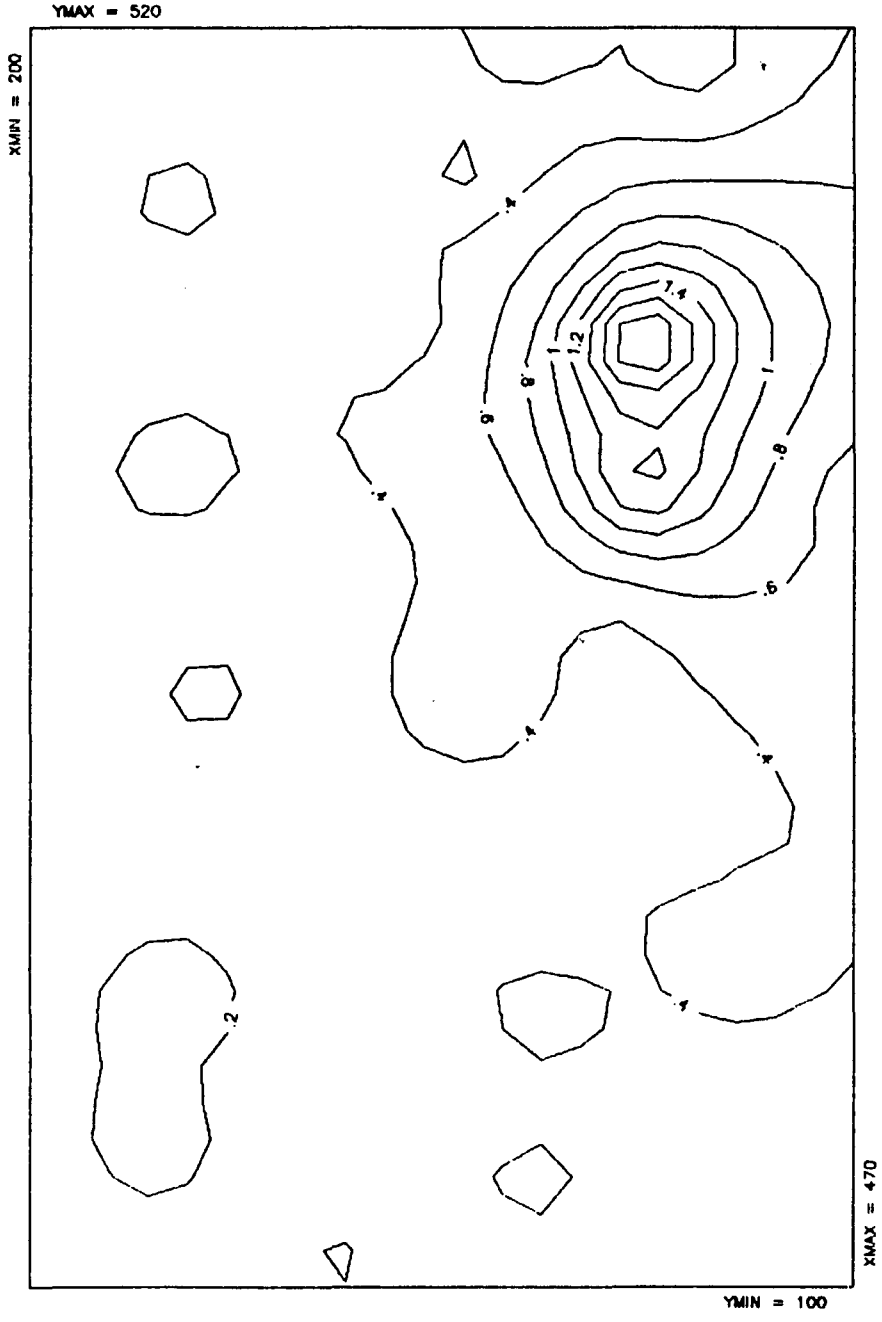

Figure B-8. Mercury veinlet geochemistry, La Prieta

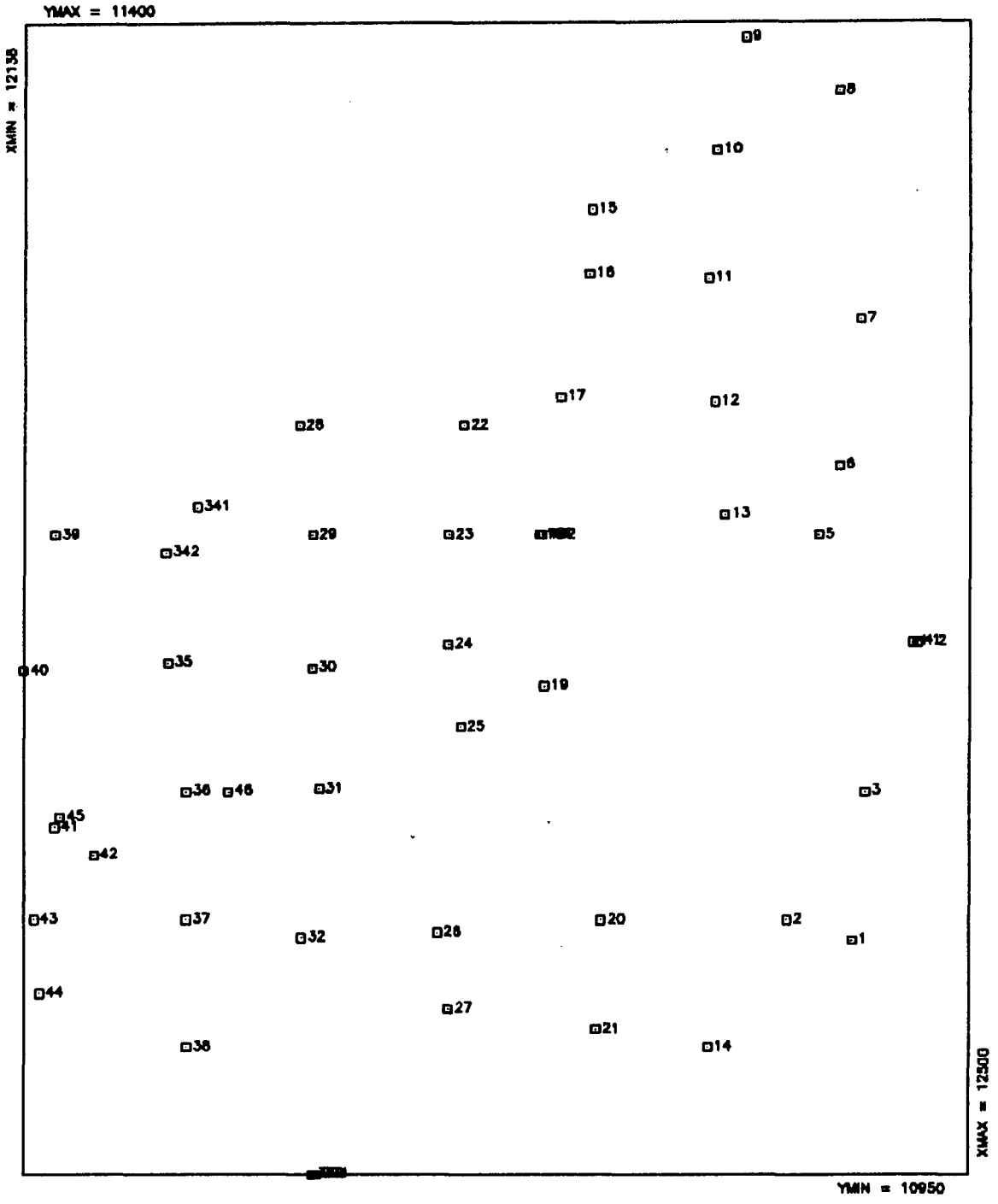

Figure B-9. Sample locations, La Escalera area

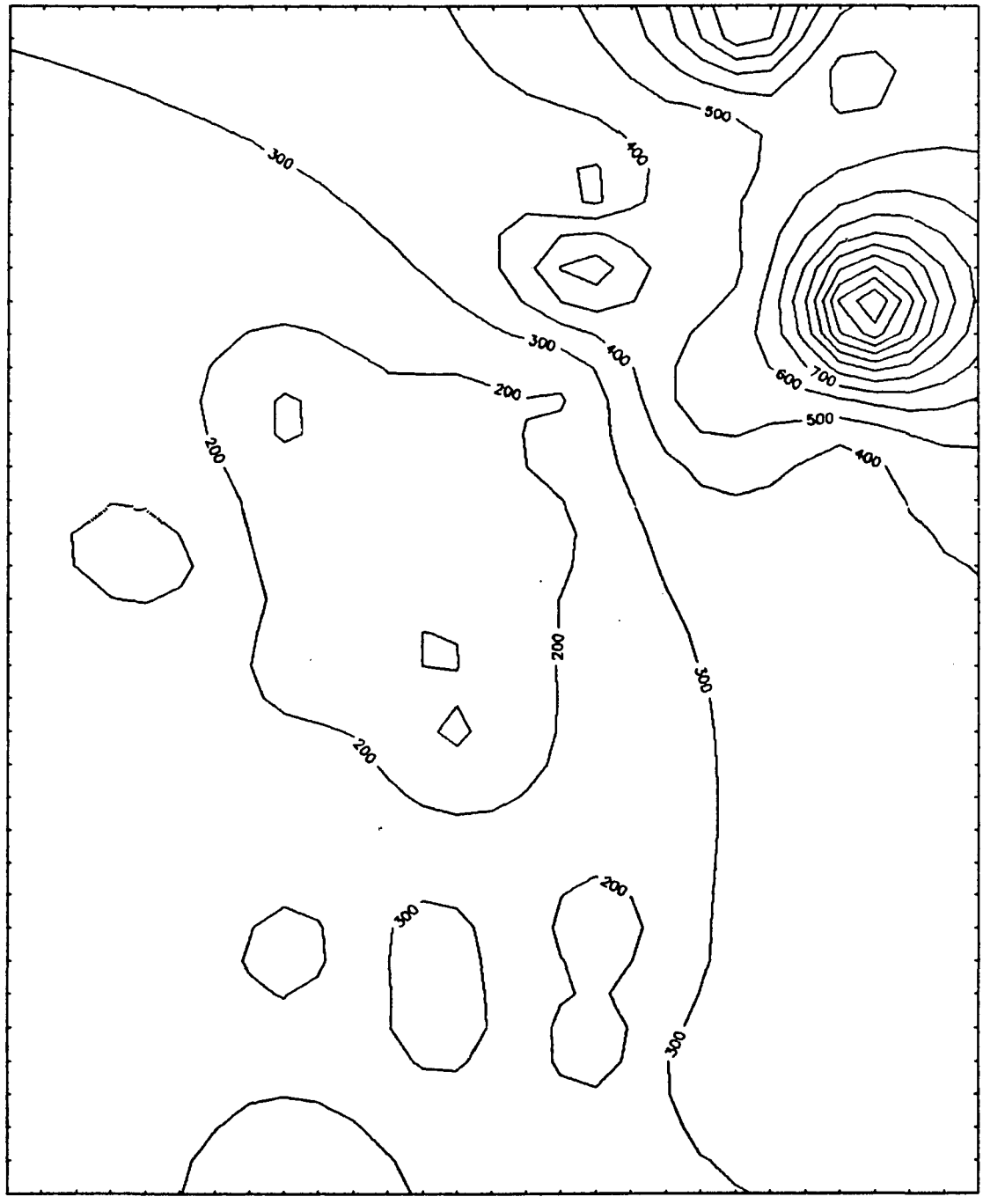

Figure B-10. Lead veinlet geochemistry, La Escalera

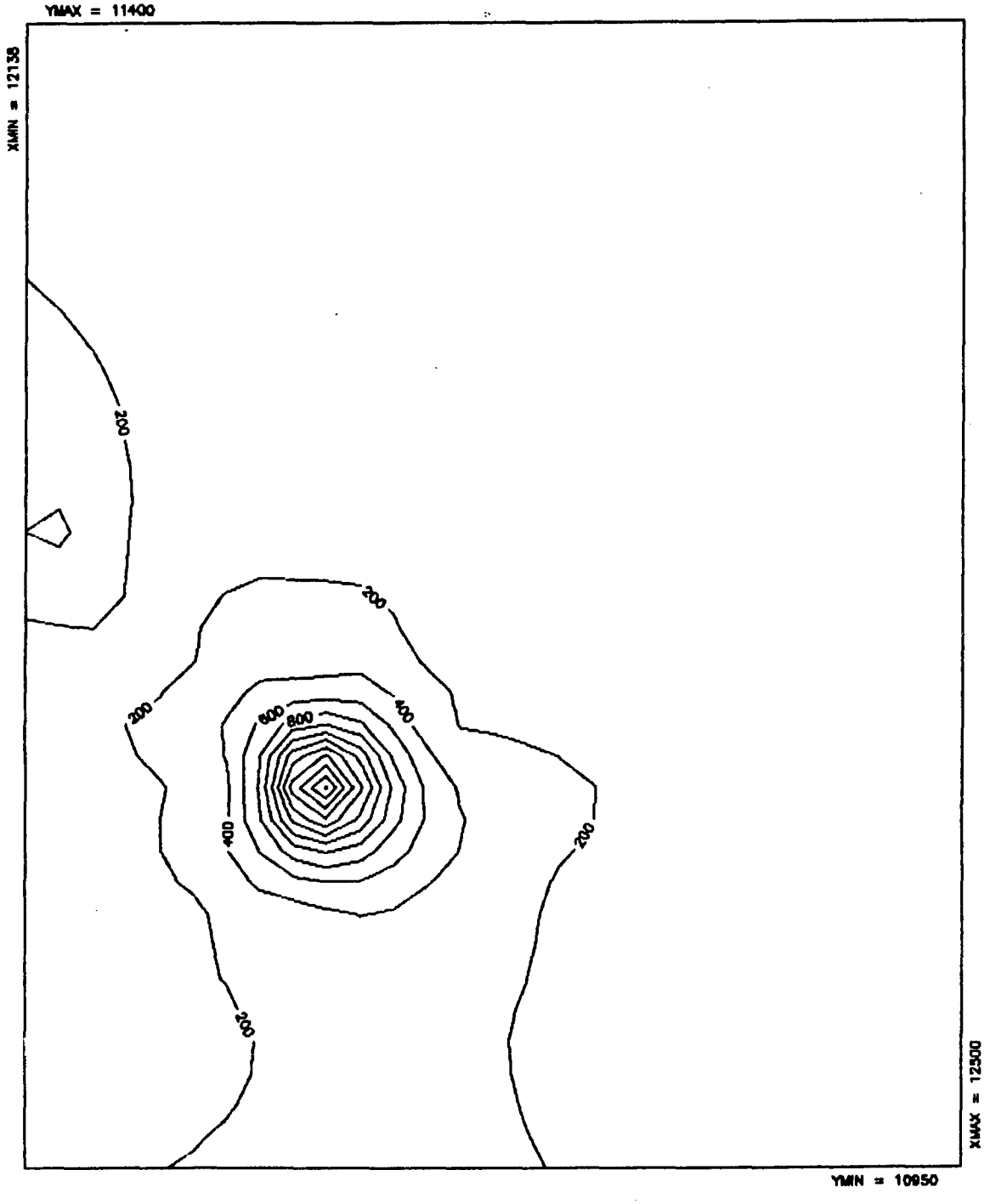

Figure B-11. Zinc veinlet geochemistry, La Escalera

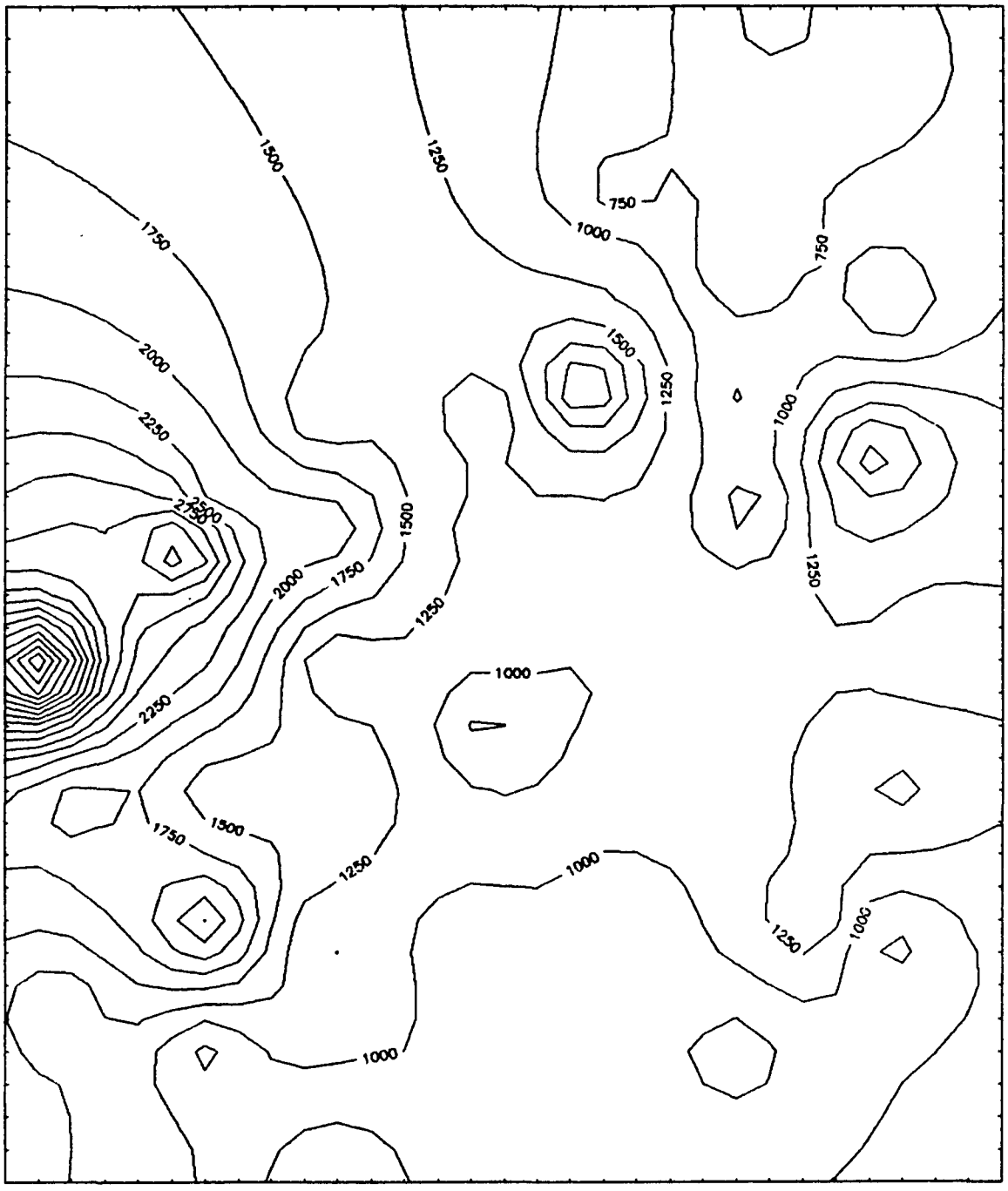

Figure B-12. Manganese veinlet geochemistry, La Escalera

Figure B-13. Molybdenum veinlet geochemistry, La Escalera

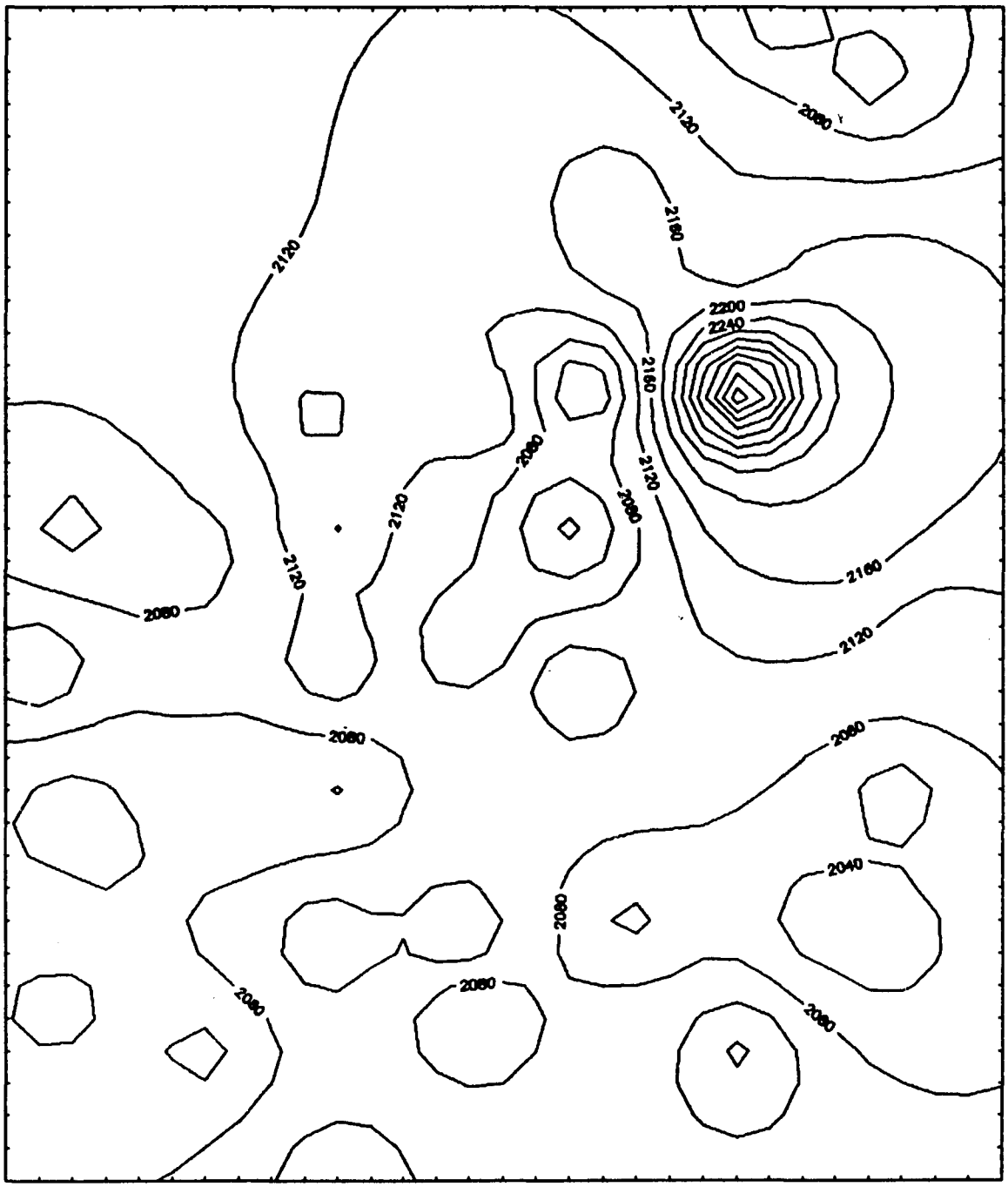

Figure B-14. Arsenic veinlet geochemistry, La Escalera

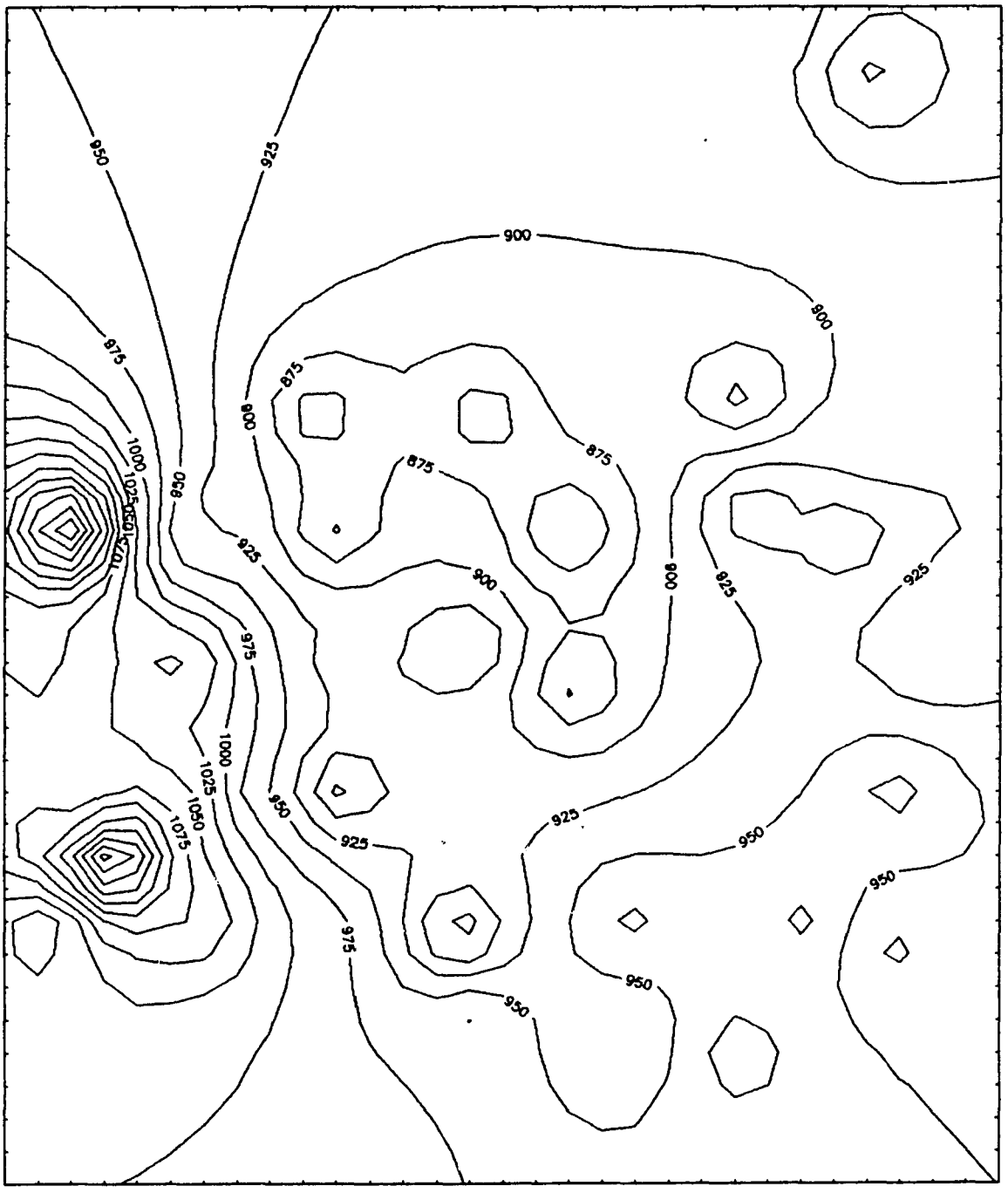

Figure B-15. Antimony veinlet geochemistry, La Escalera

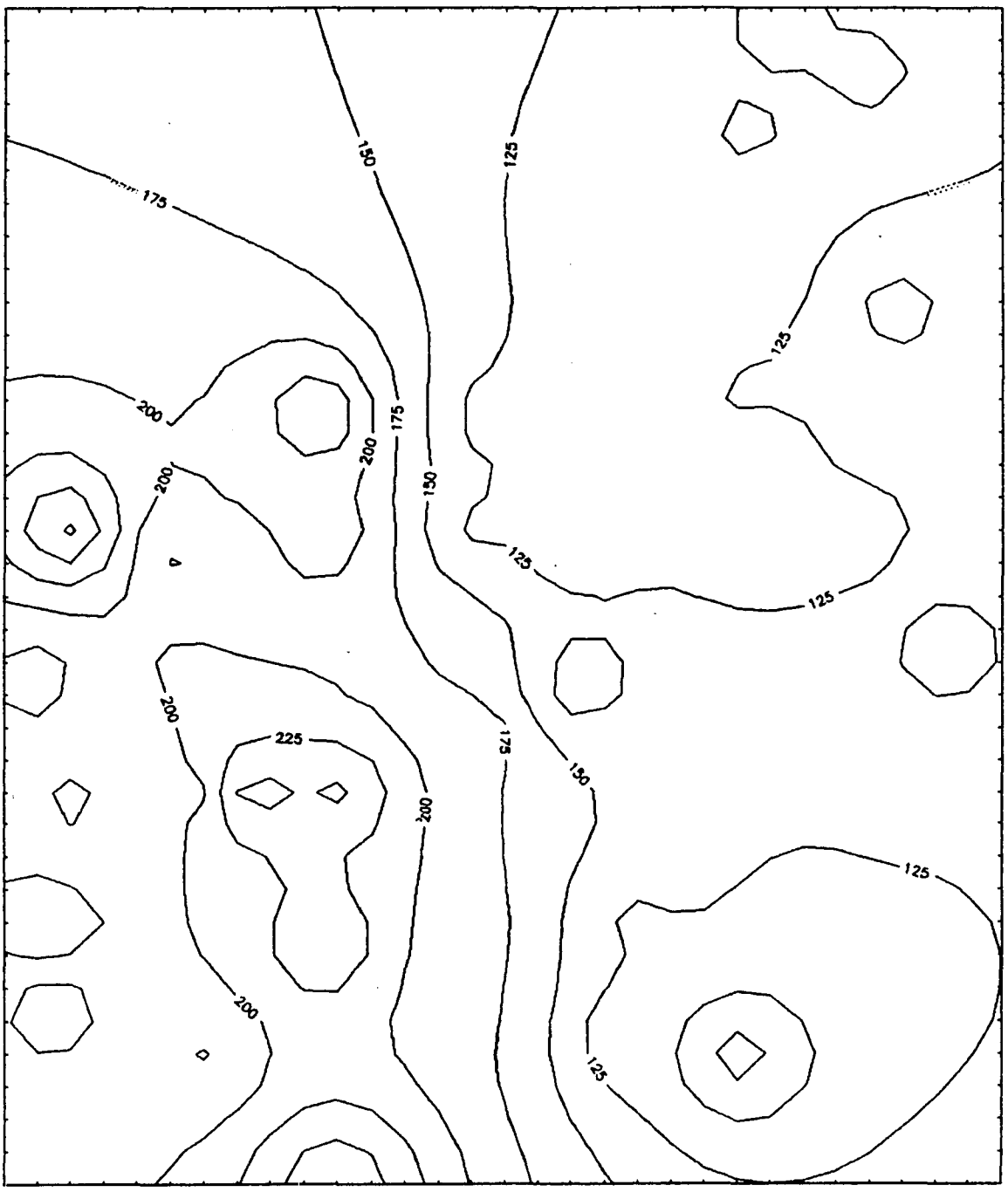

Figure B-16. Bismuth veinlet geochemistry, La Escalera

REFERENCES

Alvarez, A., 1971, Geología y mineralación en La Mina La Prieta de la Cia. Minera La Encantada, S.A., in Memoria de la IX Convención Nacional, AIMMGM, 1971, p. 225-231.

Baker, C. L., 1927, Notes on a geological exploratory traverse across the southern Sierra del Carmen and the Sierra de la Encantada in Coahuila, Mexico.

Baker, C. L., 1971, Geologic reconnaissance in the eastern Cordillera of Mexico: Geol. Soc. America Special Paper 131, 83 p.

Bateman, R., 1985, Tin-tungsten mineralization around the Canibal Creek diapir, northeastern Australia: Implications for exploration: Mineral Deposita, v. 20, p. 225-231.

Beaty, D. W., 1985, The Leadville, Colorado, district: oxygen isotopic evidence for a magmatic-hydrothermal origin [abs.]: Geol. Soc. America Abstracts with Program, v. 18, p. 521.

Beaty, D. W., 1986, Origin of the ore deposits at Gilman, Colorado; oxygen and hydrogen isotope constraints [abs.]: Geol. Soc. America Abstracts with Programs, v. 18, p. 537.

Bonet, F., 1956, Zonificación micro faunística de La Calizas Cretácicas del este de de México: Bol. Assoc. Mexicana Geologos Petroleros México, v. 8, p. 389-488.

Campa, M. F., and Coney, P. J., 1983, Tectono-stratigraphic terranes and mineral resource distributions in Mexico: Can. Jour. Earth Sci., v. 20, p. 1040-1051.

Comadurán, O., 1985, Levantamiento geológico a detalle de San Javier-La Escalera areas: La Encantada mine, Coahuila, Mexico, unpublished maps.

Comadurán, O., and Giles, D., 1975, Mapa geológico regional del distrito minero La Encantada: La Encantada mine, Coahuila, Mexico, unpublished map.

Coney, P. J., and Campa, M. F., 1984, Lithotectonic terrane map of Mexico, in Silberman, N. J., and Jones, D. L. (eds.): U.S. Geol. Survey Open-File Rept. 84-523 (map).

Coney, P. J., 1983, Un modelo tectónic de México y sus relaciones con América del Norte, América del Sur y el Caribe: Revista I.M.P., v. 15, no. 1, p. 6-15.

Conolly, H. J. C., 1936, Contour method of revealing some ore structures: Econ. Geology, v. 31, p. 235-271.

Cuevas, J. A., 1985, Analysis of subsidence and thermal history in the Sabinas Basin, northeast Mexico: M.S. thesis, Tucson, University. of Arizona, 81 p.

Deines, P., and Gold, D. P., 1969, The change in C and O isotopic composition during contact metamorphism of the Trenton Limestone by the Mount Royal pluton: Geochim. et Cosmochim. Acta, v. 33, p. 421-424.

Deines, P., Langmuir, D., and Harman, R. S., 1974, Stable carbon isotope ratios and the existence of a gas phase in the evolution of the carbonate groundwaters: Geochim. Cosmochim. Acta, v. 39, 1147-1154.

Denison, R. E., Burke, W. H., Hetherington, E.S., and Otto, J. B., 1970, Basement rocks framework of parts of Texas, southern New Mexico and northern Mexico: Midland, West Texas Geol. Soc., Pub. 71-59, p. 3-14.

Dietrich, D., McKenzie, J. A., and Song, H., 1983, Origin of calcite in syntectonic veins as determined from carbon-isotope ratios: Geology, v. 11, p. 547-551.

Emrich, K., Ehhalt, D. H., and Vogel, J. C., 1970, Carbon isotope fractionation during the precipitations of calcium carbonate: Earth Planet. Sci. Let., v. 8, p. 363-371.

Engel, A. E. J., Clayton, R. N., and Epstein, S., 1958, Variations in isotopic composition of oxygen and carbon in Leadville Limestone (Mississippi, Colorado) and its hydrothermal and metamorphic phases: Jour. Geology, v. 71, p. 238-243.

Flawn, P. T., and Maxwell, R. A., 1958, Metamorphic rocks of the Sierra del Carmen, Coahuila, Mexico: Amer. Assoc. Petroleum Geologists Bull. v. 42, p. 2245-2249.

Fleck, R. J., and Criss, R. E., 1985, Strontium and oxygen isotopic variations in Mesozoic and Tertiary plutons of central Idaho: Contr. Mineral. Petrol., v. 90, p. 291-308.

Fletcher, A. R., 1929, Mexico's lead-silver manto deposits and their origin: Eng. Mining Jour., v. 127, p. 509-513.

Friedman, I., and O'Neil, J. R., 1977, Compilation of stable isotope fractionation factors of geochemical interest, in Fleischer, M., ed., Data of geochemistry, 6th ed.: U.S. Geol. Survey Prof. Paper 440 KK.

Fritz, P., 1969, The oxygen and carbon isotopic compostion of carbonates from the Pine Point lead-zinc ore deposits: Econ. Geology, v. 64, p. 733-742.

Green, G. R., Ohmoto, H., Date, J., and Takahashi, T., 1983, Whole-rock oxygen isotope distribution in the Fukazawa-Kosaka area, Hokuroko district, Japan, and its potential application to mineral exploration: Econ. Geology Monograph 5, p. 395-411.

Guzmán, A., 1972, Notas sobre la interpretación fotogeológica de una porción de la Encantada, Edo. de Coahuila, unpublished report: México, Geotécnica, S.C., 7 p.

Hall, W. E., and Friedman, I., 1969, Oxygen and carbon isotopic composition of ore and host rock of selected Mississippi Valley deposits: U.S. Geol. Survey Prof. Paper 650-C, p. C140-C148.

Hayward, M. W., and Tripplet, W. H., 1931, Occurrence of lead-zinc ores in dolomitic limestones in northern Mexico: AIME Tech. Pub. 442, 31 p.

Hewitt, D. F., 1928, Dolomitization and ore deposition: Econ. Geology, v. 23, p. 822-962.

Humphrey, W. E., 1956, Tectonic framework of northeast Mexico: Gulf Coast Assoc. Geol. Soc. Trans., v. 6, p. 25-35.

Hunter, N. J., 1972, Regional geology and environment of ore deposition at La Encantada Mine, Coahuila, Mexico, Reporte Interno: Chihuahua, Mexico, TORMEX, S.A.,

Imlay, R. W., 1943, Evidence for Upper Jurassic landmass in eastern Mexico: Amer. Assoc. Petroleum Geologists Bull., v. 27, p. 524-549.

Lozano Ch., G., 1981, Reconocimiento estratigráfico del area La Encantada, Ocampo, Coahuila, Reporte Interno: Torrión, México, Peñoles SA. de CV.

Lozej, G. P., and Beales, F. W., 1977, Stratigraphy and structure of La Encantada Mine area, Coahuila: Geol. Soc. America, v. 88, p. 1793-1807.

Luján, G. M. A., 1975, Geología e interpretación de los cuerpos plomo-plata de La Encantada, Coahuila: AIMMGM, Memoria XI Convención Nacional, p. 531-576.

Mason, B., and Berry, L. G., 1968, Elements of mineralogy: San Francisco, Calif., Freeman, 2nd ed., 550 p.

Megaw, P. K. M., 1986. Argentiferous manganese-oxide alteration in wall and capping rocks of the Santa Eulalia district, Chihuahua, Mexico [abs.]: Geol. Soc. America Abstracts with Programs, v. 18, p.693.

Megaw, P. K. M, Ruiz, Joaquin, and Clark, K. E., 1986, High-temperature, carbonate-hosted base metal deposits of the Velardeña, Naica, and Santa Eulalia districts, northern Mexico--An overview and synthesis, in Clark, K. E., Megaw, P. K. M., and Ruiz, J., eds., Lead-zinc-silver carbonate-hosted deposits of northern Mexico, Guidebook for field and mine excursions, November 13-17, 1986: Soc. Econ. Geologists, p. 279-300.

Mining Magazine, 1980, La Encantada: January, p. 12-23.

Munskgaard, N. C., and Zeck, H. P., 1984, Oxygen-isotope systematics of a strongly recrystallized granitic rock complex, Grevillian Belt, SW Sweden: Contrib. Mineral. Petrol., v. 85, p. 67-73.

Nabelek, P. I., Labotka, T. C., O'Neil, J. R., and Papike, J. J., 1984, Contrasting fluid/rock interaction between the Notch Peak granitic intrusion and argillites and limestones in western Utah: Evidence from stable isotopes and phase assemblages: Contrib. Mineral. Petrol., v. 86, p. 25-34.

Ohmoto, H., 1986, Stable isotope geochemistry of ore deposits, in Valley, J. W., Taylor, H. P., and O'Neil, J. R., eds., Reviews in mineralogy, Vol. 16, Stable isotopes in high temperature geological processes: Mineralog. Soc. America, p. 500-555.

Ovchinnokov, L. N., and Grigorian, S. V., 1971, Primary halos in prospecting for sulfide deposits: Toronto Symposium Volume, p. 375-380.

Parslow, G. R., 1974, Determination of background and threshold in exploration geochemistry: J. Geochem. Exploration, v. 3, p. 319-336.

Pickney, D. M., and Rye, R. D., 1972, Variations of $^{18}O/^{16}O$, $^{13}C/^{12}C$, texture and mineralogy in altered limestone in the Hill mine, Cave-in-Rock district, Illinois: Econ. Geology, v. 67, p. 1-8.

Prescott, B., 1926, The underlying principles of the limestone replacement deposits of the Mexican Province I-II: Eng. Mining Jour., v. 122, p. 245-253, 289-296.

Rosas-S, A., 1983, Estudio de orientacion geoquímico del distrito minero La Encantada, reporte interno: Sonora, Mexico, SIPSA de CV.

Rose, A. W., Hawkes, H. E., and Webb, J. S., 1979, Geochemistry in mineral exploration, 2nd ed.: London, Academic Press, 657 p.

Routsala, A. P., Nordeng, S. G., and Lweege, R. J., 1969, Trace elements in accessory calcite--A potential exploration tool in the Michigan copper district: Colorado School of Mines Quart., v. 64, no. 1, p. 451-455.

Ruiz, J., Megaw, P. K., and Lofquist, D. J., n.d., Stratigraphy of the Cretaceous carbonates hosting the mineralization and Santa Eulalia and Naica, Mexico, and permeability controls on the distribution of the orebodies: accepted by Geol. Soc. America Bull., 1987.

Rye, R. O., 1966, The carbon, hydrogen, and oxygen isotopic composition of the hydrothermal fluids responsible for the lead-zinc deposits at Providencia, Zacatacas, Mexico: Econ. Geology, v. 63, p. 232-238.

Rye, R. O., and Ohmoto, 1974, Sulfur and carbon isotopes and ore genesis: A review: Econ. Geology, v. 69, p. 826-842.

Sassano, G. P., Fritz, P., and Morton, R. D., 1972, Paragenesis and isotopic composition of some gangue minerals from the uranium deposits of Eldorado, Saskatchewan, Canada: Jour. Earth Sci., v. 9, p. 141-157.

Sharpley, F. J., 1972, Report on the surface geology of the La Encantada and Los Angeles mine, and adjacent properties, Coahuila, Mexico: Unpublished report, TORMEX, A.A., 16 p.

Sheppard, S. M. E., 1986, Characterization and isotopic variations in natural waters: in Valley, J. W., Taylor, H. P., and O'Neil, J. R., eds., Reviews in mineralogy, Vol. 16, Stable isotopes in high temperature geological processes: Mineralog. Soc. America, p. 165-184.

Sinclair, A. J., 1974, Selection of threshold values in geochemical data using probability graphs: Jour. Geochem. Exploration, v. 3, p. 129-149.

So, C. S., Rye, D. M., and Shelton, K. L., 1983, C, H, O and S isotope and fluid inclusion study of the Weolag tungsten-molybdenum deposit, Korea: Fluid histories of metamorphic and ore-forming events: Econ. Geology, v. 78, 1551-1575.

Solano, R. B., 1985, Geología y mineralización del distrito minero La Encantada, Coahuila, reporte interno: Torreón, Coah., SIPSA de CV.

Solano, R. B., and Flores, G., 1983, Reporte geológico superficial del distrito minero La Encantada, Coahuila, reporte interno: Torreón, Ccoah., SIPSA de CV.

Smith, C. I., 1970, Lower Cretaceous stratigraphy, northern Coahuila, Mexico: Report of investigations N 65: Austin, University of Texas, Bureau of Economic Geology,

Smith, C. I., 1981, Review of the geologic setting, stratigraphy, and facies distribution of the Lower Cretaceous in northern Mexico, in Lower Cretaceous stratigraphy and structure, northern Mexico: West Texas Geol. Soc. 81, 74, p. 1-27.

Taylor, H. P., Jr., 1979, Oxygen and hydrogen isotope relationships in hydrothermal mineral deposits, in Barnes, H. L., ed., Geochemistry of hydrothermal deposits: New York, Hol, Rinehart and Winston, p. 236-277.

Titley, S. R., and Megaw, P. K., 1985, Carbonate hosted ores of the western Cordillera--An overviews: S.M.E., AIME Annual Meeting, New York, preprint 85-115, 17 p. 85-115,

Titley, S. R., Thompson, R. C., Haynes, R. M., Manske, S. L., Robinson, L. E., and White, S. L., 1986, Evolution of fractures and alteration in the Sierrita-Esperanza hydrothermal system, Pima County, Arizona: Econ. Geology, v. 81, p. 343-370.

Trejo, P., 1983, El proceso supergénico en La Encantada, Coahuila, in Memoria de la IV Convención Nacional, AIMMGM, 1983: p. 147-171.

Turekian, K. K., and Wedepohl, K. H., 1961, Distribution of the elements in some major units of the earth's crust: Geol. Soc. America Bull., v. 72, p. 175-182.

Valley, J. W., 1986, Stable isotope geochemistry of metamorphic rocks, in Valley, J. W., Taylor, H. P., and O'Neil, J. R., eds., Reviews in mineralogy, Vol. 16, Stable isotopes in high temperature geological processes: Mineralog. Soc. America, p. 445-479.

Veizer, J., 1983, Trace elements and isotopes in sedimentary carbonates in Reeder, R. J., ed., Reviews in mineralogy, Vol. 11, Carbonates: Mineralogy and Chemistry: Mineralog. Soc. America, p. 265-299.

Wehrenberg, J. P. and Silberman, A., 1965, Studies of base metal diffusion in experimental and natural systems: Econ. Geology, v. 74, p. 95-108.

West Texas Geological Society, 1981, Lower Cretaceous stratigraphy and structure, northern Mexico: Austin, 95 p.